



Politecnico di Torino

Corso di Laurea Magistrale in Ingegneria Aerospaziale
Dipartimento di Ingegneria Meccanica e Aerospaziale

Master's Degree Thesis

Thermal control of the avionics box for a commercial supersonic aircraft through Reverse Bootstrap cycle

Supervisors:

Prof. Paolo Maggiore

Ing. Achille Mannini

Candidate:

Luca Sarnataro s303908

Contents

1	Introduction	1
1.1	Commercial supersonic aircraft today and in the future	3
2	Refrigeration techniques	7
2.1	Brief history of the air cycle systems	8
2.2	Simple air cycle architecture (also called Turbofan)	9
2.3	Bootstrap architecture	11
2.4	Three wheel architecture (also called Simple/Bootstrap)	11
2.5	Four wheel architecture (also called Condensing Cycle)	12
3	Reverse Bootstrap system	15
3.1	Direct ram air cooling mode	16
3.2	Air cycle cooling mode	17
3.3	Ground cooling	19
3.4	Alternative configuration of the avionics cooling: distributed cold plates	20
3.5	Comparison of Direct vs. Reverse Bootstrap design	21
4	Steady-state computational model	23
4.1	Environmental conditions and intake	25
4.1.1	Ambient environmental conditions	25
4.1.2	Shock wave calculations	28
4.2	Turbine	30
4.2.1	Radial turbine: introduction	30
4.2.2	Thermodynamic calculations	32
4.2.3	Sizing calculations	35
4.3	Avionics box	45
4.3.1	Types of heat exchange	45
4.3.2	Thermal control techniques: general concepts	46
4.3.3	Avionics box configuration	48
4.3.4	Calculation process	50
4.4	Compressor	54
4.4.1	Centrifugal compressor: introduction	54
4.4.2	Thermodynamic calculations	54
4.4.3	Sizing calculations	56
4.4.4	Adiabatic efficiency verification	61
4.5	Pressure losses in the connecting pipes	64
4.5.1	Ducts pressure losses theory	64
4.5.2	Specific pressure losses data	65

5	Component's size and system performance at Design Point	69
5.1	Direct Ram Air Design Point	69
5.2	Reverse Bootstrap operation Design Point	71
5.2.1	Maximum avionics temperature	71
5.3	Shock wave and air intake	72
5.4	Air Cycle Machine (ACM)	72
5.4.1	Turbine	72
5.4.2	Compressor	76
5.5	Avionics box	78
5.5.1	Configuration	78
5.5.2	Thermal parameters	79
5.5.3	Fin selection	80
5.6	Connecting pipes	80
5.7	Complete system size and mass	80
5.8	System performance at Design Point with Reverse Bootstrap operating	81
6	Off Design Point conditions	85
6.1	Off Design point calculation procedure	86
6.1.1	Impact of Humidity on the Turbine Exhaust Temperature . .	88
6.2	Performances at Off Design points	90
7	Reliability	97
7.1	Types of reliability	97
7.2	Mean Time Between Failures (MTBF) and Failure Rate (λ)	98
7.3	Reliability relations between system components	98
7.4	Preliminary Reliability calculation for the Reverse Bootstrap Thermal Control System discussed in this thesis	99
7.5	Failure Mode and Effect Analysis (FMEA)	100
7.6	Failure Modes Effects and Criticality Analysis (FMECA)	101
8	Comments and conclusions	107
8.1	Comments	107
8.2	Conclusions	109
A	MatLab-Simulink model	111
A.1	Input blocks & ISA20 block	112
A.2	Intake block	112
A.3	Turbine block	113
A.4	Avionics box block	114
A.5	Compressor block	115
B	Component maps construction	117
C	Off Design iteration process	119
D	T_{DAR} and T_{WAR} at the turbine exhaust	121

List of Figures

1.1	Tupolev Tu-144 [14]	2
1.2	Concorde [12]	3
1.3	Boom Overture [19]	3
1.4	X-59	4
1.5	Drako	5
2.1	Dr. John Gorrie, inventor of the ice machine	8
2.2	John Gorrie’s ice machine air cycle	9
2.3	Simple air cycle	9
2.4	Bootstrap air cycle	11
2.5	Three wheel architecture	12
2.6	Four wheel architecture	13
3.1	Reverse Bootstrap system for avionics cooling	16
3.2	Direct Operation mode flow path	17
3.3	Air Cycle Operation mode flow path	18
3.4	Typical temperature-entropy diagram of a Reverse Bootstrap system running in the Air Cycle mode	19
3.5	Reverse Bootstrap configuration with cold plates	20
3.6	Reverse Bootstrap configuration for cooling of inhabited compartments	22
4.1	Humidity vs. Altitude [5]	26
4.2	Temperature, pressure and density variations through a normal shock wave	29
4.3	Radial turbine	30
4.4	Radial turbine components	31
4.5	Volute	31
4.6	Nozzle ring and rotor	32
4.7	Total-to-static adiabatic efficiency vs. Specific speed	37
4.8	Minimum number of rotor blades	39
4.9	Glassman’s minimum rotor blade number	40
4.10	Example of blade profile	41
4.11	Example of tip profile representation	41
4.12	Different types of plate fins	47
4.13	Finned tube	47
4.14	Section of a Diffusion bonded heat exchanger	48
4.15	Plate fin’s geometry	49
4.16	j and f vs. Reynolds number	50
4.17	Centrifugal compressor	54

4.18	Centrifugal compressor components	54
4.19	Total-to-static polytropic efficiency vs. Specific speed	62
4.20	Friction factor vs. Reynolds number	65
4.21	Loss coefficient vs. Reynolds number for 90° bends in circular ducts	66
4.22	Loss coefficient vs. area ratio in circular ducts for sudden area change	67
5.1	Typical mission profile of a modern supersonic aircraft	71
5.2	Air Cycle Machine CAD design	72
5.3	Turbine CAD design	73
5.4	Turbine sections	73
5.5	Triangles of velocity at turbine inlet	74
5.6	Triangles of velocity at turbine exhaust	74
5.7	Compressor CAD design	76
5.8	Compressor sections	76
5.9	Triangles of velocity at compressor inlet	77
5.10	Triangles of velocity at compressor exhaust	77
5.11	Avionics box sizes	78
5.12	Avionics box CAD section	79
5.13	Avionics box cut view	79
5.14	Avionics Box Thermal Control System CAD design	81
5.15	Thermodynamic cycle on the Temperature-Entropy plane	82
6.1	Turbine efficiency vs. Corrected speed	87
6.2	Turbine corrected mass flow vs. Expansion ratio	87
6.3	Compressor pressure ratio vs. Corrected mass flow	88
6.4	Compressor corrected head vs. Corrected mass flow	88
6.5	Turbine Performance at Off-Design conditions	90
6.6	Turbine Flow Coefficient at Off-Design conditions	90
6.7	Compressor Pressure Ratio at Off-Design conditions	91
6.8	Corrected Adiabatic Head at Off-Design conditions	91
7.1	Electrical similarity	98
7.2	Electrical similarity with redundant components	99
7.3	System block diagram	99
8.1	Reverse Bootstrap Air Cycle Machine for an ECS	108
A.1	Simulink model	111
A.2	Input blocks	112
A.3	ISA20 block	112
A.4	Connections to intake	113
A.5	Subsystem intake block	113
A.6	Turbine block (a) and subsystem turbine block (b)	114
A.7	Avionics box block (a) and subsystem avionics box block (b)	115
A.8	Connections between avionics box and iteration box	115
A.9	Compressor block (a) and subsystem compressor block (b)	116

List of Tables

3.1	Table of components	17
3.2	Table of components	18
4.1	Fin's geometrical configuration	50
4.2	Avionics box sizes	51
4.3	Thermodynamic inputs	51
5.1	Direct System Design point	70
5.2	Input parameters	71
5.3	Shock wave and air intake parameters	72
5.4	Turbine parameters	75
5.5	Compressor parameters	78
5.6	Avionics box parameters	80
5.7	Fin parameters	80
5.8	Connecting pipes pressure losses	80
5.9	Components mass	81
5.10	Reverse Bootstrap system Design point	83
6.1	Off Design conditions - Air cycle operation	85
6.2	Off Design conditions - Direct cycle operation	85
6.3	Off-Design case with vapor condensation	89
6.4	Reverse Bootstrap - Off design Case 1	92
6.5	Reverse Bootstrap - Off design Case 2	93
6.6	Reverse Bootstrap - Off design Case 3	94
6.7	Direct system - Off design Case 4	95
6.8	Direct system - Off design Case 5	96
7.1	Failure rates table	100
7.2	FMEA of the Thermal Control System of the Avionics Box	102
7.3	An exemple of FMECA layout table	104
7.4	Occurrece classification	105
7.5	Detection classification	105
7.6	Severity classification	106

Abstract

The only two supersonic aircraft that entered civil aviation service were the Russian Tupolev TU-144 (operational since December 26th, 1975 until 1978) and the Anglo/French Concorde (operational since January 21st, 1976 until October 24th, 2003). The less than brilliant commercial success of the two machines is attributable to factors of a different nature: high operating costs, maintenance problems, low sustainability of this type of aircraft. Among these, considerable importance is connected to the phenomenon of the sonic boom which occurs every time an aircraft exceeds Mach 1. In these conditions a very strong noise similar to very powerful thunder is generated, which disturbs the populations who live on the territory below. For this reason the Concorde was not allowed to fly over land at supersonic speed, limiting this main characteristic only to overflight of the oceans.

In recent times, however, there has been a revival of interest in supersonic speed connections for both tourism and business travel, whilst guaranteeing the achievement of the sustainability characteristics of the aircraft.

The work carried out in this thesis aims to contribute to the solution of the sustainability problems of new aircraft, dealing with the thermal control of the avionics that govern the operation of important on-board systems. Such device shall need minimum or 0 power, shall have small size and weight, shall be highly reliable.

The thermal control system chosen is a Reverse Bootstrap air cycle, the use of which is already well known in the "pods" of military fighter aircraft. However, in the application covered by this thesis, the environment is quite different and the duration of the mission is decidedly longer, which has been hypothesized to be three to four hours, corresponding to a flight from a European city to one in the United States or one in the Far East.

The Reverse Bootstrap works without any air bleed from the aircraft's engines and therefore its energy cost is zero because it uses the shock wave generated by flying supersonic as an energy source; the overpressure that is generated downstream of the wave is used to power a turbine that drives a compressor. At the same time, the compressor driven by the turbine, depresses the exhaust of the turbine increasing its pressure ratio and cooling the air to temperature suitable for thermal control of the electronics. The particular mechanical design of the avionics box, which will be described in detail, guarantees non-contamination of the avionics components and certainly protects them from contact with water that could come from the rain or from the turbine exhaust due to condensation of humidity. The result is a very compact (0.983 m x 0.340 m x 0.207 m) and light (1.995 kg) thermal control system of an avionics box having a thermal load from 1500 W at sea level to 400 W where it flights at Mach number 1.8.

Comments and reasoning set out at the end of the study concern the applicability of this technology also to the air conditioning system of inhabited compartments.

Sommario

Gli unici due aerei supersonici entrati in servizio nell'aviazione civile furono il russo Tupolev TU-144 (operativo dal 26 dicembre 1975 al 1978) e il Concorde anglo/francese (operativo dal 21 gennaio 1976 al 24 ottobre 2003). Il non brillante successo commerciale delle due macchine è imputabile a fattori di diversa natura: elevati costi di esercizio, problemi di manutenzione, scarsa sostenibilità di questa tipologia di velivoli. Tra questi, notevole importanza è legata al fenomeno del boom sonico che si verifica ogni volta che un aereo supera Mach 1. In queste condizioni si genera un rumore molto forte, simile a un tuono molto potente, che disturba le popolazioni che vivono sul territorio sottostante. Per questo motivo al Concorde non fu consentito sorvolare la terra a velocità supersonica, limitando questa caratteristica principale al solo sorvolo degli oceani.

Negli ultimi tempi, però, si è assistito ad un rinnovato interesse per i collegamenti a velocità supersonica sia per il turismo che per i viaggi d'affari, garantendo al tempo stesso il raggiungimento delle caratteristiche di sostenibilità degli aerei.

Il lavoro svolto in questa tesi mira a contribuire alla soluzione dei problemi di sostenibilità dei nuovi velivoli, occupandosi del controllo termico dell'avionica che governa il funzionamento di importanti sistemi di bordo. Tale dispositivo dovrà richiedere una potenza minima o nulla, dovrà avere dimensioni e peso ridotti ed essere altamente affidabile.

Il sistema di controllo termico scelto è un ciclo d'aria Reverse Bootstrap, il cui utilizzo è già ben noto nei "pod" degli aerei da caccia militari. Tuttavia, nell'applicazione oggetto di questa tesi, l'ambiente è ben diverso e la durata della missione (che è stata ipotizzata essere di tre-quattro ore corrispondenti ad un volo da una città europea ad una degli Stati Uniti o in Estremo Oriente) è decisamente più lunga.

Il Reverse Bootstrap funziona senza alcuno spillamento d'aria dai motori dell'aereo e quindi il suo costo energetico è pari a zero perché utilizza come fonte di energia l'onda d'urto generata dal volo supersonico; la sovrappressione che si genera a valle dell'onda viene utilizzata per alimentare una turbina che aziona un compressore. Allo stesso tempo il compressore deprime lo scarico della turbina aumentandone il rapporto di espansione e raffreddando l'aria ad una temperatura adatta al controllo termico dell'elettronica. Il particolare disegno meccanico della scatola avionica, che verrà descritta in dettaglio, garantisce la non contaminazione dei componenti avionici e sicuramente li protegge dal contatto con l'acqua che potrebbe provenire dalla pioggia o dagli scarichi della turbina per condensazione dell'umidità. Il risultato è un sistema di controllo termico molto compatto (0.983 m x 0.340 m x 0.207 m) e leggero (1.995 kg) di una scatola avionica con un carico termico da 1500 W al livello del mare a 400 W alla quota di 16000 m, dove vola a Mach 1,8.

Al termine dello studio si discute sui pro e i contro dell'applicabilità di tale tecnologia anche al sistema di climatizzazione dei vani abitati.

Chapter 1

Introduction

The objective of this thesis is to design and characterize a reverse bootstrap refrigeration system applied to an avionics box for commercial supersonic aircraft.

Supersonic aircraft for commercial use are an ambitious step forward in the evolution of air transportation. They are aircraft capable of flying faster than the speed of sound (Mach 1).

Supersonic flight would drastically transform air transportation in a matter of years: it would allow to fly from New York to London in about 3.5 hours, compared to 7-8 hours for conventional aircraft. That would produce easier connections around the world, which would benefit both general and business travelers: indeed, overnight flights would no longer be needed, and jet-lag would no longer be an issue.

Commercial-use designs for supersonic aircraft have been dropped, in the past, essentially because of the following issues:

1. The noise caused by sonic booms, associated with shock waves created when an object traveling through the air exceeds the speed of sound, which generate a considerable amount of noise pollution. When an aircraft travels through the atmosphere, it continuously produces air-pressure waves: if the aircraft exceeds the speed of sound, these waves combine and form shock waves which travel forward from the generation or "release" point. Sonic booms from large supersonic aircraft can be particularly loud, so much so that they disturb people and even, in extreme cases, damage structures. They have led to the prohibition of routine supersonic flights over land. This phenomenon, though unavoidable, can be mitigated through modern technologies, based on the study of shock waves.
2. Sustainability is a crucial issue in the aeronautical environment, therefore supersonic aircraft, as well as the subsonic ones, have to contain fuel consumption within the limits established by regulations. Particularly challenging is to respect these limitations during the mission segments of take-off and acceleration to cruise speed.
3. The cost per seat of a supersonic airliner is significantly higher than that of a subsonic airliner. Supersonic flight requires more powerful engines, producing the increase of manufacturing and maintenance costs. Furthermore, the higher

stresses on the airplane's structure require the use of expensive materials, and also increase the maintenance costs. Finally, noise mitigation costs must be considered. All these issues have to be overcome, in order to make supersonic flight available not only for high income people.

The only two supersonic aircraft to ever enter service for civilian use were Tupolev Tu-144 and Concorde. A brief overview of them follows:

- **Tupolev Tu-144**

Tupolev Tu-144 (Figure 1.1) was the first supersonic airliner to ever enter service (first flight on December 31st, 1968, entered service on December 26th, 1975); it was designed by *OKB*, developed by *Tupolev* and built by *VASO*. Tu-144 was equipped with 4 turbofan engines with afterburner, and it could reach Mach 2.15 at maximum cruise speed. On the aircraft were applied a double-delta wing and two canards, one on each side of the front section. As the Tu-144 was intended for flying over the Urss territory, it had to fly at a 17000 *m* altitude, in order to limit noise pollution.

In 1978, following an accident during an engine test, Urss suspended supersonic flight for commercial use. One of the main reasons was also the economic unsustainability of the project: a Tu-144 flight cost almost twice as much as a conventional flight, hence the aircraft was often half-full, while maintenance and fuel were very expensive.



Figure 1.1: Tupolev Tu-144 [14]

- **Concorde**

Concorde (Figure 1.2) was a supersonic airliner produced by *British Aerospace* (UK) and *Aérospatiale* (France) (first flight on March 2nd, 1969, entered service on January 21st, 1976). It was very similar to Tu-144 in terms of weight, dimensions and configuration: infact, they both had delta wings and adjustable front section to improve visibility during landing.

It was equipped with 4 turbojet engines (turbofan size would have been excessive) with afterburner, produced by Rolls-Royce, and it could reach Mach 2.04 at maximum cruise speed.

The huge fuel consumption (17 litres per passenger, every 100 km travelled), the high production and maintenance costs made the ticket price three times

1.1. COMMERCIAL SUPERSONIC AIRCRAFT TODAY AND IN THE FUTURE

higher than a first class ticket on a conventional airliner. Because of that, and after an accident occurred at Charles de Gaulle (Paris) on July 25th, 2000, when all passengers and crew and 4 people on the ground died, Concorde was retired on October 24th, 2003.



Figure 1.2: Concorde [12]

1.1 Commercial supersonic aircraft today and in the future

Overture

Today, several companies and agencies are working on supersonic commercial aircraft design: one of them is *Overture* (Figure 1.3), proposed by *Boom Supersonic*. It is a 64-80 passenger supersonic airliner, designed to fly at Mach 1.7 over water, at an altitude of 60000 *ft*, with a range of 4250 nautical miles. Boom has received orders, including purchases and options from American Airlines, United Airlines, and Japan Airlines for a total of 130 aircraft.

Overture's wing configuration is a conventional compound delta for low supersonic



Figure 1.3: Boom Overture [19]



Figure 1.4: X-59

drag; it needs to address the nose-up attitude on landing. Airframe maintenance costs are expected to be similar to those of other carbon fiber airliners. The Overture is expected to not be louder at takeoff than current airliners. Supersonic jets could be exempted from the FAA takeoff noise regulations, reducing their fuel consumption by 20–30% by using narrower engines optimized for acceleration over limiting noise. There will be 4 engines, called *Boom Symphony*: they are two spool medium bypass turbofans, also developed by *Boom Supersonic*. Symphony is designed to be powered only by sustainable aviation fuel (SAF).

Boom targets \$5,000 fares for a New York-to-London round-trip, while the same on Concorde cost \$20,000 adjusted for inflation.

X-59

Lockheed Martin X-59 QueSST (Fig.1.4) is a low-boom flight demonstrator, under development by NASA and built by Lockheed Martin; its preliminary design process started in 2016, and the first test flight is expected by the end of 2023.

X-59 will be able to reach Mach 1.4 at an altitude of 55000 *ft*, and it will be equipped with a *F414-GE-100* engine by General Electric.

Purpose of the *X-59* program is to study and develop an aircraft geometry which allows to prevent, or at least delay, the coalescence of the compression waves that generates the shock wave. Thanks to the high elongation of the fuselage, this aircraft could generate a sonic boom equal to one thousandth of that of a conventional supersonic aircraft.

An interesting detail about *X-59* is the absence of a forward-facing window inside the pilot cabin: it will be substituted by a 4K monitor, which will display images from two cameras located on the nose of the aircraft. This system, beyond allowing the pilot to safely see traffic in the flight path, provides additional visual aids for airport approaches, landings and takeoffs.

It has to be noted that *X-59* is not meant to actually transport passengers, but its boom-reduction technology could help to lift the current bans on supersonic flight overland and it could be implemented on aircraft suitable to passenger transportation.



Figure 1.5: Draco

Drako

Drako is a concept hypersonic plane, conceived by french designers to be used on the routes that today are traveled by B-777, B-787, A-330 and A-350, between Europe and North America and between Asia and North Pole.

Drako would be able to reach and overcome Mach 3, allowing to fly from Paris to New York in about 2 hours. It would be equipped with two TBCC (Turbine Based Combined Cycle) engines. This technology allows to use the most efficient mode for any mission's segment: at low speed the engine will work as a Turbofan, while at high speed it will work as a Ramjet.

The realization of this prototype is expected not before 2050, since there are many problems to overcome, in terms of materials, fuel and refrigeration system.

As described in this Introduction, shock waves associated with supersonic flight can be a problem in terms of noise, airframe damaging, interaction with boundary layer, increased drag. On the other hand, the compression of the ambient airflow after the shock waves, could be exploited for the avionic and/or cabin cooling, avoiding or at least reducing the compressor bleed and the associated performance losses.

It is known that the Reverse Bootstrap technology is already efficiently applied for the avionics thermal control of the fighter aircrafts. However, one of the main targets of this thesis is the exploitment of the Reverse Bootstrap technology for the avionics cooling and the preliminary evaluation of its extension to the cabin temperature control in commercial flights.

Chapter 2

Refrigeration techniques

Pneumatic power has several purposes on board an aircraft, depending on its category and size, such as:

1. Cabin pressurization and conditioning;
2. Tanks pressurization and venting;
3. Engine start;
4. Ice protection;
5. Actuators feeding;

The Pneumatic System is powered by high/moderate pressure flow and, depending on its source, the distinction between bleed and bleedless systems arises:

- *Bleed system*
It's the traditional architecture of the Pneumatic System. High pressure high temperature air is taken from engine compressor stages, and driven through ducts.
- *Bleedless system*
There is no engine bleed, while the Pneumatic System's source is ambient air, compressed through a dedicated compressor driven by an electric motor or, in the case of this thesis, ram air compressed by the pressure recovery effects associated with supersonic flight.
This kind of architecture has no negative impact on engine's efficiency, since all the airflow entering the engine is used to produce thrust. Also, the removal of the large ducts used in bleed systems to transport air from the engine to the airframe allows to gain space and reduce weight, as well as reduce maintenance costs.

This thesis deals with the thermal control of avionics installed on board supersonic civil aircraft whose use is expected in the near future, but which are already in the development phase. Two main types of refrigeration systems exist:

- *Air cycle refrigeration systems*
Compressed air, bled from one stage of the engine compressor or coming from a dedicated compressor, expands through a turbine, producing work, while

its temperature and pressure reduce. This cold air is used to refrigerate the utilities (avionics, inhabited compartments). In such systems the refrigerant fluid (air) never changes its phase, remaining always gas. The quantity of heat to be removed strictly depends from the level of the bleed pressure, therefore the associated energetic cost is always high.

The most part of the commercial aircraft are equipped with such systems.

- *Vapour cycle refrigeration systems*

It is a closed loop cycle, in which the heat load is absorbed during the evaporation of a refrigerant fluid, synthetically produced. Then, the fluid passes through a compressor, increasing its pressure and temperature, and finally it cools down in a condenser, where the heat is rejected in a heat sink (usually ambient air). Through an expansion valve, the coolant flows back to the evaporator.

Vapour cycle systems are much more efficient than air cycle systems from a thermodynamic point of view, but they have a limited range of temperature in which they can operate, higher maintenance costs and ecological impact.

This thesis deals with the application of the "Reverse Bootstrap cycle". It follows, in the next section, an overview of the main types of air cycle refrigeration systems.

2.1 Brief history of the air cycle systems



Figure 2.1: Dr. John Gorrie, inventor of the ice machine

The first application of air cycle refrigeration dates back to 1851. It is attributed to Dr. John Gorrie, an American physician, scientist and mayor of Apalachicola, Florida. He believed that cooling the sickrooms, through ice, would have been helpful to cure yellow fever patients, who were plentiful in that swampy area.

Gorrie's idea was to realize an ice maker machine, based on an air cycle system (Figure 2.2):

1. Ambient air was compressed by a wooden piston, moving into a cylinder and powered by a steam engine. Consequently, air pressure and temperature increased.
2. Compressed, hot air was then cooled down at constant pressure, passing through tubes refrigerated by water.
3. Refrigerated air expanded into a second cylinder, further reducing its temperature.
4. Cold air passed through tubes, immersed into a container full of water.

2.2. SIMPLE AIR CYCLE ARCHITECTURE (ALSO CALLED TURBOFAN)

5. Water in the container freezes.

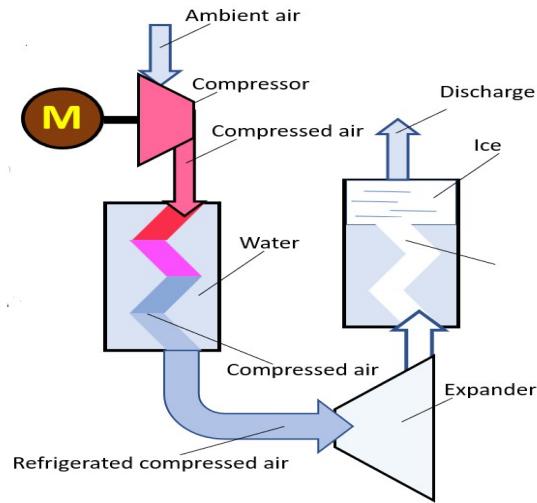


Figure 2.2: John Gorrie's ice machine air cycle

Gorrie obtained the patent in 1851, but never succeeded in selling his machine on the market. His studies were resumed by Einstein who, together with Leo Szilard, between 1928 and 1933 improved Gorrie's technology and registered 45 patents in this field. These so-called 'cold air machines' were used to guarantee food preservation at sea, transporting frozen meat from South America, New Zealand and Australia, and were also installed in land-based cold stores.

Basically, the air cycle machines dominated the marine refrigeration sector at the end of XIX century, until they were replaced by more efficient (and more reliable) vapour compression systems using CO_2 .

2.2 Simple air cycle architecture (also called Turbofan)

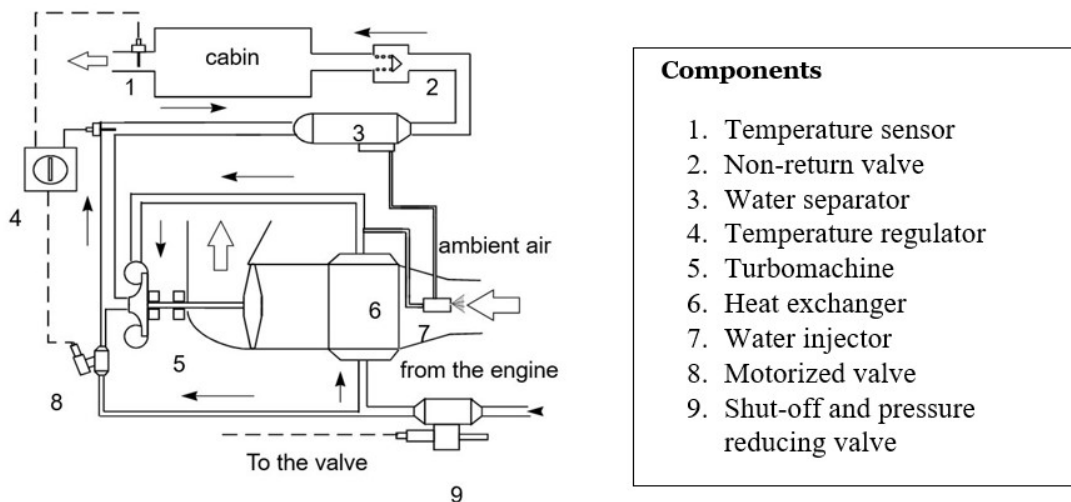


Figure 2.3: Simple air cycle

The most basic airborne air cycle system is shown in Figure 2.3. High temperature high pressure bleed air from the engine compressor passes through a shut-off and pressure reduction valve (9), and then it is cooled down by an heat exchanger (6) placed into a static intake of the aircraft.

The airflow expands through a turbine (5), reaching a lower temperature than the ambient air. The work produced by the expansion is used to move a fan keyed onto the turbine shaft: the fan sucks air from the environment, which is used to vent the heat exchanger.

The cold air from the turbine refrigerates the utilities (avionics, inhabited compartments).

If the combination of temperature, pressure and humidity conditions is above the saturation condition, vapor present in the air condenses during the expansion. Condensation is an exothermic reaction, so the temperature of the air increases during the expansion: the lower the level of humidity in the air, the lower temperature can be reached at the turbine discharge.

At the turbine discharge, the air carries liquid water; for this reason, a water separator (3) is needed. The air/liquid moisture enters the water separator passing through a special fabric which exerts a coalescing action on the air/water flow, agglomerating the micro-drops discharged by the turbine into larger drops.

Some corrugations on the internal surface of the separator give a swirling motion to the water/air flow; the transported water drops are separated from the air and pushed against the internal surface thanks to centrifugal force. The water flows along the surface and collects at the bottom of the separator from where it is expelled.

If temperature levels at turbine discharge are below $0^{\circ}C$, condensed water can freeze, blocking the airflow: hence, a temperature sensor is placed at the water separator inlet, sending a signal to an electronic regulator if temperature reaches $2^{\circ}C$. The regulator activates the motorized valve (8), which opens injecting hot air.

Separated water is recovered: it is sprayed into the exchanger intake and it evaporates again, lowering the cooling air temperature. In this way, the most part of the cooling lost by the condensation during the expansion is recovered; higher system efficiency and lower cabin temperature are reached. However, the lost cooling is not 100% recovered; this depends on several factors: efficiency of the separator, size of the water droplets, geometry of the air intake, orientation of the water injector to favour re-evaporation.

A non-return valve (2) is placed between the water separator discharge and the cabin, in order to prevent fast cabin depressurization in case of accidental breakage of a hose or a component of the system.

When heating (or just partial cooling) is required, hot air bled upstream of the turbine (or the heat exchanger) is injected upstream of the water separator, through the motorized valve.

The limit of this architecture is the dependence from the operating condition of the engine: when it is in *idle* conditions, or in any case at low *rpm*, the efficiency of the cycle is lower as the air entering the system is less compressed. The only solutions are either to increase the engine *rpm* or to take the bleed air from the last stages of the engine compressor. Either way, the energy consumption is often unacceptable.

This architecture has been applied on several aircraft, such as MB-326, G-91, F-104, T-38, A-4, F-89, B-52, Fokker-100.

2.3 Bootstrap architecture

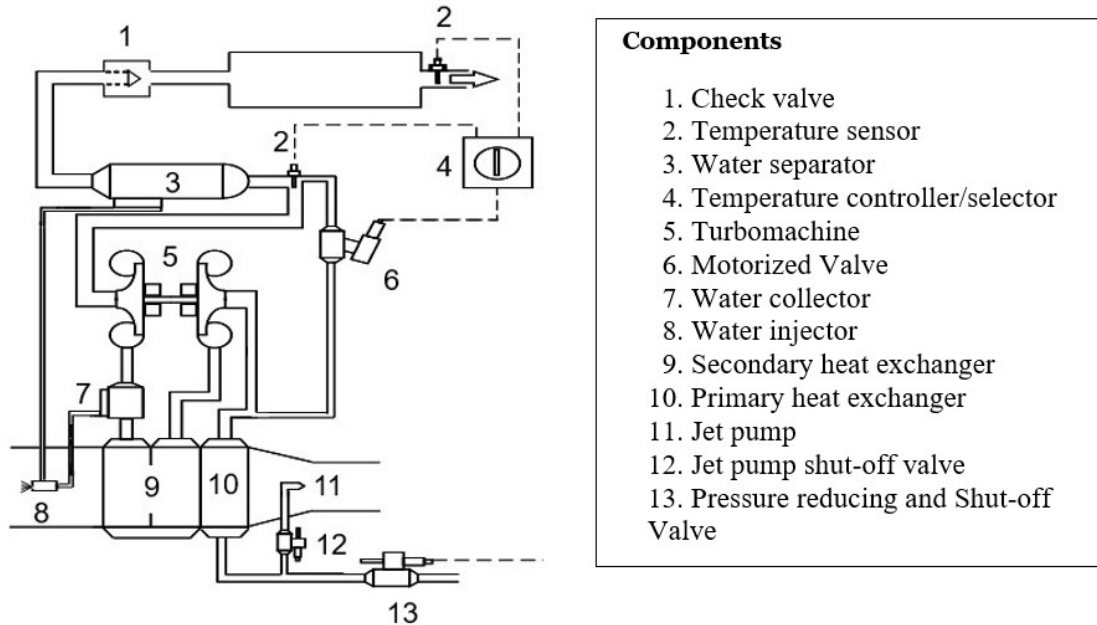


Figure 2.4: Bootstrap air cycle

Figure 2.4 describes the Bootstrap air cycle.

This system is similar to Turbofan with an important difference: the work produced by the turbine is not used to drive a fan for ventilation of the heat exchanger, but it is utilized to drive a compressor keyed onto the same turbine shaft. Purpose of this compressor is to increase the pressure of the air bled from the engine compressor in order to have a higher turbine pressure ratio. This is a very important help to the system performance in any condition, particularly when the engine is in idle.

Some of the aircraft provided with Bootstrap refrigeration system are ATR-72, B-727, F-16, AM-X, MB-339.

However, on the other end, the Bootstrap architecture shows some drawback when compared with the Turbofan. This is the ventilation of the heat exchanger that in Turbofan was achieved by mean of the fan directly driven by the turbine, that in Bootstrap drives the compressor. A couple of solution exists:

1. an electric fan can be installed in order to suck or push the ventilation air;
2. a jet pump system powered by the engine bleed can be installed downstream the heat exchanger.

In both cases the devices operate on ground and at low flight speed.

2.4 Three wheel architecture (also called Simple/Bootstrap)

The *Three wheel architecture* is a combination between the *Simple air cycle* and *Bootstrap* architectures. The turbine drives both the fan and the compressor, all

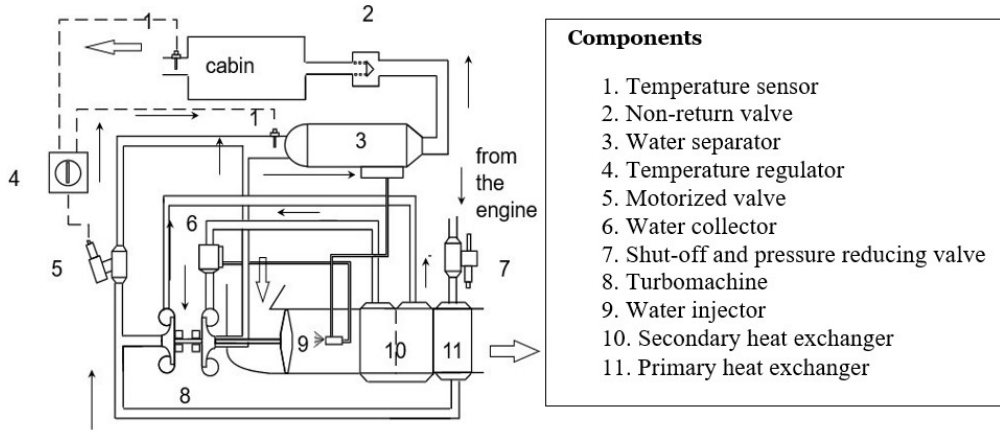


Figure 2.5: Three wheel architecture

keyed on the same shaft. Under the same boundary conditions, *three wheel's* thermodynamic performances are less efficient than *Bootstrap's*, as about 20% of the power generated in the turbine is used to move the fan.

All the considerations made for *Simple air cycle* and *Bootstrap* architectures also apply in this case.

The *three wheel architecture* has two main advantages:

1. removal of the electric motor as the fan is driven by the turbine: that implies reduced weight, size and costs and increased reliability;
2. the static intake generates much less aerodynamic drag compared to a dynamic one.

For an helicopter *three wheel* is often the best solution, while for a jet aircraft the choice between *three wheel* and *Bootstrap* has to be evaluated, as it depends on several factors.

Three wheel architecture has been applied on A-320, A-330, A-340, B-747, B-767, P-180, DC-10, L-1011, EH-101.

2.5 Four wheel architecture (also called Condensing Cycle)

The *four wheel* architecture (Figure 2.6) is characterized by four rotors keyed onto the same shaft: a compressor, a fan and two turbine stages.

Bleed air from the engine passes through the shut-off valve and then it is possibly refrigerated by a primary heat exchanger, otherwise it goes directly into the compressor. After being compressed (and heated at the same time), the airflow is refrigerated at constant pressure into a secondary heat exchanger, fed by ambient air sucked by the fan.

Subsequently, the air is further cooled down into a condenser, fed by cold air discharged from the first turbine stage. In this phase, vapor present in the air condenses: liquid water is collected in the water collector and then sprayed into the ambient air which refrigerates the secondary heat exchanger. So, liquid water re-evaporates, lowering ambient air temperature and improving heat exchange.

2.5. FOUR WHEEL ARCHITECTURE (ALSO CALLED CONDENSING CYCLE)

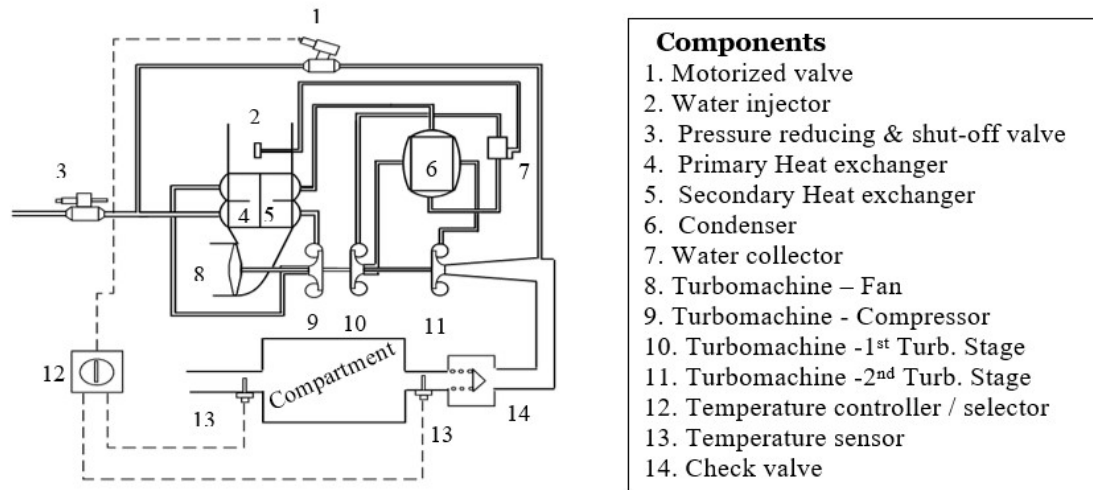


Figure 2.6: Four wheel architecture

After the water collector, the airflow expands into the first turbine stage, before going into the cold side of the condenser. Here, it is heated by the air from the other side, so it needs to further expand into the second turbine stage, reaching lower temperature levels.

Finally, it flows into the compartments which need to be refrigerated.

This solution allows to exploit the condensation heat into the second turbine stage, improving cycle efficiency and therefore reducing exchanger's size and weight.

Temperature control is implemented by a by-pass valve in the first turbine stage, which keeps the temperature at the condenser inlet above 1°C at low altitude.

A by-pass valve in the second turbine stage controls the temperature at the system's discharge.

The *four wheel* architecture implies several advantages:

1. improving cycle's efficiency (by about 10%);
2. higher refrigeration capacity;
3. removal of the low pressure water separator, with consequent no need for maintenance;
4. the problem of freezing conditions into the condenser is solved without excessively increasing its size and weight (as it happens in traditional cycles with one turbine stage);
5. contrary to what happens in the traditional anti-ice solutions, there is no hot air periodically introduced into the condenser, as it would reduce system's performances.

This system has been installed on B-767-400, B-777, A-380, ERJ-170/190.

Chapter 3

Reverse Bootstrap system

The cooling of the avionics on board of the fighters is usually done by means of pods, special air cycle or vapor cycle systems installed under the wing or the fuselage of the aircraft.

In order to cool the inhabited compartments and the avionics, either aircraft supplied air or closed cycle (vapor compression) refrigerators are used ¹. Both systems have advantages and drawbacks, as well as the systems already briefly mentioned in the previous paragraphs. Indeed, air systems are lighter, more reliable but energetically less efficient than vapor cycle which are heavier and require also heavier maintenance. The Reverse Bootstrap system is used for avionics cooling on board of fighters ([10], [13]). It has an important advantage on the classic bootstrap: it does not need any engine bleed. This systems usually have a dual mode of operation:

1. Direct ram air cooling which corresponds to the flight conditions with pressure difference between turbine inlet and ambient pressure lower than 14 kPa ;
2. Reverse Bootstrap operation which corresponds to the flight conditions with pressure difference between turbine inlet and ambient pressure not lower than 14 kPa .

Such air cycle cooling requires no electrical power during flight since all of the power is supplied by captured ram air. A small amount of electrical power is required for ground cooling.

This dual-mode cooling system has been investigated and found to have numerous advantages on other cooling systems.

The functional schematic of a reverse bootstrap system for avionics cooling, applicable to the dual mode operations, is shown in Figure 3.1.

In both modes (*Direct ram air* or *Reverse Bootstrap*) the ram air enters the intake and passes through a water separator (1) which is designed to remove approximately 80 percent of the liquid water when the aircraft is flying through the rain. Although the cooling system is tolerant of water, it is desirable to remove most of it in the inlet region. The flow path then depends on which mode of operation is being used.

¹On pressurized aircraft, the air cycle systems fed by engine bleed air are used because they can easily allow the pressurization of the inhabited compartments.

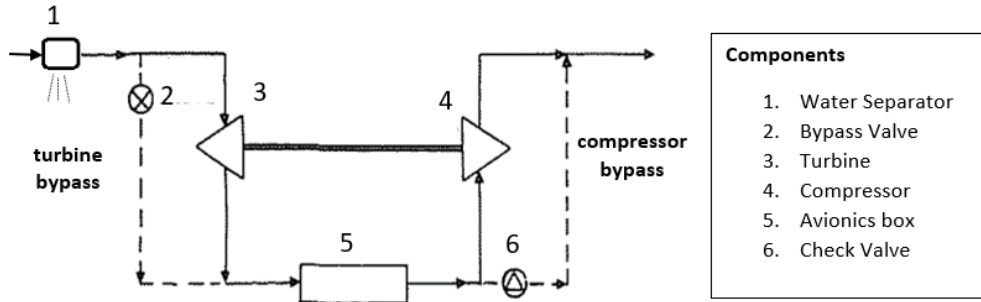


Figure 3.1: Reverse Bootstrap system for avionics cooling

3.1 Direct ram air cooling mode

In the ram air cooling mode, the turbine bypass valve (2) is open and the ram air is ducted directly to the avionics box (5). The by-pass valve is controlled by the pressure switch (7) that opens the valve when the pressure drop between the turbine inlet and the ambient is lower than 14 kPa (about 2 psi) and closes it at higher Pressure Drops. In the first case the system works in direct mode by-passing the air cycle subsystem, while in the second case the system operates through the reverse bootstrap cycle.

The pressure drop (turbine inlet-ambient pressure) controlled by the dedicated switch depends from the flight Mach number and the altitude. 14 kPa are reached at sea level approximately at $\text{Mach} = 0.5$. and $\text{Mach} = 1.1$ at 15000 m . The switchover from ram air cooling to air cycle cooling, and vice versa, occurs at nearly the optimum speed to maximize cooling capacity.

The flow path of the system in the Direct Operation mode is more clearly depicted in Figure 3.2.

In the Direct Operation mode the air enters directly the avionics equipment flowing on the finned walls of the avionics box, removing the heat load by combined effects of thermal conduction and forced convection². At the exhaust of the avionics the air is discharged into the container of the system which is equipped with one or more check valves (6) allowing the discharge to the external ambient; this is possible due to the over pressure between the internal volume of the system container and the external ambient when the system is operating in *direct ram air* mode. Any water accumulated in the container is also discharged together with the air through the check valves which are kept in open position.

²A detailed description of the architecture of the avionics equipment box is given at paragraph 4.3

3.2. AIR CYCLE COOLING MODE

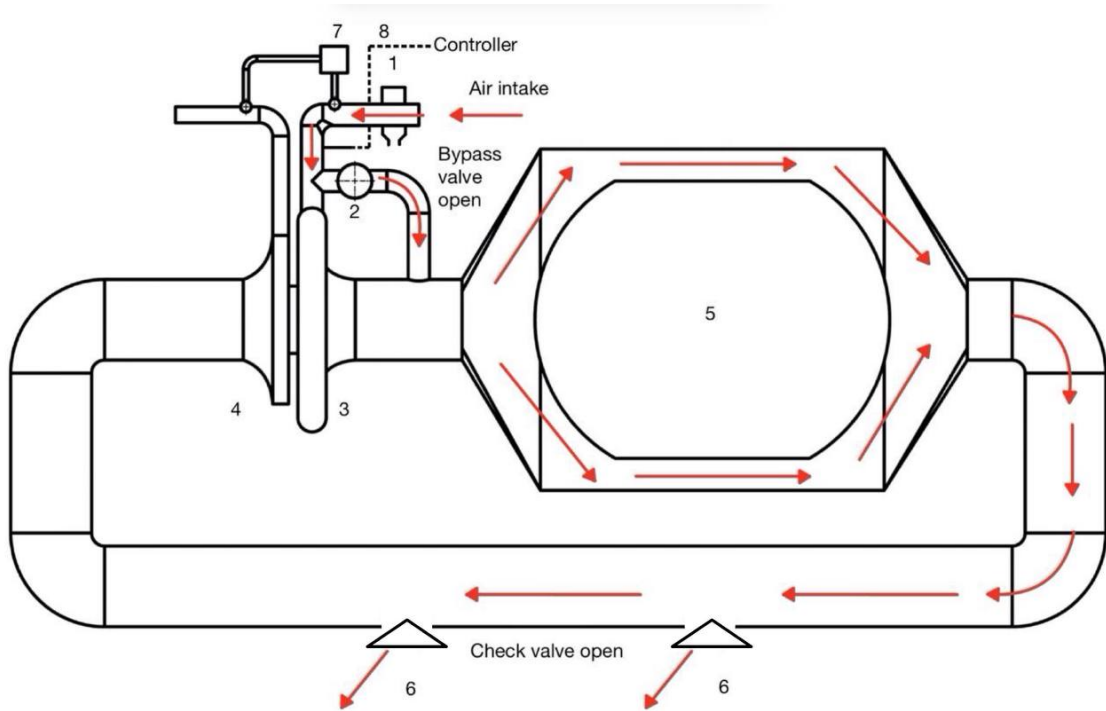


Figure 3.2: Direct Operation mode flow path

Components	
1	Water Separator
2	By-Pass Valve
3	Turbine
4	Compressor
5	Avionics Box
6	Check Valve
7	Pressure Switch
8	Temperature Sensor

Table 3.1: Table of components

3.2 Air cycle cooling mode

In the air cycle cooling mode, the turbine bypass valve (2) is closed and the ram air is directed to the turbine inlet.

The flow path of the system in Air Cycle Operation mode is shown in Figure 3.3. If the flight velocity is higher than the sonic one (as in the most part of the flight envelope) a sonic shock will happen with a consistent increase of the pressure on the static ambient. Using this compressed air to drive a turbine, a certain amount of work will be produced together with the reduction of the air temperature. The cooling effects will be increased by reducing the turbine exhaust pressure by means of a compressor driven by the turbine. Such compressor depresses the turbine exhaust section, increasing the turbine pressure ratio. In this way, the cooling effect will be produced avoiding any engine bleed with a non-negligible energy cost saving. On the other hand, it must be noted that this technology gives advantages if the compartment to be cooled can be at lower pressure than the ambient static one, like

in the case considered in this thesis; in other cases (e.g.: inhabited compartments) the Reverse Bootstrap solution could be still used, but an intermediate loop consisting of a heat exchanger, a hydraulic pump, a tank, a fan, a controller shall be necessary³.

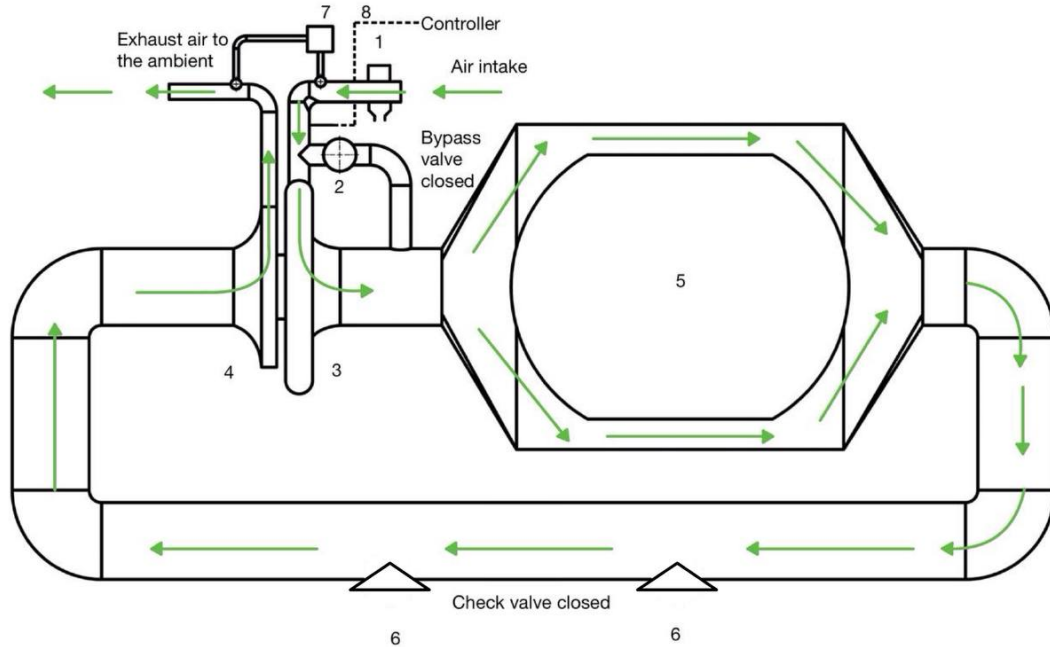


Figure 3.3: Air Cycle Operation mode flow path

Components	
1	Water Separator
2	By-Pass Valve
3	Turbine
4	Compressor
5	Avionics Box
6	Check Valve
7	Pressure Switch
8	Temperature Sensor

Table 3.2: Table of components

The cold air discharged by the turbine is directed to the avionics equipment where it flows through the external finned faces of the avionics box, removing the heat load without any physical contact with the electronic components inside.

The by-pass valve (component 2 in Figures 3.2 and 3.3) has a double purpose:

1. to select the operation mode of the system (open/closed; direct/air cycle operation mode);
2. to modulate the turbine exhaust temperature by mean of a turbine by/pass in order to avoid icing at the turbine exhaust in cold days. The sensor (n.8 in

³See para 3.5 for more complete description.

3.3. GROUND COOLING

system schematic of Figures 3.2 and 3.3) measures the dry bulb temperature at the turbine exhaust and sends a signal to the electronic controller (included in the avionics box) which drives the by-pass valve in order to keep the turbine exhaust temperature at values $>2^{\circ}\text{C}$.

The airflow then enters the compressor, installed on the same shaft of the turbine and mechanically driven by it, which helps the system efficiency in two ways:

1. depressing the turbine discharge to pressure levels lower than the ambient static pressure;
2. sucking and driving the air coming from the avionics box to the external ambient.

Negative differential pressure during air cycle cooling keeps check valves closed since the internal container pressure is less than ambient.

A typical temperature-entropy diagram of such a system, is shown in Figure 3.4.

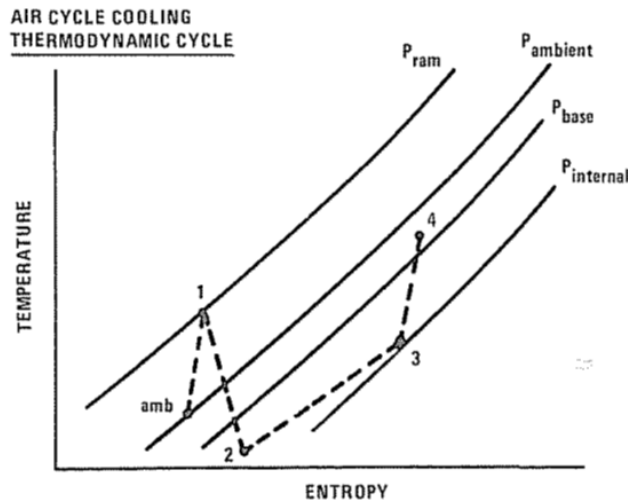


Figure 3.4: Typical temperature-entropy diagram of a Reverse Bootstrap system running in the Air Cycle mode

The air cycle cooling mode is generally referred to as a "*Reverse Bootstrap Cycle*". This terminology stems from the fact that the captured ram air does not initially flow through the compressor, but rather is expanded through the turbine.

3.3 Ground cooling

For extended periods of equipment operation on the ground, a supplementary cooling technique is required. The problem comes from the absence of ram air which is mandatory for any reverse bootstrap system operation. The candidate approaches are:

- a. a single large fan placed in an external trolley connected upstream of the reverse bootstrap using an adapter;

- b. a fan integral with the reverse bootstrap system acting to pull the outside air through the ram air inlet into the system container.

In both approaches, the turbine bypass valve is open and the system is effectively in the ram air cooling mode.

The determination of the preferred ground cooling approach depends on many factors:

1. required flow rates;
2. system pressure drops;
3. packaging constraints;
4. ambient conditions;
5. potential interference with the air cycle and ram air cooling modes during flight operation;
6. weight, reliability, logistics issues.

This trade-off study could be the target of a separate effort and is not covered in this thesis.

Considering that the aircraft having the reverse bootstrap system on board should operate from medium/large airports with appropriate facility level, it seems at a first approach with a separate fan on a trolley is the best one, at least for the moment.

3.4 Alternative configuration of the avionics cooling: distributed cold plates

Sometimes stringent installation requirements could not allow the solution discussed in the previous paragraphs. A different approach could be considered, consisting in avionics component groups attached to dedicated cold plates cooled by a liquid, recirculated by a pump, rejecting the avionics heat into an exchanger cooled by the air coming from the turbo-machine on the other side. A functional system schematic is shown in Figure 3.5.

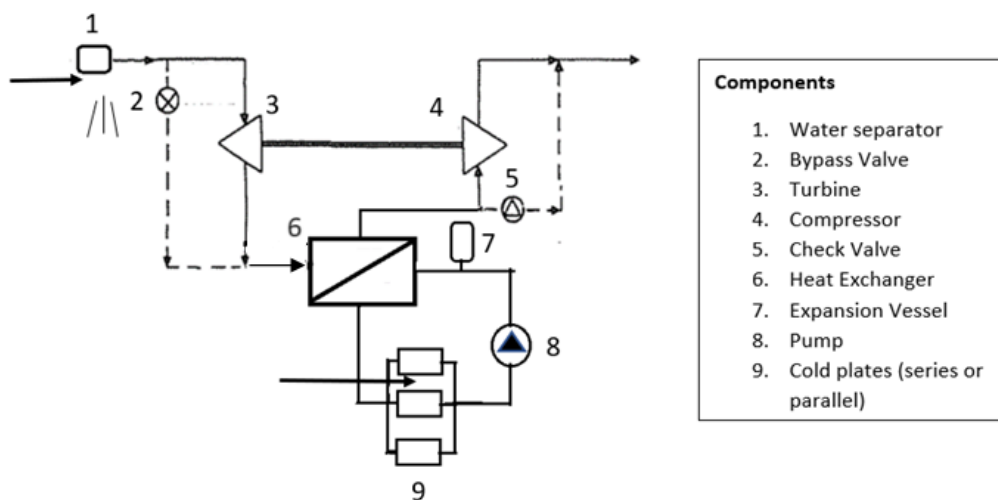


Figure 3.5: Reverse Bootstrap configuration with cold plates

3.5 Comparison of Direct vs. Reverse Bootstrap design

1. Direct and Reverse Bootstrap are both based on the same principle: compressed air, flowing in a turbine, reduces its pressure and, at the same time, its temperature. The cold air produced can be introduced into the compartment to be cooled, removing a quantity of heat and reducing the compartment temperature.
2. The Direct Bootstrap bleeds the air from a stage of the engine compressor, subtracting an amount of air which was compressed to contribute to the engine thrust production; the total engine thrust and engine efficiency are therefore reduced to allow the cooling effect.

On the other hand, in the Reverse Bootstrap, the compressed air is taken directly from the ambient, downstream the shock wave which generates in flights at supersonic speed, avoiding any deterioration of the engine performance.

3. In both systems, like in all other air cycle systems, the cooling produced is proportional to the expansion ratio achieved in the turbine. In the direct bootstrap cycle, an increase of the expansion ratio can be achieved by bleeding the air from a higher stage of the compressor with increasing energy costs. In the reverse bootstrap, at a datum flight speed, there is a datum air pressure after the shock wave, therefore the only possibility for an expansion ratio increase is the reduction of the turbine exhaust pressure that could lead to a depressed cycle because the exhaust from the turbine is at lower pressure than the static ambient pressure.
4. In a Direct Bootstrap air cycle, one or two heat exchangers are present in the system:
 - the first heat exchanger could be installed upstream of the compressor in case of incompatibility between the bleed temperature and the material of the tubing and of the system components;
 - a second heat exchanger is located immediately after the compressor in order to remove the compression heat before to enter into the turbine. In any case, the temperature of the air entering the turbine is always higher than the ambient air which cools the heat exchanger, due to its efficiency which never reaches 100%.

On the other hand, in the Reverse Bootstrap system, the air enters the turbine at a temperature always lower than in the direct configuration. Because of the absence of the heat exchangers, the Reverse Bootstrap system is in principle lighter and more efficient than the Direct one.

5. The advantages of the Reverse Bootstrap on the Direct one, as already discussed, are achievable if the compartment to be cooled can tolerate the low pressure (e.g.: avionics compartments). If we want to exploit the advantages of the Reverse Bootstrap configuration also for the thermal control of a pressurized compartment (e.g.: inhabited cabins), the system schematic shall include the modifications shown in Figure 3.6.

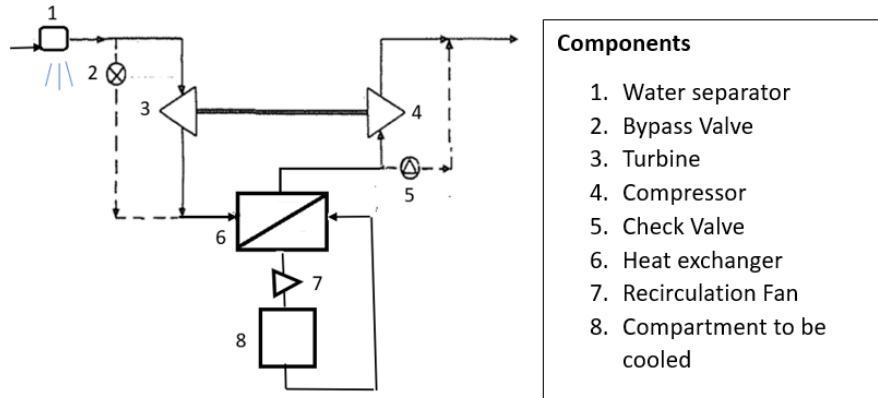


Figure 3.6: Reverse Bootstrap configuration for cooling of inhabited compartments

At the turbine exhaust the air enters an heat exchanger where the heat of the compartment to be cooled is removed and rejected outside through the air sucked by the compressor. An extra fan is needed to circulate the air in the compartment to be cooled.

A careful trade-off shall be performed in order to evaluate the convenience of such solution vs. a classic direct bootstrap.

The analysis will concern, as a minimum:

- pressurization of the inhabited compartments;
- heating of the inhabited compartments;
- ventilation of the inhabited compartments;
- structural aspect of the heat exchanger;
- total system weight;
- reliability.

Chapter 4

Steady-state computational model

In this chapter, all the equations used to model the airflow evolution through the cycle, such as conservation equations or power balances, and to carry out the design of the turbomachinery will be described.

The airflow starts his path before the intake, after the supersonic shock wave. The ambient air, compressed by the shock wave, enters the intake and reaches the radial turbine where it expands to pressure levels lower than the ambient; at the same time, due to expansion, the air is cooled. No air is bled from the engine compressor; just ambient air compressed by the shock wave is used.

Cold exhausted air from the turbine passes through the avionics box, carrying out the task of cooling the electronics contained in it.

After having accomplished its duty, the airflow is compressed by a centrifugal compressor, driven by the radial turbine, and then expelled into the environment.

The simulation has been realized using SIMULINK: it is a modeling, simulation and analysis software, which allows to create block diagrams and solve dynamic systems. On SIMULINK it is possible to implement *Matlab Function blocks*: each one of these blocks contains all the equations utilized in that particular segment of the model, implemented into MATLAB functions.

Station nomenclature

- 0 : environmental conditions;
- i : after shock;
- 1 : turbine inlet;
- 2 : turbine outlet;
- 3 : avionics box inlet;
- 4 : avionics box outlet;
- 5 : compressor inlet;
- 6 : compressor outlet;
- e : exhaust.

Symbols nomenclature

T	static temperature
p	static pressure
ρ	static density
T^0	total temperature
p^0	total pressure
ρ^0	total density
R	universal gas constant
c_p	specific heat at constant pressure
γ	specific heat ratio
g	gravitational acceleration
λ	temperature gradient with altitude
M	Mach number
z	altitude
\dot{m}	mass flow rate
Q	volume flow rate
F	corrected mass flow rate
α	absolute speed angle
β	relative speed angle
η	efficiency
β_T/β_C	turbine/compressor pressure ratio
P_T/P_C	turbine/compressor power
L_t/L_c	turbine/compressor work
Φ, Ψ	velocity ratios
U	peripheral speed
C	absolute speed
W	relative speed
a	sound speed
ω	angular speed
N	number of revolutions
n_s	specific number of revolutions
R_n	radius at station "n"
D_n	diameter at station "n"
A	area
b_n	channel height at station "n"
k_B	restriction factor
Z	number of blades
f	friction factor

sp	blade spacing
l_{th}	throat length
C_p	pressure recovery coefficient
$\frac{s}{c}$	pitch to chord ratio
Pr	Prandtl number
Re	Reynolds number
μ	absolute viscosity
Q_t	thermal load
h_{fcc}	forced convection coefficient
L	length
C_D	drag coefficient
q	dynamic pressure

Subscripts nomenclature

t	tip
h	hub
T	turbine
v	volute
C	compressor
r	radial component
u	tangential component
ts	total to static
i	inner
o	outer
ext	external
is	isentropic
tot	total
max	maximum
min	minimum
$stat$	stator
LE	leading edge
TE	trailing edge
th	throat
D	diffuser
fr	frontal
ff	free flow
av	avionics
h	hydraulic

4.1 Environmental conditions and intake

The intake component plays a key role in ensuring adequate airflow to cool the aircraft electronic systems, while ensuring optimal performance under various environmental and flight conditions. Environmental conditions, in particular altitude and flight Mach number, are necessary for the design of the intake, as they significantly influence the air density and, consequently, the available air flow rate.

In addition, the flight Mach number, affects the efficiency of the air compression process and consequently, its design must take into account these critical variables to ensure effective cooling of the on-board avionics in a wide range of operational scenarios.

4.1.1 Ambient environmental conditions

The input values from the ambient condition are:

- flight Mach number M_0 ;
- altitude z .

From the altitude, ambient pressure and temperature are derived by means of the ISA equations.

The following relations apply:

$$\begin{aligned} T_z &= T_0 + \lambda z \\ dz &= \frac{dT}{\lambda} \\ dp &= -\frac{Pg}{\lambda RT} dT \end{aligned}$$

where

- R : universal gas constant;
- λ : temperature gradient;
- T_0 : temperature at zero altitude (ISA+20);
- p_0 : pressure at zero altitude;
- T_z : temperature at altitude z .

By integrating, the final formula is obtained:

$$p_z = p_0 \left(\frac{T_z}{T_0} \right)^{-\frac{g}{R\lambda}}$$

and consequently the expression of density

$$\rho_z = \frac{p_z}{RT_z}$$

This equations are valid within the troposphere. However, a supersonic aircraft will fly also at stratospheric altitudes, where temperature, pressure and density rates are different.

Specifically, temperature remains constant through the stratosphere ($\lambda = 0$). Using the previous equations it is possible to evaluate the conditions at the tropopause altitude ($\bar{T}, \bar{p}, \bar{\rho}$). Now, knowing that $T_z = \bar{T}$ it is possible to express the differential equation for stratosphere:

$$dp = -\frac{p g}{R \bar{T}} dz$$

By integrating it, this result is obtained:

$$p_z = \bar{p} e^{\frac{-g}{R \bar{T}}(z-\bar{z})}$$

$$\rho_z = \bar{\rho} e^{\frac{-g}{R \bar{T}}(z-\bar{z})}$$

4.1.1.1 Humidity

Also the humidity of the air plays an important role on the thermo-physics of the atmosphere.

In this thesis, according to [5] of Massachusetts Institute of Technology, it has been assumed the following:

- absolute humidity of 0 g/kg at altitude $z = 16000 \text{ m}$ (design point);
- variation of the humidity vs. altitude, as shown in Figure 4.1.

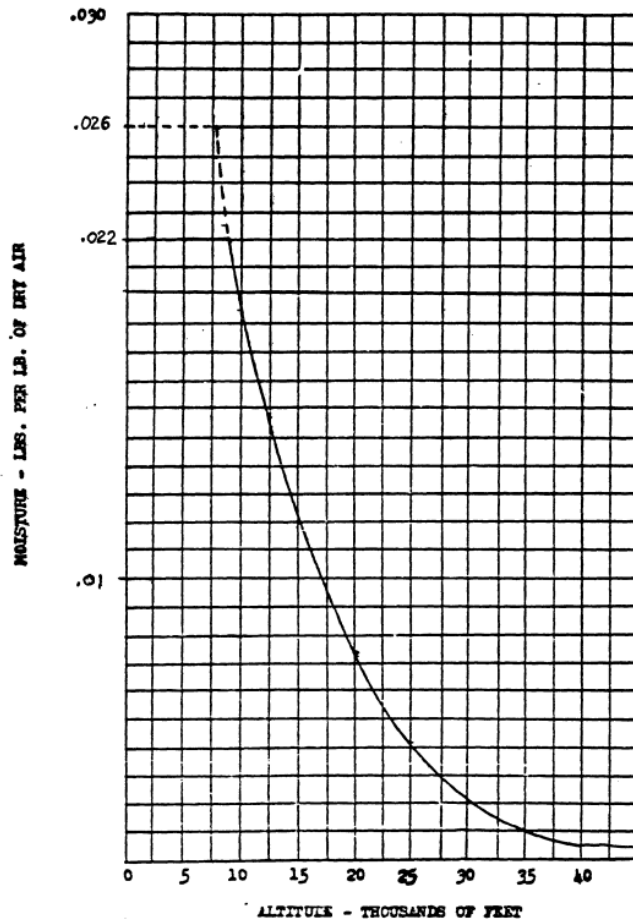


Figure 4.1: Humidity vs. Altitude [5]

The impact of humidity on performances of a Reverse Bootstrap like the system considered in this thesis is usually lighter than in an Environmental Control System based on a classic Air Cycle systems (e.g. equipment for inhabited compartment air conditioning).

Impact of humidity on Bootstrap cycle for ECS

Such negative impact is due to the fact that the water vapor carried by the air, during the expansion in the turbine, condensates while the air temperature decreases with the latent heat injection from the vapor to the air. In this condition, while the air temperature decreases, its final value is surely higher than the temperature that could be reached by the dry air: the fluid exhausted from the turbine therefore consists of a mixture of humid air and liquid water.

Due to the effect of vapor condensation on the temperature of the air expanding in the turbine, at the turbine exhaust we have two distinct temperatures: Wet Air Rated Temperature (T_{WAR}) which is the effective temperature measured by a dry bulb thermometer, and Dry Air Rated Temperature (T_{DAR}) which is the temperature achieved by the air if the carried water can totally re-evaporate.

However, even if the losses of cooling are not negligible, a partial recovery is possible on the classical ECS in the following way.

The mixture air/moisture is introduced in a water separator before to enter the compartment to be thermally controlled. At the water separator discharge, the air is introduced into the compartment, while the liquid water is sprayed into the ambient airflow which cools the heat exchanger of the Environmental Control System. Here the water re-evaporates, decreasing in a sensible way the temperature of the ambient air to the heat exchanger and the turbine inlet temperature with a beneficial effect on the overall system.

It is impossible to completely recover the turbine cooling losses for the following reasons:

- the efficiency of the water separators is less than 1; usually it is about 85/90%;
- a certain quantity of water is lost in the distribution circuit and, even if re-evaporates, is not well in contact with the air and does not affect its temperature;
- the water removed from the separator is injected into the cold airflow to the heat exchanger and its cooling effect directly impacts this flow, not the cabin flow which receives just an indirect effect;
- the direction of the water could not be the right one to favour a sufficient evaporation with a good cooling effect. In this regard, it should be noted that the installation of the water injector in the air intake is decided after a careful experimental campaign; the results strictly depend on the aerodynamic field that is established in the air intake and this varies with flight conditions. It is therefore very likely that in practice the water is not injected in such a position as to favour optimal re-evaporation.

Impact of humidity on the Reverse Bootstrap Cycle of the present study

Coming back to the system of our present interest, the situation of the loss and recovery of the cooling effect connected to the humidity is not critical at all. Also in this case, the humid air while expanding in the turbine generates water and the turbine exhaust temperature of the humid air is higher than the temperature associated to the dry air for the said reasons. However, the difference with the inhabited compartment ECS consists in:

- the air/water mixture is immediately introduced into the avionics box: no water separator is installed;
- air/water flows through the gap around the box which is full of fins brazed to the external faces of the box;
- in the gap the liquid water re-evaporates (partially or entirely) removing from the air the latent evaporation heat.

This is an important advantage deriving from the special configuration of the Avionics Box¹, in addition to the total guarantee of absence of FOD² and accidental contact between water and avionics components.

4.1.2 Shock wave calculations

In this study the assumption that inside the intake the flow is compressed by a single, normal shock wave is made. So, as the conditions before the shock wave (environmental conditions) are known, it is possible to calculate the after the normal shock wave, using the corresponding equations. This equations ([3]) are meant for a normal, steady shock wave, with the hypothesis of ideal gas, and they are derived from the balance equations for mass, momentum and energy.

$$\begin{aligned}
 T_i^0 &= T_0^0 \\
 \frac{T_i}{T_0} &= \frac{(2\gamma M_0^2 - \gamma + 1)(\gamma - 1 + \frac{2}{M_0^2})}{(\gamma - 1)^2} \\
 \frac{p_i}{p_0} &= \frac{2\gamma M_0^2 - \gamma + 1}{\gamma + 1} \\
 \frac{p_i^0}{p_0^0} &= [(\gamma + 1)^{-(\gamma+1)} (\gamma - 1 + \frac{2}{M_0^2})^\gamma (2\gamma M_0^2 - \gamma + 1)]^{\frac{1}{1-\gamma}} \\
 M_i^2 &= \frac{(\gamma - 1) M_0^2 + 2}{2\gamma M_0^2 - (\gamma - 1)}
 \end{aligned}$$

Through the normal shock wave the flow becomes subsonic ($M_i < 1$), there is an increase of static pressure and static temperature, while total pressure decreases and total temperature remains constant, as the normal shock wave is homoenergetic. This trends are showed in Figure 4.2.

¹See paragraph 4.3.3 for design details.

²FOD = Foreign Object Damage.

4.1. ENVIRONMENTAL CONDITIONS AND INTAKE

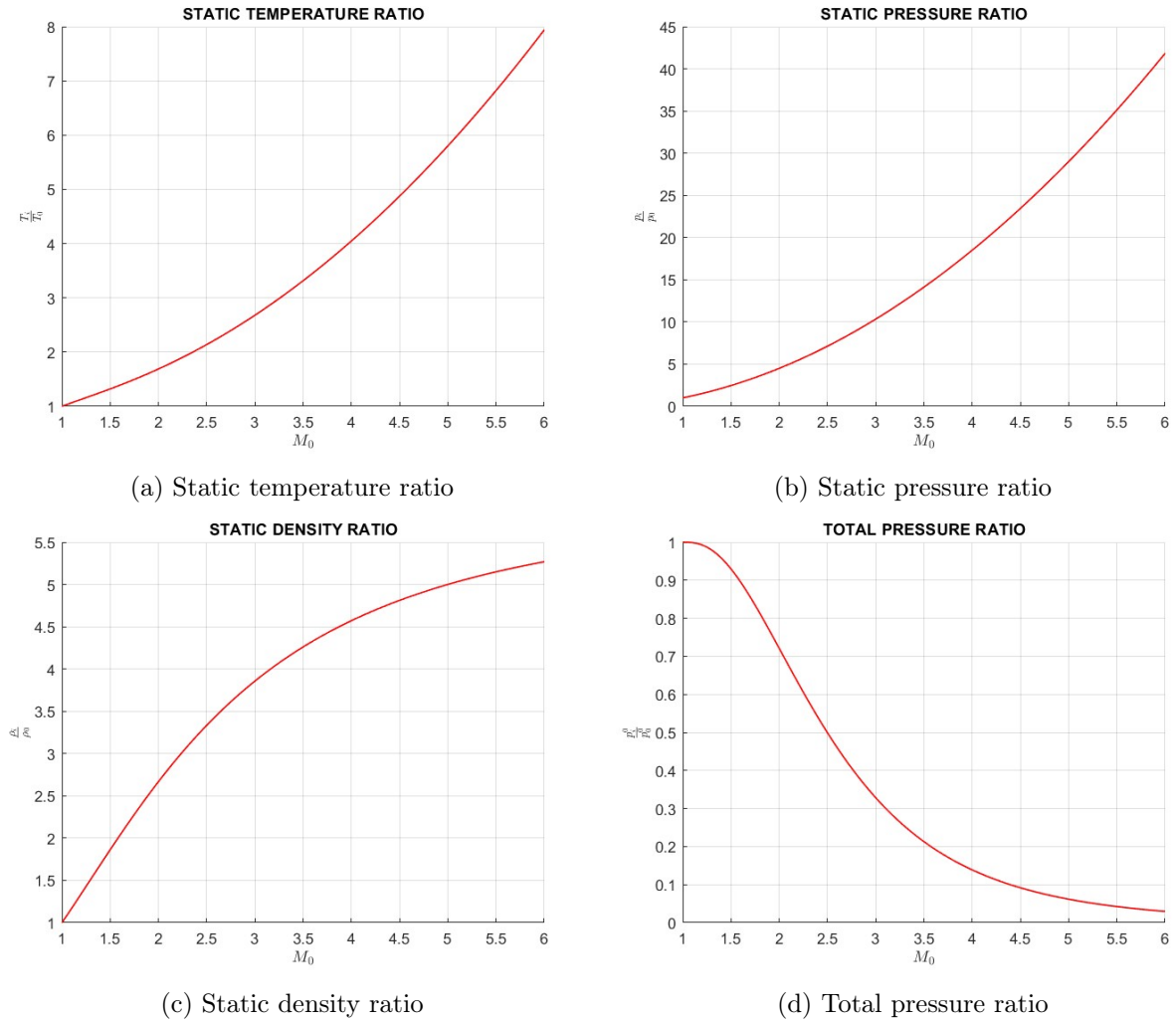


Figure 4.2: Temperature, pressure and density variations through a normal shock wave

There are other types of shock waves, beside the normal ones: if they are not perpendicular to the speed vector upstream of them, they are called *oblique shock waves*.

Oblique shock waves are called *weak* if the downstream flow is supersonic and *strong* if it is subsonic; usually, the strong solution does not occur, except when the flow needs to match downstream high pressure conditions.

Oblique shock waves are preferable in a supersonic engine intake, since they result in smaller entropy increase and reduced stagnation pressure losses if compared to the normal shock waves. For these reasons, many supersonic aircraft's engines are provided with intake ramps: these plate-like devices allow to deflect the airflow from the longitudinal direction, creating a certain number of oblique shock waves in order to reduce the Mach number and increase the pressure.

However, since the study of the flow in a supersonic engine intake goes beyond the objectives of this thesis, it has been decided to assume that the airflow is compressed by a single, normal shock wave. This assumption is certainly a simplification of what really happens in the engine intake, but it is also a conservative assumption, since the total pressure losses are higher through a normal shock wave than they would be through a series of oblique shock waves.

4.2 Turbine



Figure 4.3: Radial turbine

4.2.1 Radial turbine: introduction

A radial gas turbine is a turbomachine in which the flow enters in perpendicular direction to the shaft. It consists in a fixed part, the *volute*, in which the flow rotates and receives a tangential component of velocity, and a rotating part, the *rotor*, which is set in motion by the flow, which expands producing work. Eventually, between the volute and the rotor, a stator with fixed blades, called *nozzle ring*, can be placed. Also, sometimes there is a diffuser, located after the rotor, whose utility is to recover part of the high kinetic energy of the exhausted airflow.

While an axial turbine is "impacted" by the working fluid, the latter is smoothly orientated perpendicular to the axis of rotation: that results in reduced mechanical and thermal stress. Consequentially, a radial turbine is more efficient, and allows to reach higher pressure ratios per stage than an axial turbine.

On the other hand, because of the heavy and expensive rotor, a radial turbine loses its advantages at high power ranges and high flow rates. Furthermore, it can't be used for high temperature applications, as the cooling of radial rotor stages is more difficult than it is for axial stages.

The turbine stations, shown in Figure 4.4, are described afterwards.

Volute

As previously described, the flow enters the turbine radial to the axis: so, it is necessary to give it a swirl component of velocity before entering the rotor. The volute (Figure 4.5) is a spiral shape component, in which the airflow expands and gains a tangential component of velocity: for this reason, the volute cross section decreases as the azimuthal angle increases along the turbine axis.

4.2. TURBINE

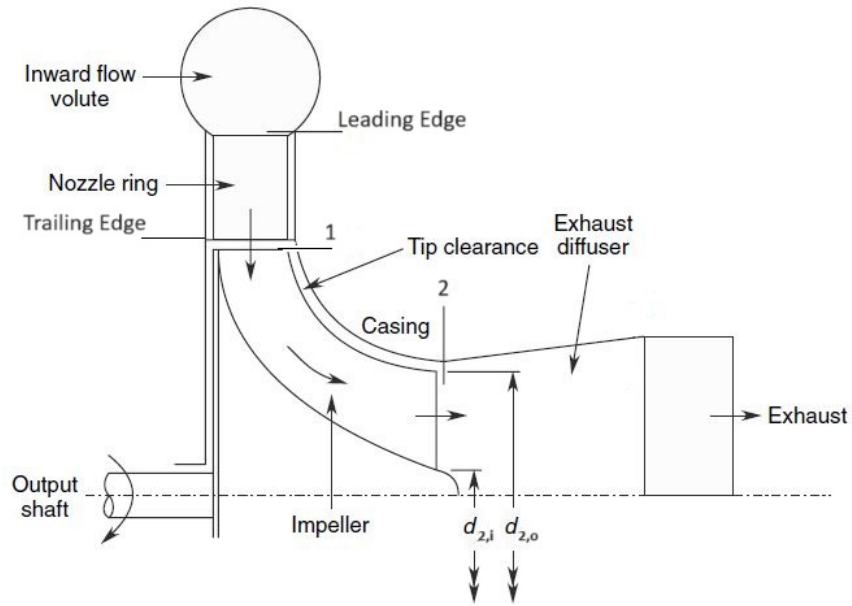


Figure 4.4: Radial turbine components

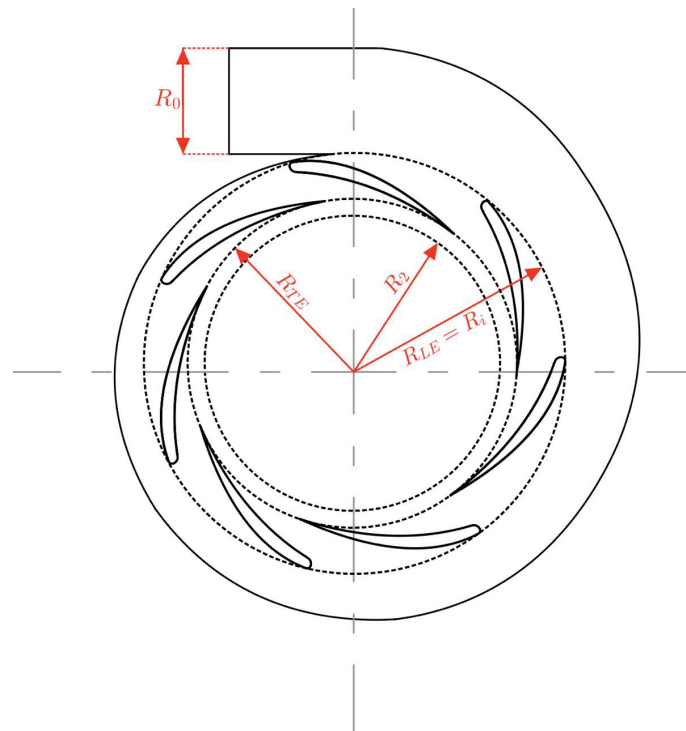


Figure 4.5: Volute

Nozzle ring

The nozzle ring is fixed blading component placed between the volute and the rotor. It accelerates the airflow and gives it a tangential component of velocity.

Its main purpose is to limit flow distortion after the volute, making it more uniform and establishing a desired flow angle.

Often the nozzle ring is not utilized, in order to reduce cost and size of the turbine, as well as simplifying the design. In this case, there is a decreased efficiency of the

turbine, due to the non-uniformity of the flow; however, it is also observed that an architecture without a stator has an higher efficiency (compared to the nozzle ring architecture) in off-design conditions.

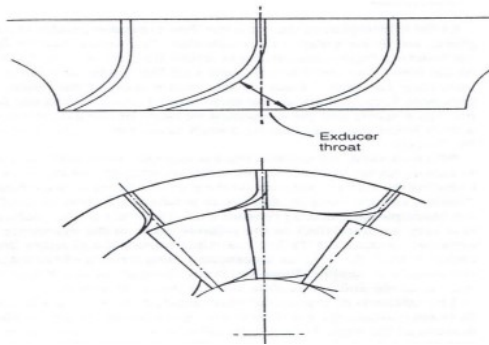


Figure 4.6: Nozzle ring and rotor

Rotor

The airflow enters the rotor at its outer radius, with the relative component of velocity that is tangent to the blade (at least at design point), and moves towards the rotor's inner radius.

In this phase, the airflow produces work, while reducing its tangential component of velocity: that generates a pressure gradient along the channel.

At the rotor outlet, the radial component of velocity is almost irrelevant, as the axial and tangential components are much higher.

The rotor is the turbine's component in which there are the most significant energy losses, due to friction between air and blades and flow separation in the space between blades and casing. For this reason, the rotor has a major influence on turbine's efficiency.

Furthermore, the rotor also influences the mass flow rate which passes through the turbine: indeed the channel's geometry determines such flow rate, and the outlet section is particularly critical.

Diffuser

The flow coming out of the impeller has an elevated kinetic energy, especially in large size turbines: this energy can be recovered using a diffuser, placed after the rotor outlet.

Through the diffuser, the airflow is compressed while reducing its speed: that allows to increase the pressure rate in the rotor, with a consequent raise of the power transferred to the shaft.

However, a diffuser is often not used, as it increases turbine's size, creating problems in terms of size, installation and weight.

4.2.2 Thermodynamic calculations

The calculation process described in this section follows [32]. The following data are given as inputs:

- p_1^0 : total inlet pressure;

4.2. TURBINE

- T_1^0 : total inlet temperature;
- p_2 : static outlet pressure;
- α_1 : inlet absolute velocity angle;
- $\beta_{2,o}$: outlet relative velocity angle at outer radius;
- $\eta_{T,ts}$: total-to-static isentropic efficiency;
- Φ, Ψ : velocity ratios, related to losses, which depend on Reynolds and Mach numbers.

The inlet conditions are known from the previous calculations, while p_2 is a design data: it has to be chosen considering the need to create a depressed environment at the turbine discharge, in order to cool down the airflow as required. The angles, velocity ratios and efficiency values are determined by experience.

As the inlet and outlet pressures are known, the turbine total-to-static pressure ratio can be found:

$$\beta_{T,ts} = \frac{p_1^0}{p_2} \quad (4.1)$$

From the isentropic relations it is possible to calculate the isentropic total-to-static temperature drop (ΔT_{is}) and then, through the definition of $\eta_{T,ts}$, the total-to-static temperature drop (ΔT_{tot}) is found. The latter allows to obtain the discharge total temperature and, as $\beta_{T,ts}$ is known, also the static one.

$$\Delta T_{is} = T_1^0 \left[1 - \left(\frac{p_2}{p_1^0} \right)^{\frac{\gamma-1}{\gamma}} \right] \quad (4.2)$$

$$\eta_{T,ts} = \frac{\Delta T_{tot}}{\Delta T_{is}} \quad (4.3)$$

$$T_2^0 = T_1^0 - \Delta T_{tot} \quad (4.4)$$

$$T_2 = T_1^0 \left(\frac{p_2}{p_1^0} \right)^{\frac{\gamma-1}{\gamma}} \quad (4.5)$$

As in the following lines flow velocities are calculated, it is now defined the velocity nomenclature:

- U : peripheral velocity;
- W : relative velocity;
- C : absolute velocity;
- a : sound speed.

From the definition of $\eta_{T,ts}$, the $\frac{U_1}{a_0}$ ratio can be obtained (where a_0 is the speed of sound at the total inlet temperature), and then, as a_0 is known, U_1 can be calculated:

$$\eta_{T,ts} = \frac{\Delta T_{tot}}{\Delta T_{is}} = \frac{(\gamma - 1) \left(\frac{U_1}{a_0} \right)^2}{1 - \left(\frac{p_2}{p_1^0} \right)^{\frac{\gamma-1}{\gamma}}} \quad (4.6)$$

$$U_1 = \frac{U_1}{a_0} \sqrt{\gamma R T_1^0} \quad (4.7)$$

Through the velocity triangle at the rotor inlet, the absolute and relative components of speed are obtained, and then the correspondent Mach numbers:

$$C_1 = \frac{U_1}{\sin \alpha_1} \quad (4.8)$$

$$W_1 = C_1 \cos \alpha_1 \quad (4.9)$$

$$M_{C_1} = \frac{C_1}{\sqrt{\gamma RT_1}} = \frac{\frac{U_1}{a_0}}{\sin \alpha_1 \sqrt{1 - \frac{\gamma-1}{2} \frac{\left(\frac{U_1}{a_0}\right)^2}{\sin^2 \alpha_1}}} \quad (4.10)$$

$$M_{W_1} = M_{C_1} * \cos \alpha_1 \quad (4.11)$$

An important parameter to calculate, useful in this phase but also in the design process, is the ratio between the outer outlet radius and the inlet radius of the rotor, $\frac{R_{2,o}}{R_1}$. It is derived from the definition of $\eta_{T,ts}$, expressing ΔT_{tot} as follows:

$$\Delta T_{tot} = \frac{U_1 C_{u1}}{c_p} \quad (4.12)$$

$$C_{u1} = U_1 \quad (\beta_1 = 0^\circ) \quad (4.13)$$

$$c_p = \frac{\gamma}{\gamma - 1} R \quad (4.14)$$

$$\frac{\Delta T_{tot}}{T_1^0} = (\gamma - 1) \frac{U_1^2}{\gamma RT_1^0} = (\gamma - 1) \left(\frac{U_1}{a_0}\right)^2 \quad (4.15)$$

$$\eta_{T,ts} = \frac{2}{2 + \frac{1}{\sin^2 \alpha_1} \left(\frac{1}{\Phi^2} - 1\right) + \left(\frac{R_{2,o}}{R_1}\right)^2 \left(\frac{1}{\Psi^2 \sin^2 \beta_{2,o}} - 1\right)} \quad (4.16)$$

Now, through equation (4.15) and the following relations, the Mach numbers at the rotor outlet can be found:

$$C_2 = U_{2,o} \cot \beta_{2,o} = \frac{R_{2,o}}{R_1} U_1 \cot \beta_{2,o} \quad (4.17)$$

$$T_2 = T_2^0 - \frac{C_2^2}{2c_p} = T_1^0 - \Delta T_{tot} - \frac{C_2^2}{2c_p} \quad (4.18)$$

$$M_{W_{2,o}} = \frac{W_{2,o}}{\sqrt{\gamma RT_2}} = \frac{\frac{R_{2,o}}{R_1} U_1}{\sin \beta_{2,o} \sqrt{\left(\frac{a_0}{U_1}\right)^2 - (\gamma - 1) \left[1 + \left(\frac{R_{2,o}}{R_1}\right)^2 \frac{\cot^2 \beta_{2,o}}{2}\right]}} \quad (4.19)$$

$$M_{C_2} = M_{W_{2,o}} \cos \beta_{2,o} \quad (4.20)$$

Consequently, it is obtained

$$C_2 = M_{C_2} \sqrt{\gamma RT_2} \quad (4.21)$$

$$W_{2,o} = \frac{C_2}{\cos \beta_{2,o}} \quad (4.22)$$

$$U_{2,o} = W_{2,o} \sin \beta_{2,o} \quad (4.23)$$

Finally, knowing the value of the speed at the rotor outlet, it is possible to calculate

4.2. TURBINE

the total outlet pressure and the total-to-total efficiency from their definitions:

$$p_2^0 = p_2 \left(1 + \frac{\gamma - 1}{2} M_{W_{2,o}}^2\right)^{\frac{\gamma}{\gamma-1}} \quad (4.24)$$

$$\eta_T = \frac{\eta_{T,ts}}{1 - \frac{C_2^2}{2c_p \Delta T_{is}}} \quad (4.25)$$

4.2.2.1 Impact of humidity

In paragraph 4.1.1.1 the effects of the ambient humidity on the Reverse Bootstrap system performances have been mentioned and qualitatively discussed.

The process to calculate the effective turbine exhaust temperature of the humid air and liquid water content is shown in Appendix D.

The re-evaporation of the condensed water in the gap around the avionics box will not be considered in this thesis: it will be assumed that just the humid, saturated air passes through the fins, entering the gap with the temperature T_{WAR} calculated according to Appendix D. This is a conservative assumption since the evaporation of the liquid water would remove the latent heat from the air, helping the refrigeration of the Avionics box.

4.2.3 Sizing calculations

Objective of this activity ([32]) is to determine all the significant sizes of the turbine, especially radii and thicknesses.

4.2.3.1 Rotor sizing

Input of this process are:

- the thermodynamic conditions obtained in the previous paragraph;
- k_{B1} : restriction factor, which corrects the mass flow rate and primarily depends on thickness and number of the rotor blades;
- k_{B2} : restriction factor, which corrects the mass flow rate taking into account the finite blade thickness and the boundary layers along the blades and the walls;
- $\frac{R_{2,i}}{R_1}$: ratio between the inner outlet radius and the inlet radius.

In this section, station "1" will be considered the rotor inlet, not the turbine inlet.

First of all, the ratio between inner and outer radius at the rotor outlet can be calculated:

$$\frac{R_{2,i}}{R_{2,o}} = \frac{R_{2,i}}{R_1} \frac{R_1}{R_{2,o}} \quad (4.26)$$

The next step is to calculate the axial thickness at the inlet station (b_1) and the inlet radius (R_1): it is done starting from the definitions of the flow rate functions F_1 and F_2 , respectively at the inlet and outlet station.

Using equations (4.27) and (4.28), derived from the isentropic relations, it is possible to develop the definition of F_1 as in equation (4.29), and then obtain its value.

$$\frac{T_1}{T_1^0} = 1 - \frac{\gamma - 1}{2} \frac{(U_1/a_0)^2}{\sin^2 \alpha_1} \quad (4.27)$$

$$\frac{p_1}{p_1^0} = \left[1 - \frac{\gamma - 1}{2} \frac{(U_1/a_0)^2}{\Phi^2 \sin^2 \alpha_1} \right]^{\frac{\gamma}{\gamma-1}} \quad (4.28)$$

$$\frac{\dot{m} \sqrt{R T_1^0}}{p_1^0 \pi R_1^2 \frac{b_1}{R_1} k_{B1}} = F_1 = \frac{2 \sqrt{\gamma} \left(\frac{U_1}{a_0} \right) \cot \alpha_1 \left[1 - \frac{\gamma-1}{2} \frac{(U_1/a_0)^2}{\Phi^2 \sin^2 \alpha_1} \right]^{\frac{\gamma}{\gamma-1}}}{1 - \frac{\gamma-1}{2} \frac{(U_1/a_0)^2}{\sin^2 \alpha_1}} \quad (4.29)$$

Similarly, at the rotor discharge, equations (4.30) and (4.31) (also derived from the isentropic relations) are used together with the expression of ξ_A to develop the definition of F_2 as shown in equation (4.33), and so calculate it.

$$\frac{T_2}{T_1^0} = 1 - (\gamma - 1) \left(\frac{U_1}{a_0} \right)^2 \left[1 + \left(\frac{R_{2,o}}{R_1} \right)^2 \frac{\cot^2 \beta_{2,o}}{2} \right] \quad (4.30)$$

$$\frac{p_2}{p_1^0} = \left(\frac{T_1^0 - \Delta T_{is}}{T_1^0} \right)^{\frac{\gamma}{\gamma-1}} = \left[1 - \frac{\gamma - 1}{\eta_{T,ts}} \left(\frac{U_1}{a_0} \right)^2 \right]^{\frac{\gamma}{\gamma-1}} \quad (4.31)$$

$$\xi_A = \frac{\pi(R_{2,o}^2 - R_{2,i}^2)}{\pi R_1^2} = \left(\frac{R_{2,o}}{R_1} \right)^2 \left[1 - \left(\frac{R_{2,i}}{R_{2,o}} \right)^2 \right] \quad (4.32)$$

$$\frac{\dot{m} \sqrt{R T_1^0}}{p_1^0 \pi R_1^2 \xi_A k_{B2}} = F_2 = \frac{\sqrt{\gamma} \left(\frac{U_1}{a_0} \right) \left(\frac{R_{2,o}}{R_1} \right) \cot \beta_{2,o} \left[1 - \frac{\gamma-1}{\eta_{T,ts}} \left(\frac{U_1}{a_0} \right)^2 \right]^{\frac{\gamma}{\gamma-1}}}{1 - (\gamma - 1) \left(\frac{U_1}{a_0} \right)^2 \left[1 + \left(\frac{R_{2,o}}{R_1} \right)^2 \frac{\cot^2 \beta_{2,o}}{2} \right]} \quad (4.33)$$

Combining equations (4.29) and (4.33) it is possible to obtain the ratio $\frac{b_1}{R_1}$, as

$$\frac{F_1}{F_2} = \frac{\xi_A k_{B2}}{\frac{b_1}{R_1} k_{B1}} = \frac{\left(\frac{R_{2,o}}{R_1} \right)^3 \left[1 - \left(\frac{R_{2,o}}{R_{2,i}} \right)^2 \right] k_{B2}}{\frac{b_1}{R_1} k_{B1}}$$

and then, through equation (4.29), R_1 is calculated.

Knowing the ratios $\frac{b_1}{R_1}$, $\frac{R_{2,o}}{R_1}$, $\frac{R_{2,i}}{R_1}$, it is easy to obtain the values of b_1 , $R_{2,o}$ and $R_{2,i}$. The channel thickness at the rotor discharge can easily be found as $b_2 = R_{2,o} - R_{2,i}$. The rotational speed (ω if expressed in *rad/s*, N if expressed in *rpm*) can be found as $\omega = \frac{U_1}{R_1}$.

Then, the specific speed has to be evaluated, in order to verify (and possibly modify) the chosen value for the adiabatic efficiency. It has been chosen to consider the non dimensional specific speed, since it can be used in any system of units. This parameter's definition is showed in equation (4.34). It has been chosen, as it usually is for gas turbines, to use the discharge volume flow rate (defined as in equation (4.35)).

4.2. TURBINE

$$n_s = \frac{\omega Q^{1/2}}{(c_p \Delta T_{is})^{3/4}} \quad (4.34)$$

$$Q_2 = \pi R_{2,o}^2 \left[1 - \left(\frac{R_{2,i}}{R_{2,o}} \right)^2 \right] k_{B2} U_{2,o} \cot \beta_{2,o} \quad (4.35)$$

With the calculated value of the specific speed it is possible to derive the new value of the total-to-static efficiency, entering the diagram showed in Figure 4.7, which is reworked from the data of the NASA report [18].

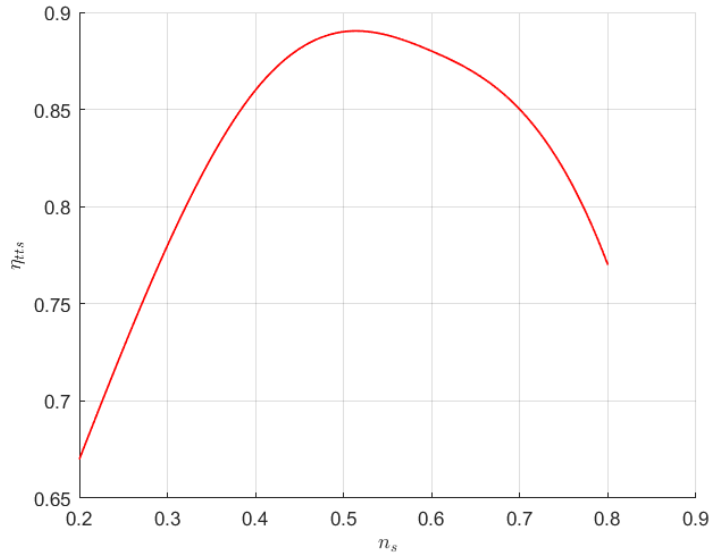


Figure 4.7: Total-to-static adiabatic efficiency vs. Specific speed

The value of the total-to-static efficiency is iterated, as described, until convergence, with a tolerance of $\pm 2\%$

4.2.3.2 Calculation of the minimum rotor blade and stator vane number

It is necessary to evaluate the minimum number of rotor blades (Z_{min}) that allows to not have flow reversion. The Jamieson criteria has been followed. Jamieson demonstrated that, for an incompressible fluid in a radial machine, the variation of radial velocity with the angle is:

$$\frac{\partial C_r}{\partial \theta} = -2\omega r \quad (4.36)$$

That means that the maximum and minimum radial speeds are respectively:

$$C_{r,max} = C_r + \frac{1}{2} \Delta C_r = C_r + \omega r \Delta \theta$$

$$C_{r,min} = C_r - \frac{1}{2} \Delta C_r = C_r - \omega r \Delta \theta$$

where C_r is the average radial speed and $\Delta \theta = \frac{2\pi}{Z}$ is the angular distance between the blades. In order to find Z_{min} , the limiting case has to be evaluated. In that case:

- $r = R_1$
- $C_{r,min} = 0$

So, $\Delta\theta$ can be expressed as in equation (4.37). But, at the rotor inlet, the radial velocity can be expressed as $C_r = \frac{U_1}{\tan \alpha_1}$, so $\Delta\theta$ can be found as in (4.38). Finally, as previously defined, Z_{min} is calculated in equation (4.39).

$$\Delta\theta = \frac{C_r}{\omega R_1} = \frac{C_r}{U_1} \quad (4.37)$$

$$\Delta\theta = \frac{1}{\tan \alpha_1} \quad (4.38)$$

$$Z_{min} = \frac{2\pi}{\Delta\theta} = 2\pi \tan \alpha_1 \quad (4.39)$$

According to [24], the minimum rotor blade number for a radial turbine can be found with the following formula,

$$Z_{min} = 2\pi \frac{\cos(\frac{\pi}{2} - \alpha_1)}{\sin(\frac{\pi}{2} - \alpha_1)}$$

which exactly correspond to (4.39).

[4] suggests, when comparing with test evidence, that these calculated values are too high and should be decreased with a factor 0.7. That makes the final formula:

$$Z_{min} = 1.4\pi \frac{\cos(\frac{\pi}{2} - \alpha_1)}{\sin(\frac{\pi}{2} - \alpha_1)}$$

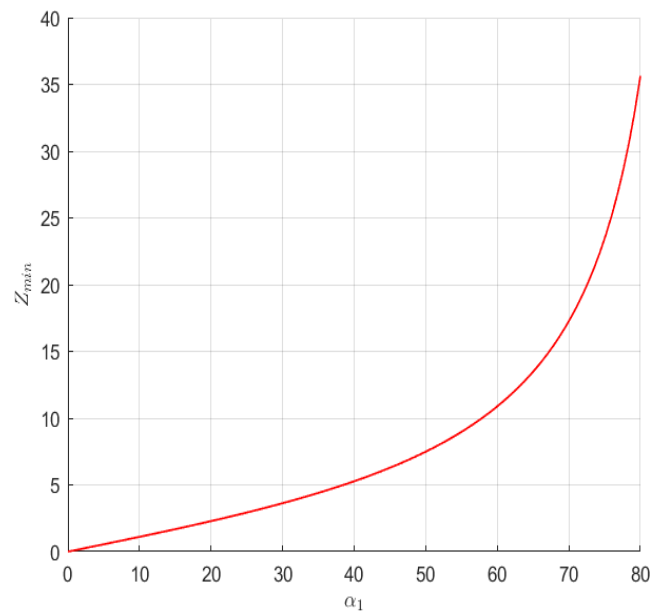
Results for both cases are shown in Figure 4.8.

However, this formula gives a high blade number, very often not compatible with the small turbine design.

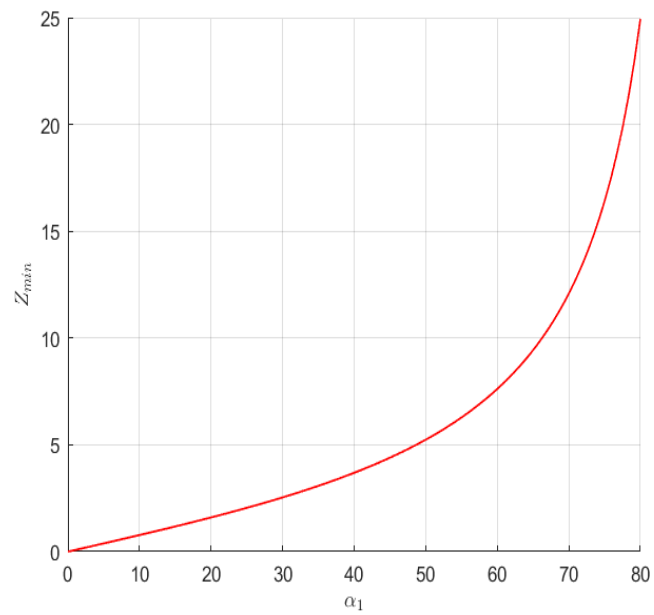
According to Glassman, the minimum number of the impeller blades can be calculated using formula (4.40), giving the results shown in Figure 4.9 where also the comparison between the number of blades derived from the experimental formula (dotted line) and the theoretical one is shown. The difference of the results is more evident at low angle α_1

$$Z_{min} = \frac{\pi}{30}(\alpha_1 + 20^\circ) \cot \alpha_1 \quad (4.40)$$

4.2. TURBINE



(a) Uncorrected



(b) Corrected

Figure 4.8: Minimum number of rotor blades

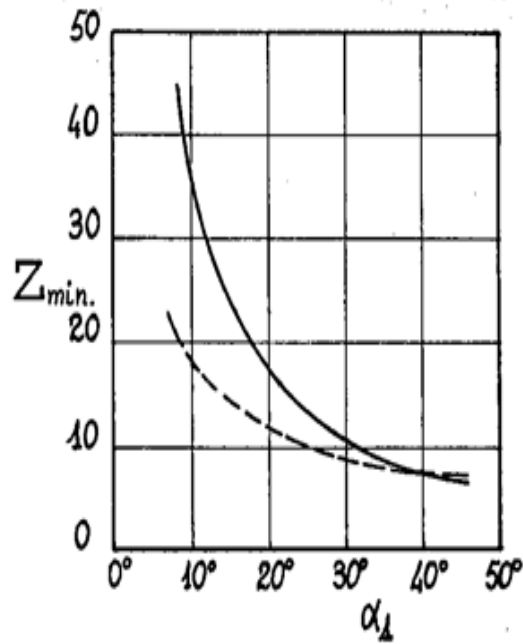


Figure 4.9: Glassman's minimum rotor blade number

Another correlation used to calculate the number of the rotor blade is:

$$Z_{min} = \frac{2\pi}{\arcsin\left(\frac{1}{\Phi}\right)}$$

where Φ is the ratio between the absolute flow velocity at the rotor exhaust and the peripheral speed at the same station (*velocity ratio*).

Whichever is the method of calculation of the number of impeller blades, the number of the stator vanes shall be always higher than the blade one and prime number in order to avoid vibrations and resonance between rotor and stator.

4.2.3.3 Rotor blade channel definition

As all the main dimensions of the turbine impeller have been calculated, now it is possible to represent the meridional view of the blade profile. It has been assumed, following [15], that the hub profile is formed of one circular arc, while the tip profile is formed of two circular arcs, with their common normal at 45° to axis, as shown in Figure 4.10.

Following the scheme in Figure 4.10 and setting the angle φ to 10° , it is possible to derive:

$$x = (r_2 - r_{1H}) \left(\frac{1}{\cos \varphi} - \tan \varphi \right) - b_2$$

$$y = r_2 - r_{1T}$$

4.2. TURBINE

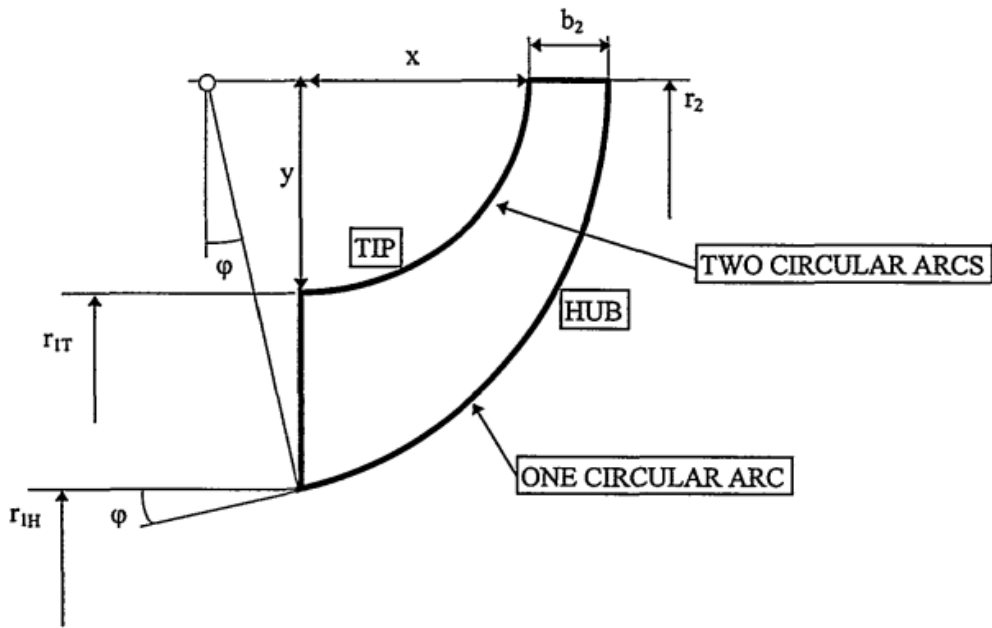


Figure 4.10: Example of blade profile

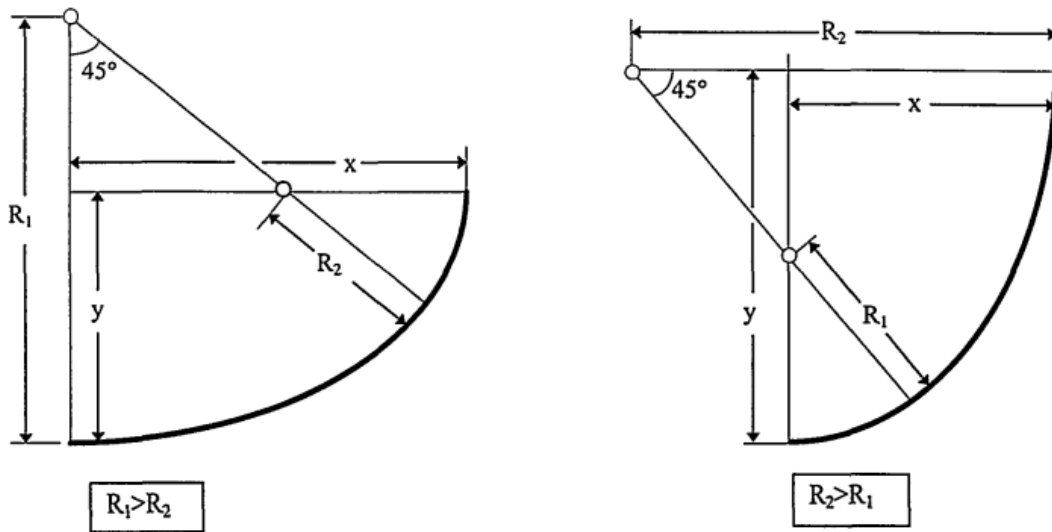


Figure 4.11: Example of tip profile representation

The tip profile is more complicated, as the center of the two arcs moves depending on which radius is the largest. Following the nomenclature of Figure 4.11, the magnitude of the two radius can be calculated:

$$x - R_2 = R_1 - y$$

$$R_1 - R_2 = \sqrt{2}(R_1 - y)$$

Hence

$$R_1 = \frac{x + (1 - \sqrt{2})y}{2 - \sqrt{2}}$$

$$R_2 = \frac{(1 - \sqrt{2})x + y}{2 - \sqrt{2}}$$

Now that x , y , R_1 and R_2 are known (note that in this case R_1 and R_2 are not the turbine rotor inlet and discharge radii), it is possible to represent the blade profile.

4.2.3.4 Volute sizing

The volute is designed by assuming that its cross section is circular (with a radius r_v , diameter D_v) and that the tangential speed C_{ui} at the inner radius R_i remains constant.

In this section, the volute diameter will be calculated as function of the azimuthal angle ψ .

Input of this process are:

- R_i : inner radius of the volute;
- all the thermodynamic conditions at the volute inlet;
- f : friction factor.

According to the law of conservation of the angular momentum for frictionless flows, the product between tangential speed and radius remains constant:

$$C_{ui} R_i = C_u (R_i + r_v) \quad (4.41)$$

C_{ui} is the tangential component of speed at the inner radius, C_u is the mean tangential speed at a certain angle ψ , where the radius of the volute cross section is r_v .

If Q (equation (4.42)) is the total volume flow rate entering the volute, the volume flow rate at the angle ψ is:

$$Q = \frac{\dot{m}}{\rho_1} \quad (4.42)$$

$$\frac{Q(360 - \psi)}{360} = \pi r_v^2 C_u = \pi r_v^2 \frac{C_{ui} R_i}{(R_i + r_v)} \quad (4.43)$$

By remodeling equation (4.43) the following relation is obtained:

$$\frac{\left(\frac{r_v}{R_i}\right)^2}{1 + \frac{r_v}{R_i}} = \frac{Q(1 - \frac{\psi}{360})}{\pi R_i^2 C_{ui}} = b \quad (4.44)$$

So, for every value of ψ between 0° and 360° , b can be calculated. Hence, r_v is obtained by solving a simple second degree equation:

$$\frac{r_v}{R_i} = \frac{b}{2} + \sqrt{b + \frac{b^2}{4}} \quad (4.45)$$

4.2. TURBINE

The friction effect is taken into account increasing r_v to r_{vf} , according to these empirical relations:

$$\frac{r_{vf}}{r_v} = \frac{1}{\sqrt[4]{1 - \Delta q}}$$

$$\Delta q = 0.0233 f c \log \left[\frac{\sqrt{2c} + 3\sqrt{360}}{\sqrt{2c} + 3\sqrt{360 - \psi}} \right]$$

$$c = \frac{(360)(2\pi)V_{ui}R_i^2}{Q}$$

Finally, it is possible to calculate the outer volute radius, measured from the turbine axis: this is useful to evaluate the size of the turbine.

$$R_{v,ext} = R_i + 2r_{vf} \quad (4.46)$$

4.2.3.5 Nozzle ring sizing

Objective of this paragraph is to calculate the inlet and outlet angles of the nozzle ring vanes. Inputs of this process are:

- $\frac{R_{TE}}{R_1}$: ratio between the nozzle ring's trailing edge radius and the rotor's inlet radius;
- $\frac{R_1}{R_{LE}}$: ratio between the rotor's inlet radius and the nozzle ring's leading edge radius;
- Z_{stat} : number of nozzle ring vanes.

First of all, since the value of R_1 is known from the rotor sizing, the leading edge and trailing edge radii can be obtained using the ratios in input:

$$R_{LE} = \frac{R_1}{\frac{R_1}{R_{LE}}}$$

$$R_{TE} = R_1 \frac{R_{TE}}{R_1}$$

Since the leading edge of the nozzle ring coincides with the inner radius of the volute R_i , the tangential component of speed at this stage is already known ($C_{uLE} = C_{ui}$). On the other hand, the radial component of speed is obtained from the definition of volumetric flow rate (4.49), after calculating the flow passage area at the leading edge (4.48), assuming that the nozzle ring has the same axial depth as the rotor inlet (4.47):

$$b_{LE} = b_{TE} = b_1 \quad (4.47)$$

$$A_{LE} = 2\pi R_{LE} b_{LE} \quad (4.48)$$

$$C_{rLE} = \frac{Q}{A_{LE}} \quad (4.49)$$

Now, the absolute speed and its correspondent angle can be calculated:

$$C_{LE} = \sqrt{C_{uLE}^2 + C_{rLE}^2} \quad (4.50)$$

$$\alpha_{LE} = \arctan \left(\frac{C_{uLE}}{C_{rLE}} \right) \quad (4.51)$$

At the trailing edge, the tangential component of speed can be obtained by assuming that the vaneless space between the nozzle ring and the rotor is frictionless, so the conservation of angular momentum can be applied:

$$C_{uTE} R_{TE} = C_1 \sin \alpha_1 R_1 \quad (4.52)$$

$$C_{uTE} = \frac{R_1}{R_{TE}} C_1 \sin \alpha_1 \quad (4.53)$$

The radial component, instead, is calculated through an iteration, assuming that total temperature and total pressure remain constant along the volute and the nozzle ring:

$$0. \quad C_{rTE} = 0$$

$$1. \quad T_{TE} = T_{TE}^0 - \frac{C_{uTE}^2 + C_{rTE}^2}{2c_p}$$

$$2. \quad p_{TE} = p_{TE}^0 \left(\frac{T_{TE}}{T_{TE}^0} \right)^{\frac{\gamma}{\gamma-1}}$$

$$3. \quad \rho_{TE} = \frac{p_{TE}}{RT_{TE}}$$

$$4. \quad C_{rTE} = \frac{\dot{m}}{\rho_{TE} 2\pi R_{TE} b_{TE}}$$

C_{rTE} starting value is 0. Then, the static temperature is derived from the total temperature, knowing the value of the absolute speed (at the first iteration it has only a tangential component). The static pressure is obtained from the isentropic relation, while the density is calculated through the ideal gas law. Hence, a new value for C_{rTE} is found through the definition of mass flow rate, and the loop continues until C_{rTE} converges.

Now it is possible to obtain, as well as it was done for the leading edge, the absolute speed and its correspondent angle:

$$C_{TE} = \sqrt{C_{uTE}^2 + C_{rTE}^2} \quad (4.54)$$

$$\alpha_{TE} = \arctan \left(\frac{C_{uTE}}{C_{rTE}} \right) \quad (4.55)$$

Finally, using the geometric relation showed in (4.57), it is possible to determine the diameter of the "throat" between the nozzle ring's vanes:

$$sp_{TE} = \frac{2\pi R_{TE}}{Z_{stat}} \quad (4.56)$$

$$l_{th} = sp_{TE} \cos \alpha_{TE} \quad (4.57)$$

where sp_{TE} is the spacing of the nozzle ring's vanes at the trailing edge.

4.3 Avionics box

The Avionics Box contains the electronic components which are the source of the heat to be dissipated. Indeed, in order to ensure the correct functioning of these devices, their temperature needs to be maintained within a certain range. The safe temperature range is different depending on the electronic components technology and on its final use (i.e.: commercial, military, space applications). In our study case, advanced electronic components which tolerate temperatures till to $170^{\circ}C$ have been considered (more details at para 5.2.1).

Generally speaking, the heat can be removed from a source and rejected into a sink by mean of different ways; an overall analysis shall be performed in the design phases and the appropriate heat exchange method shall be selected.

Brief descriptions of the types of heat exchange and of the thermal control techniques are reported in the following paragraphs.

4.3.1 Types of heat exchange

The passage of heat from a system to another can happen if two conditions persist:

1. there is a temperature differential between the systems;
2. the systems are not separated by an adiabatic wall.

According to the *second law of Thermodynamics*, the heat propagates in the direction of decreasing temperature: that is true for all types of heat exchange.

There are three heat exchange mechanisms: **conduction**, **convection** and **radiation**. Conduction and radiation only consist in heat transmission, while convection also implies a mass transfer. In nature it is rare that just one of this mechanisms takes place: generally, they are associated in different combinations.

Conduction

It is the mechanism of energy transmission due to interaction between particles with different energy levels. It can happen in solids, liquids and gases: in fluids it is due to molecules collision during their chaotic motion, while in solids it is due to molecule vibration and free electrons.

The heat load transmitted via conduction through a flat plate is defined by the *Fourier's law*:

$$Q_{cond} = -\lambda A \frac{\Delta T}{\Delta x}$$

where

- λ is the thermal conductivity of the material;
- A is the surface of the plate (normal to the heat exchange direction);
- Δx is the plate thickness;
- ΔT is the temperature difference between the faces of the plate.

Convection

It is the energy transfer mechanism between a solid surface and a moving fluid adjacent to it. Convection consists in the combined effects of conduction and mass transfer. The heat exchange is higher for higher flow speed.

Two types of convection can be distinguished:

Forced convection when the fluid is forced to flow along the solid surface by "external forces" (for example if it is moved by a fan).

Natural (or Free) convection when the fluid motion is caused by forces induced by a density difference, which is due to temperature variation in a gravitational field.

The heat load transmitted via convection is expressed in the *Newton's law*:

$$Q_{conv} = h A \Delta T$$

where h is the convective heat exchange coefficient.

Radiation

It is the energy transfer mechanism which takes place through electromagnetic waves, generated from the variation of the electronic configuration of atoms and molecules. Radiation does not need a material medium, since electromagnetic waves can propagate also in vacuum. The heat transmission happens at the speed of light. Every body with a temperature higher than 0 K emits a thermal radiation.

The heat load emitted via radiation from a surface A is expressed in the *Boltzmann's law*:

$$Q_{em} = \epsilon \sigma A T^4$$

where

- ϵ is the emissivity of the surface;
- σ is the Boltzmann constant;
- T is the temperature of the surface.

So, the heat load exchanged via radiation between two bodies "a" and "b" is:

$$Q_{rad} = \epsilon \sigma A (T_a^4 - T_b^4)$$

4.3.2 Thermal control techniques: general concepts

Compact heat exchangers

Compact heat exchangers (**CHE**) play an important role in the aeronautics industry by addressing the critical need for efficient thermal management within the constraints of space, weight, and performance requirements. Their versatility, compactness, and ability to optimize heat transfer make them indispensable components in various aircraft systems, contributing significantly to safety, efficiency, and passenger comfort.

The peculiarity of compact heat exchangers is the high surface area-to-volume ratio, that allows to enhance heat transfer efficiency. Depending on the application, various types of augmented heat transfer surfaces are used, such as:

Plate fin heat exchangers

This category of CHE is characterised by having secondary heat transfer surfaces, also called *fins*, between the plates. The fins have two main functions: first of all they act as secondary heat transfer surfaces, reducing the hydraulic diameter and so improving the heat transfer coefficient; then, they also carry mechanical load due to differential pressure between the sides of the heat exchanger.

There are many types of PFHE, some of which are showed in Figure 4.12:

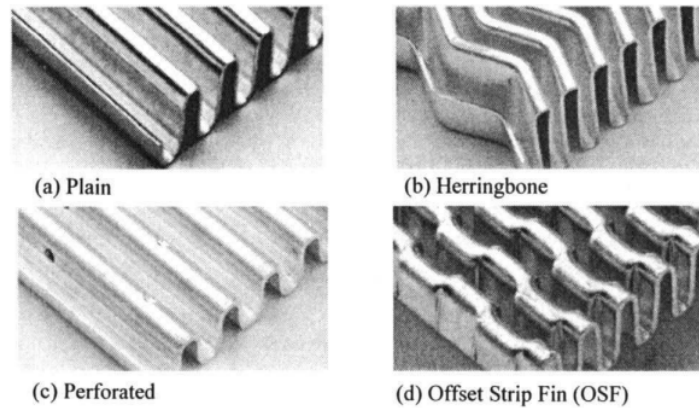


Figure 4.12: Different types of plate fins

Tube-fin heat exchangers

Finned tube exchangers (Figure 4.13) were used for many years for different applications, such as locomotive radiators, air cooling and steam condensers. They consist in tubes where fins have been added on the outside (and/or on the inside) in order to increase the contact area with the fluid (so the heat exchange). It is possible to have either a single spiroidal fin or a finned pack.

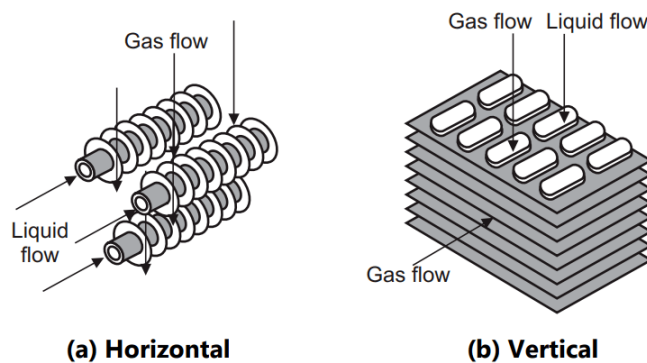


Figure 4.13: Finned tube

Diffusion bonded heat exchangers

They are formed by the diffusion bonding of a stack of plates, in which microchannels for flow passage are photochemically etched. The diffusion bonding process includes a thermal soaking period to allow grain growth, thereby enabling an interface-free join between the plates.

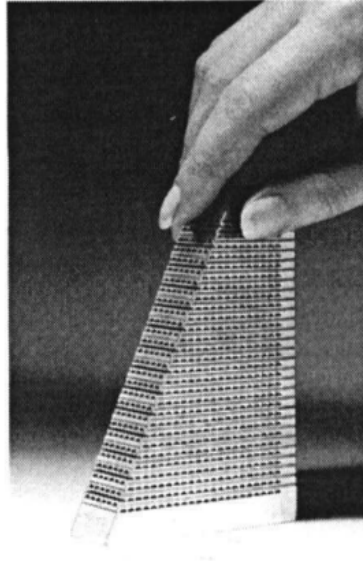


Figure 4.14: Section of a Diffusion bonded heat exchanger

4.3.3 Avionics box configuration

The avionics consists of a metal box containing the components attached to its internal faces. The heat generated by the components is transferred by conduction to the external faces of the box which have a fin brazed on them. Here the heat is removed by forced convection by the cold air coming from the turbine and flowing in a gap wrapping the box. The fin is located inside the gap, brazed on the external faces and to another upper metal sheet.

The original design of the avionics box allows full protection of the electronic components against water and any FOD contamination because they are closed in the box without any contact with the external environment.

Due to its original design, such item is not properly a heat exchanger, neither a pure box: it is an integrated unit containing the avionic components and allowing at the same time the dissipation of the internally generated heat together with full isolation from external water and FOD.

The heat transfer, via convection, between the avionics box's surface and the airflow allows to maintain the surface at the safe temperature of less than 170°C in any phase of the flight envelope. The configuration of the fins is reported in Figure 4.15. The geometrical parameters are:

- h : fin height;
- s : fin spacing;
- t : fin thickness;
- a : plate thickness;
- L : fin wavelength;
- A : wave amplitude.

Other important parameters are:

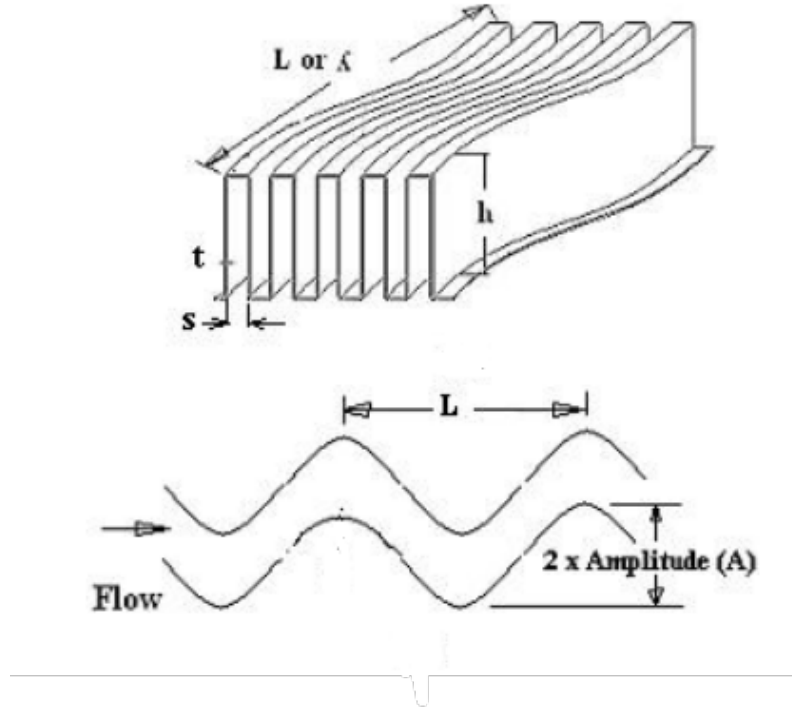


Figure 4.15: Plate fin's geometry

- β_f : ratio of total transfer area to volume between plates;
- r_h : flow passage hydraulic radius;
- α_f : ratio of total transfer area to total exchanger volume;
- $\frac{F_a}{T_a}$: ratio of fin area to total area;
- σ_f : ratio of free-flow area to frontal area.

The fin selected for the present application has been specifically designed: it is wavy type which generally allows highest performance in terms of Colburn factor j and associated minimum pressure losses derived from the Fanning factor f .

The geometrical data of the fin are shown in Table 4.1. Colburn (j) and Fanning (f) factors have been calculated according to the process reported in paper by L. Sheik and Ch. Ranganayakulu of Aeronautical Development Agency in Bangalore [16].

The applicable mathematical relations are:

For Laminar range ($100 < Re < 800$)

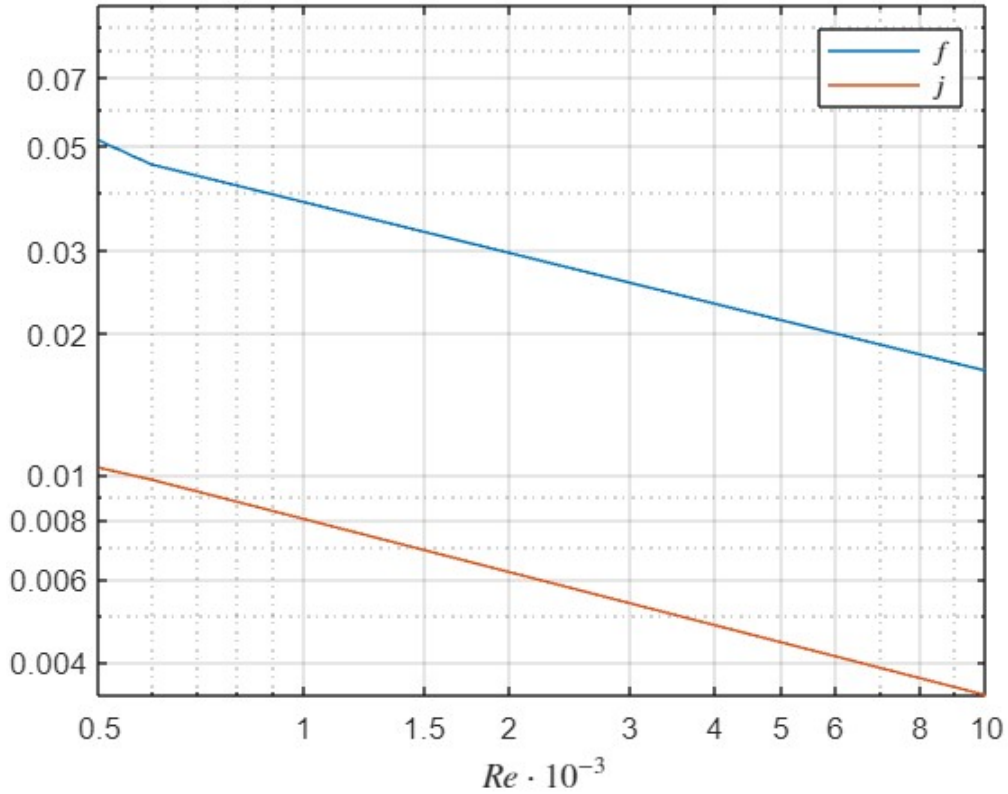
$$f = 9.827 Re^{-0.705} (h/s)^{0.322} (2A/s)^{-0.394} (L/2A)^{-0.603}$$

$$j = 2.348 Re^{-0.786} (h/s)^{0.312} (2A/s)^{-0.192} (L/2A)^{-0.432}$$

For Turbulent range ($1000 < Re < 15000$)

$$f = 10.628 Re^{-0.359} (h/s)^{0.264} (2A/s)^{-0.848} (L/2A)^{-1.931}$$

$$j = 0.242 Re^{-0.375} (h/s)^{0.235} (2A/s)^{-0.288} (L/2A)^{-0.553}$$


 Figure 4.16: j and f vs. Reynolds number

<i>Parameter</i>	<i>Symbol</i>	<i>Value</i>	<i>Unit</i>
Hydraulic radius	r_h	0.378	mm
Fin height	h	2.70	mm
Fin thickness	t	0.150	mm
Fin spacing	s	1.20	mm
Fin wavelength	L	9.50	mm
Wave amplitude	A	0.985	mm
Transfer area/ Volume between plates	β_f	2645.5	m^{-1}
Fin area/Total area	$\frac{F_a}{T_a}$	0.72	-

Table 4.1: Fin's geometrical configuration

4.3.4 Calculation process

4.3.4.1 Fins calculations

Inputs of this process are listed in Table 4.2 and Table 4.1.

4.3. AVIONICS BOX

<i>Parameter</i>	<i>Symbol</i>	<i>Value</i>	<i>Unit</i>
Air side length	L_{air}	400	<i>mm</i>
Traversal side length	L_t	200	<i>mm</i>
No-flow side length	L_{nf}	5.7	<i>mm</i>

Table 4.2: Avionics box sizes

The ratios α_f and σ_f are derived from the geometrical inputs (their expressions are taken from [17]):

$$\sigma_f = \frac{h \beta_f r_h}{h + a}$$

$$\alpha_f = \frac{\sigma_f}{r_h}$$

Knowing the sizes of fins and avionics box, the frontal area (A_{fr}), the free-flow area (A_{ff}) and the total exchanger volume (V_{tot}) can be obtained. Then, through the definition of α_f , the total heat exchange area A_{tot} is calculated:

$$A_{fr} = L_{nf} \cdot L_t$$

$$A_{ff} = \sigma_f A_{fr}$$

$$V_{tot} = A_{fr} \cdot L_{air}$$

$$A_{tot} = \alpha_f V_{tot}$$

4.3.4.2 Thermodynamic calculations

Inputs of this process are listed in Table 4.3.

<i>Parameter</i>	<i>Symbol</i>	<i>Value</i>	<i>Unit</i>
Air entering temperature	T_3	281.6	<i>K</i>
Air entering pressure	p_3	12.49	<i>kPa</i>
Avionics box's surface safe temperature	T_{av}	150	<i>°C</i>
Aluminium thermal conductivity	k_{al}	173	$\frac{W}{mK}$
Air Prandtl number	Pr	0.7	-
Air dynamic viscosity	μ	$1.99 \cdot 10^{-5}$	<i>Pa · s</i>

Table 4.3: Thermodynamic inputs

This calculation process follows [17]. First of all, the value of the mass flow rate \dot{m} has to be calculated. Since it is derived from the expression of the heat load (4.58), the value of the avionics box's exhaust air temperature (T_4) is needed. It is obtained through an iterative calculation: initially the value of T_4 is estimated, then it is re-calculated and the iteration starts again until T_4 converges. The same goes for the avionics exhaust pressure (p_4).

$$\dot{m} = \frac{Q_t}{c_p (T_4 - T_3)} \quad (4.58)$$

Now, the specific volumes at stations 3 (V_3) and 4 (V_4) and their mean value (V_m) are calculated.

$$\begin{aligned} V_3 &= \frac{RT_3}{p_3} \\ V_4 &= \frac{RT_4}{p_4} \\ V_m &= \frac{V_3 + V_4}{2} \end{aligned}$$

In order to calculate the values of f and j , the Reynolds number is needed: it is calculated from its definition (4.60), where G is the ratio between the mass flow rate and the free-flow area (notice that, since the flow passes through four finned surfaces, assumed of the same size, in equation (4.59) A_{ff} is multiplied by 4).

$$G = \frac{\dot{m}}{4 A_{ff}} \quad (4.59)$$

$$Re = \frac{D_h G}{\mu} \quad (4.60)$$

The Colburn number is used to calculate the Stanton number (St), and then the forced convection heat transfer coefficient (h_{fcc}), as follows:

$$St = \frac{j}{Pr^{2/3}} \quad (4.61)$$

$$h_{fcc} = St \cdot G \cdot c_p \quad (4.62)$$

In order to calculate the heat removed by the air from the surface of the avionics box, the efficiency of the fin shall be taken into account. This value is lower than 1 because the temperature along the fin height is not uniform: it decreases from the avionics surface temperature at that point till to a lower value at the tip of the fin. The efficiency of the fin (4.63) is calculated by the following procedure:

$$\begin{aligned} m &= \sqrt{\frac{2 h_{fcc}}{k_{al} t}} \\ ml &= m \cdot h \end{aligned}$$

$$\eta_f = \frac{\tanh(ml)}{ml} \quad (4.63)$$

Then, the overall heat exchanger efficiency (η_o) can be derived:

$$\eta_o = 1 - \frac{F_a}{T_a} (1 - \eta_f) \quad (4.64)$$

Now the new value $T_{4_{new}}$ can be calculated, equalizing the heat exchanged via convection between the avionics box surface and the air to the heat removed by the air:

$$\begin{aligned} \dot{m} c_p (T_4 - T_3) &= \eta_o h_{fcc} A_{tot} (T_{av} - T_{4|_{new}}) \\ T_{4|_{new}} &= T_{av} - \frac{\dot{m} c_p (T_4 - T_3)}{\eta_o h_{fcc} A_{tot}} \end{aligned} \quad (4.65)$$

4.3. AVIONICS BOX

$T_{4_{new}}$ will be introduced into the next iteration together with the new value of the avionics discharge pressure. According to [17], the pressure drop is:

$$dp = \frac{G^2}{2} V_3 \left[(1 + \sigma_f^2) \left(\frac{V_4}{V_3} - 1 \right) + f \frac{L_{aria}}{r_h} \frac{V_m}{V_3} \right] \quad (4.66)$$

where the first term is the contribution of flow acceleration (due to heating) and the second term is the contribution of friction. The small contributions of entry and exit losses are neglected.

The updated value of p_4 can finally be derived as

$$p_4 = p_3 - dp \quad (4.67)$$

and the iteration starts again from the turbine inlet until T_4 and p_4 converge.

4.4 Compressor



Figure 4.17: Centrifugal compressor

4.4.1 Centrifugal compressor: introduction

The centrifugal compressor is a turbomachine provided with a rotating impeller and a bladed diffuser, in which the airflow enters axially. Air is sucked by the so called *impeller eye*, the central part of the impeller, and it is put in rotation. The airflow pressure increases along the channel, balancing the centrifugal force.

There is a further static pressure increase through the diffuser: here, the flow is slowed down, in order to convert kinetic energy into pressure energy. Usually, the compressor is designed to equally split the static pressure increase between the impeller and the diffuser.

Different is the total pressure situation: it only increases through the impeller, as it performs work on the fluid. On the other hand, through the diffuser there is a total pressure reduction, due to friction losses.

At the diffuser discharge, the airflow is collected by a single volute or multiple collectors.

It follows a scheme of the compressor's components:

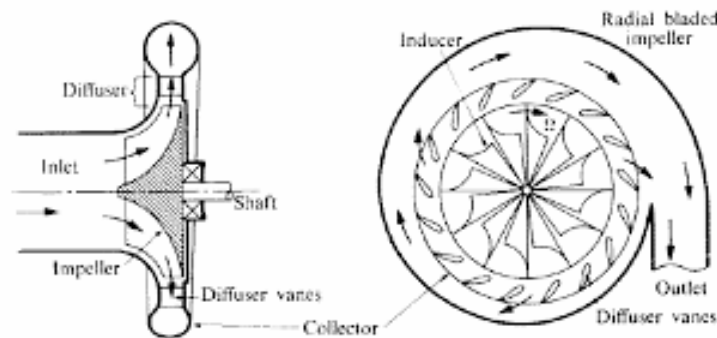


Figure 4.18: Centrifugal compressor components

4.4.2 Thermodynamic calculations

The following data are given as inputs:

- p_5 : static inlet pressure;

4.4. COMPRESSOR

- p_6 : static outlet pressure;
- T_5^0 : total inlet temperature;
- \dot{m} : mass flow rate;
- M_5 : inlet Mach number;
- η_C : total-to-total isentropic efficiency.

In this system architecture, all the mechanical power developed into the turbine is used to move the compressor, so the power balance at the spool is $P_C = P_T$.

Knowing the value of the power, the discharge total pressure can be found, as

$$T_6^0 = \frac{P_C}{\dot{m} c_p} + T_5^0 \quad (4.68)$$

Then, also from the definition of compressor power, and using the isentropic relations, the compressor pressure ratio β_C can be calculated:

$$P_C = \frac{1}{\eta_C} \dot{m} c_p T_5^0 (\beta_C^{\frac{\gamma-1}{\gamma}} - 1) \quad (4.69)$$

$$\beta_C = \left(\frac{\eta_C P_C}{\dot{m} c_p T_5^0} + 1 \right)^{\frac{\gamma}{\gamma-1}} \quad (4.70)$$

Now, since the static inlet pressure T_5 is obtainable as in (4.71), the inlet velocity C_5 can be found as in (4.72), from the definition of Mach number. C_5 is assumed to be purely axial ($\alpha_1 = 0^\circ$).

$$T_5 = \frac{T_5^0}{1 + \frac{\gamma-1}{2} M_5^2} \quad (4.71)$$

$$C_5 = M_5 \sqrt{\gamma R T_5} \quad (4.72)$$

From the ideal gas law, the flow density ρ_5 can be calculated, while the inlet total pressure p_5^0 is obtained as in (4.74) :

$$\rho_5 = \frac{p_5}{R T_5} \quad (4.73)$$

$$p_5^0 = p_5 \left(\frac{T_5^0}{T_5} \right)^{\frac{\gamma}{\gamma-1}} \quad (4.74)$$

Since the discharge static pressure is the ambient pressure and the discharge total pressure can be obtained through the pressure ratio β_C (4.75), the outlet static temperature T_6 can be calculated as well, and consequently the discharge absolute speed C_6 is derived in (4.77):

$$p_6^0 = \beta_C p_5^0 \quad (4.75)$$

$$T_6 = T_6^0 \left(\frac{p_6}{p_6^0} \right)^{\frac{\gamma-1}{\gamma}} \quad (4.76)$$

$$C_6 = \sqrt{2c_p(T_6^0 - T_6)} \quad (4.77)$$

$$\rho_6 = \frac{p_6}{R T_6} \quad (4.78)$$

4.4.3 Sizing calculations

4.4.3.1 Rotor sizing

In this phase, stations 1 and 2 will be referred respectively to the rotor inlet and outlet.

Inputs of the sizing process are:

- β_{b2} : backsweep angle;
- β_2 : relative velocity angle at rotor outlet;
- N : rotational speed;
- $\frac{R_{1h}}{R_{1t}}$: ratio between hub and tip inlet radii;
- $\frac{C_{1t}}{C_1}$: ratio between the absolute inlet speed at the tip and at the mean radius;
- $\frac{W_2}{W_{1t}}$: ratio between the relative discharge speed and the tip relative inlet speed
- $C_{p,2-3}$: pressure recovery factor between rotor discharge and diffuser outlet.

From the expression of the mass flow rate (4.79), and having $\frac{R_{1h}}{R_{1t}}$ as input, the tip radius can be calculated as in (4.80) :

$$\dot{m} = \rho_1 C_1 \pi (R_{1t}^2 - R_{1h}^2) \quad (4.79)$$

$$R_{1t} = \sqrt{\frac{\dot{m}}{\rho_1 C_1 \pi [1 - (\frac{R_{1h}}{R_{1t}})^2]}} \quad (4.80)$$

Consequently R_{1h} , the inlet channel height b_1 and the mean square radius R_1 are easily obtained:

$$R_{1h} = \left(\frac{R_{1h}}{R_{1t}} \right) R_{1t}$$

$$b_1 = R_{1t} - R_{1h}$$

$$R_1 = \sqrt{\frac{R_{1h}^2 + R_{1t}^2}{2}}$$

Since the compressor rotational speed is the same as the turbine, the rotational speed at station 1 can be obtained (4.81) and, from the velocity triangle, also the relative speed (4.82) and its correspondent angle β_1 (4.83) are calculated:

$$U_1 = \omega R_1 \quad (4.81)$$

$$W_1 = \sqrt{C_1^2 + U_1^2} \quad (4.82)$$

$$\beta_1 = \arcsin \left(\frac{U_1}{W_1} \right) \quad (4.83)$$

Since the ratio $\frac{W_2}{W_{1t}}$ is an input of the problem, W_{1t} needs to be calculated in order to obtain the relative outlet speed W_2 . Also the ratio $\frac{C_{1t}}{C_1}$ is an input, so it is possible

4.4. COMPRESSOR

to derive the inlet tip absolute speed C_{1t} and then repeat the previous steps in order to obtain W_{1t} :

$$\begin{aligned} C_{1t} &= \left(\frac{C_{1t}}{C_1} \right) C_1 \\ U_{1t} &= \omega R_{1t} \\ W_{1t} &= \sqrt{U_{1t}^2 + C_{1t}^2} \\ W_2 &= \left(\frac{W_2}{W_{1t}} \right) W_{1t} \end{aligned}$$

The peripheral speed at rotor outlet U_2 can be derived through the expression of *specific work*: the latter can be calculated by its definition (4.84), since the total temperatures at rotor inlet and outlet are known (T^0 remains constant through the diffuser, so the total temperature at rotor discharge is T_6^0). The specific work can also be expressed as function of U_2 and of the tangential component of absolute velocity C_{u2} as in (4.85). From the velocity triangle, C_{u2} can be related to U_2 , W_2 and β_2 as in (4.86), then U_2 can be found.

$$L_c = \frac{1}{\eta_C} c_p (T_6^0 - T_5^0) \quad (4.84)$$

$$L_c = U_2 C_{u2} \quad (4.85)$$

$$C_{u2} = U_2 - W_2 \sin \beta_2 \quad (4.86)$$

$$U_2 = \frac{W_2 \sin \beta_2 + \sqrt{4L_c + W_2^2 \sin^2 \beta_2}}{2} \quad (4.87)$$

In order to obtain the absolute speed's (C_2) magnitude, its radial and tangential components will be calculated. C_{u2} is derived from (4.86). Since the relative speed and the absolute speed have the same tangential component ($C_{r2} = W_{r2}$), from the velocity triangle C_{r2} can be derived. Then, C_2 is obtained.

$$C_{r2} = W_{r2} = W_2 \cos \beta_2 \quad (4.88)$$

$$C_2 = \sqrt{C_{r2}^2 + C_{u2}^2} \quad (4.89)$$

Now, the outlet radius R_2 and the absolute speed angle α_2 can easily be calculated:

$$R_2 = \frac{U_2}{\omega} \quad (4.90)$$

$$\alpha_2 = \arctan \left(\frac{C_{u2}}{C_{r2}} \right) \quad (4.91)$$

In order to complete the rotor sizing, the channel height b_2 at the discharge has to be found: it can be done through the expression of the discharge section A_2 (4.92), which can be calculated from the mass flow rate as in (4.93).

$$A_2 = 2\pi R_2 b_2 \quad (4.92)$$

$$\dot{m} = \rho_2 C_{r2} A_2 \quad (4.93)$$

Since the value of the density ρ_2 is needed, also p_2 and T_2 have to be derived, in order to apply the ideal gas law. As previously discussed, the value of T_2^0 is known

(it is the same total temperature of the compressor discharge), so T_2 can easily be found in (4.94). On the other hand, the value of p_2^0 is unknown, so the calculation of p_2 will be a little different. First of all, the ratio $\frac{p_2}{p_2^0}$ can be obtained as in (4.95). Then, the magnitude of p_2^0 can be found from the definition of the pressure recovery coefficient $C_{p,2-3}$ (4.96). In this nomenclature, station "3" is the diffuser outlet (so the compressor discharge). Then, p_2 is derived.

$$T_2 = T_2^0 - \frac{C_2^2}{2c_p} \quad (4.94)$$

$$\frac{p_2}{p_2^0} = \left(\frac{T_2}{T_2^0} \right)^{\frac{\gamma}{\gamma-1}} \quad (4.95)$$

$$C_{p,2-3} = \frac{p_3 - p_2}{p_2^0 - p_2} \quad (4.96)$$

$$p_2^0 = \frac{p_3}{C_{p,2-3} - \left(\frac{p_2}{p_2^0} \right) (C_{p,2-3} - 1)} \quad (4.97)$$

$$p_2 = \left(\frac{p_2}{p_2^0} \right) p_2^0 \quad (4.98)$$

The representation of the meridional view of the blade profile follows the same process described in paragraph 4.2.3.3.

4.4.3.2 Minimum number of rotor blades and stator vanes

The minimum number of blades is calculated using a formula by Stodola:

$$Z = \frac{2\pi \cos \bar{\beta}}{\frac{s}{c} \log \left(\frac{D_2}{D_1} \right)} \quad (4.99)$$

where $\frac{s}{c}$ is the blade's pitch to chord ratio and $\bar{\beta}$ is the average blade angle ($\bar{\beta} = \frac{\beta_1 + \beta_2}{2}$).

Another method of calculation is the use of the following formula, similar to that already shown for turbine rotor blade calculation:

$$Z = \frac{2\pi}{\arcsin \left(\frac{1}{\Phi (1+M_r^2)^{0.5}} \right)} \quad (4.100)$$

where Φ is the velocity ratio and M_r is the relative Mach number at rotor tip.

For the calculation of the number of stator vanes, the same principle discussed for the turbine case is applied.

4.4.3.3 Diffuser sizing

In this paragraph the conditions through the diffuser, in terms of temperature, pressure, speed and speed angle will be evaluated, in order to determine the size of the diffuser, in terms of geometrical area.

Inputs of this phase are:

- $\frac{R_{LE}}{R_2}$: ratio between the rotor discharge radius and diffuser's leading edge radius;

4.4. COMPRESSOR

- $\frac{p_{th}^0}{p_2^0}$: ratio between the diffuser's throat total pressure and the rotor discharge total pressure;
- $C_{p,2-th}$: pressure recovery factor between the rotor discharge and the diffuser's throat.

It is assumed that there is no friction in the vaneless space between the rotor tip and the diffuser's leading edge, so the total pressure and temperature remain constant ([8] and [6]).

$$\begin{aligned} p_{LE}^0 &= p_2^0 \\ T_{LE}^0 &= T_2^0 \end{aligned}$$

It is also assumed that the diffuser has the same axial depth as the rotor tip ($b_D = b_2$). Knowing the value of the ratio $\frac{R_{LE}}{R_2}$, R_{LE} can be found (4.101), and then the geometrical inlet area A_{LE} can also be calculated as in (4.102):

$$R_{LE} = \frac{R_{LE}}{R_2} R_2 \quad (4.101)$$

$$A_{LE} = 2\pi R_{LE} b_D \quad (4.102)$$

It is also assumed that the angular momentum remains constant in the vaneless space, so the tangential component of absolute speed at the leading edge can be derived:

$$C_{uLE} = \frac{C_{u2} R_2}{R_{LE}} \quad (4.103)$$

The radial component C_{rLE} is instead found by trial and error. Initially, it is assumed that $C_{rLE} = 0$, and the static temperature T_{LE} is calculated from the corresponding total temperature, as if the speed had only a tangential component. Then, since T_{LE} , T_{LE}^0 and p_{LE}^0 are known, p_{LE} is calculated. ρ_{LE} is obtained from the ideal gas law, and that allows to calculate C_{rLE} through the expression of mass flow rate. At this point the C_{rLE} value is updated and steps from 1 to 4 are repeated until C_{rLE} converges.

$$0. \quad C_{rLE} = 0$$

$$1. \quad T_{LE} = T_{LE}^0 - \frac{C_{uLE}^2 + C_{rLE}^2}{2c_p}$$

$$2. \quad p_{LE} = p_{LE}^0 \left(\frac{T_{LE}}{T_{LE}^0} \right)^{\frac{\gamma}{\gamma-1}}$$

$$3. \quad \rho_{LE} = \frac{p_{LE}}{RT_{LE}}$$

$$4. \quad C_{rLE} = \frac{\dot{m}}{\rho_{LE} A_{LE}}$$

At this point, the remaining conditions at the leading edge (absolute speed magnitude, Mach number, angle α_{LE}) can be found:

$$C_{LE} = \sqrt{C_{uLE}^2 + C_{rLE}^2} \quad (4.104)$$

$$M_{LE} = \frac{C_{LE}}{\sqrt{\gamma R T_{LE}}} \quad (4.105)$$

$$\alpha_{LE} = \arctan \left(\frac{C_{uLE}}{C_{rLE}} \right) \quad (4.106)$$

The value of the total temperature at the diffuser's throat is already known, since it remains constant along the stator, while the value of the total pressure can be found from the ratio $\frac{p_{th}^0}{p_2^0}$, so:

$$T_{th}^0 = T_2^0 \quad (4.107)$$

$$p_{th}^0 = \frac{p_{th}^0}{p_2^0} p_2^0 \quad (4.108)$$

Furthermore, from the definition of the pressure recovery factor between the rotor discharge and the diffuser's throat (4.109), the static pressure p_{th} can be obtained and, consequently, also T_{th} is calculated (4.110):

$$C_{p,2-th} = \frac{p_{th} - p_2}{p_2^0 - p_2} \quad (4.109)$$

$$T_{th} = T_{th}^0 \left(\frac{p_{th}}{p_{th}^0} \right)^{\frac{\gamma-1}{\gamma}} \quad (4.110)$$

Hence, knowing both the static and total temperature, it is possible to evaluate speed (4.111) and Mach number (4.112). Then, after calculating the density value from the ideal gas law, the throat area is obtained from the mass flow rate (4.114):

$$C_{th} = \sqrt{2c_p(T_{th}^0 - T_{th})} \quad (4.111)$$

$$M_{th} = \frac{C_{th}}{\sqrt{\gamma R T_{th}}} \quad (4.112)$$

$$\rho_{th} = \frac{p_{th}}{R T_{th}} \quad (4.113)$$

$$A_{th} = \frac{\dot{m}}{\rho_{th} C_{th}} \quad (4.114)$$

Finally, the diffuser's exit conditions are already known from the system calculations: the compressor discharge area can be calculated as:

$$A_6 = \frac{\dot{m}}{\rho_6 C_6} \quad (4.115)$$

4.4.3.4 Volute sizing

The sizing process of the compressor volute is similar to the one of the turbine, described in paragraph 4.2.3.4. As well as the turbine volute, the compressor one is assumed to have a round section, which linearly decreases with the azimuthal angle ψ .

Inputs of this process are:

- flow conditions at compressor discharge, which were previously calculated;
- rotor outlet radius R_2 , obtained from rotor sizing;
- $\frac{R_{TE}}{R_2}$: ratio between diffuser trailing edge radius and R_2 .

4.4. COMPRESSOR

The volumetric flow rate can be derived from its definition, knowing the mass flow rate and the air density at compressor discharge. Since the speed C_6 is known, it's easy to derive the volute section $A_{coll,ex}$ and its radius $R_{coll,ex}$.

The volute inner radius coincides with the diffuser trailing edge radius R_{TE} , obtained through the ratio $\frac{R_{TE}}{R_2}$.

$$\begin{aligned} Q &= \frac{\dot{m}}{\rho_6} \\ A_{coll,ex} &= \frac{Q}{C_6} \\ R_{coll,ex} &= \sqrt{\frac{A_{coll,ex}}{\pi}} \\ R_i &= R_{TE} = \frac{R_{TE}}{R_2} R_2 \end{aligned}$$

Applying the law of conservation of angular momentum for frictionless flow, as well as it was done in paragraph 4.2.3.4, the volute radius R_c can be found, for each value of ψ , as

$$\frac{R_c}{R_i} = \frac{b}{2} + \sqrt{b + \frac{b^2}{4}}$$

where b is

$$b = \frac{Q(1 - \frac{\psi}{360})}{\pi R_i C_6}$$

The only difference between this case and the turbine volute sizing calculations is that the angle $\psi = 0^\circ$ corresponds to the volute exit, while in paragraph 4.2.3.4 it referred to the volute inlet.

4.4.4 Adiabatic efficiency verification

As well as it was done for the turbine, the adiabatic efficiency's value (both total-to-total and total-to-static) needs to be verified and, if necessary, iterated.

In this paragraph the process of calculation of the total-to-total and total-to-static adiabatic efficiencies is described. the process is taken from [26].

First of all, the total-to-static polytropic efficiency ($\eta_{pol,ts}$) is calculated as function of the specific speed (n_s): this dependence is shown in figure 4.19, while the specific speed is calculated from its definition (4.116):

$$n_s = \frac{\omega \sqrt{\frac{\dot{m}}{\rho_5}}}{H_{ad}^{3/4}} \quad (4.116)$$

where H_{ad} is the adiabatic head and it is calculated as follows:

$$H_{ad} = R \frac{\gamma}{\gamma - 1} T_5^0 \left[\left(\frac{p_6^0}{p_5^0} \right)^{\frac{\gamma-1}{\gamma}} - 1 \right] \quad (4.117)$$

The maximum value of the total-to-static polytropic efficiency ($\eta_{max,pol,ts}$) is set to 0.88.

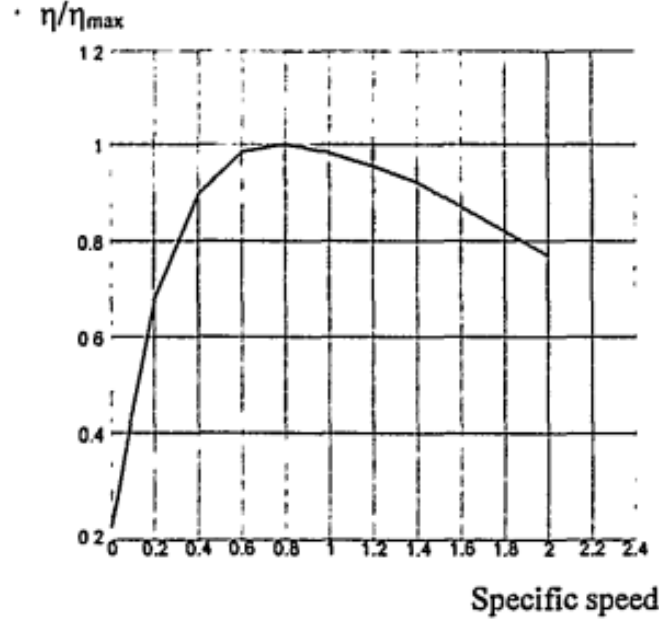


Figure 4.19: Total-to-static polytropic efficiency vs. Specific speed

Now it is possible to calculate the uncorrected value of the total-to-static adiabatic efficiency:

$$\eta_{ts,unc} = \frac{\left(\frac{p_6}{p_5}\right)^{\frac{\gamma-1}{\gamma}} - 1}{\left(\frac{p_6}{p_5}\right)^{\frac{\gamma-1}{\gamma \cdot \eta_{pol,ts}}} - 1}$$

This value, in order to be accurate for the compressor of interest of this thesis, needs to be corrected. [26] proposes three corrections:

1. Reynolds correction:

$$\Delta\eta_{ts} = (1 - \eta_{ts}) \left[\left(\frac{1.5 \cdot 10^7}{Re} \right)^n - 1 \right]$$

where Re is the Reynolds number at impeller tip diameter and $n \approx 0.2$.

2. $M_{W5,t}$ correction:

$$\begin{aligned} & \text{if } M_{W5,t} > 1 \\ \Delta\eta_{ts} &= \lambda(M_{W5,t} - 1) \\ & \text{else } \Delta\eta_{ts} = 0 \end{aligned}$$

where $M_{W5,t}$ is the relative Mach number at rotor inlet, while $\lambda \approx 0.1$.

3. M_6 correction:

$$\Delta\eta_{ts} = (1 - \eta_{ts}) \cdot (M_6 - 0.1) \left[1 + \frac{\gamma - 1}{2} M_6^2 \right]^{\frac{\gamma-1}{\gamma}}$$

Now, the corrected value of the total-to-static adiabatic efficiency can be found:

$$\eta_{ts} = \eta_{ts,unc} - \sum \Delta\eta_{ts}$$

4.4. COMPRESSOR

Finally, the value of the total-to-total adiabatic efficiency (η_{tt}) can be obtained from its definition (4.121), using the new values of T_6^0 and p_6^0 calculated with the new η_{ts} . The used equations are the following:

$$\eta_{ts} = \frac{T_5^0}{T_6 - T_5^0} \left[\left(\frac{p_6}{p_5^0} \right)^{\frac{\gamma-1}{\gamma}} - 1 \right] \quad (4.118)$$

$$T_6^0 = T_6 \left(1 + \frac{\gamma-1}{2} M_6^2 \right) \quad (4.119)$$

$$\frac{p_6}{p_6^0} = \left(\frac{T_6}{T_6^0} \right)^{\frac{\gamma}{\gamma-1}} \quad (4.120)$$

T_6 is derived from (4.118), and it is used to calculate T_6^0 from (4.119). Then, from the isentropic relation (4.120), p_6^0 is obtained.

The total-to-total adiabatic efficiency is then calculated:

$$\eta_{tt} = \frac{T_5^0}{T_6^0 - T_5^0} \left[\left(\frac{p_6^0}{p_5^0} \right)^{\frac{\gamma-1}{\gamma}} - 1 \right] \quad (4.121)$$

As well as it was done for the turbine, the value of η_{tt} is iterated until convergence, with a tolerance of $\pm 2\%$.

4.5 Pressure losses in the connecting pipes

Turbine, compressor and avionics box are connected by ducts, which imply pressure losses with associated impact on the total system performances.

In the next paragraphs, the equations used to model the pressure losses and the theory behind them will be discussed; since both between stations 2 and 3 and between stations 4 and 5 the Mach number is less than 0.3, the assumption of incompressible flow will be made in all the following considerations. It can be observed from the mass conservation that, for an incompressible flow in a constant section tube, the flow speed remains constant. Indeed

$$\dot{m} = \rho A V = \text{const}$$

and, since $\rho, A = \text{const}$ also $V = \text{const}$. This leads to the fact that, when the duct area is constant, the pressure losses are only static, while the dynamic component of total pressure does not change.

Theory and equations in this section are taken from [29].

4.5.1 Ducts pressure losses theory

In a real fluid, frictional forces, due to viscosity, exist: these forces are generated by the shearing stresses between the streamlines, and they are proportional to the viscosity and the velocity gradient perpendicular to the flow, according to Newton's equation (4.122):

$$\frac{F}{S} = \mu \frac{dV}{dx} \quad (4.122)$$

The shear stress causes a force along the wall of the duct, proportional to the area of the surface in contact with the fluid, which is called *drag* or *friction force*.

In classical aerodynamic theory, the drag force acting on a surface with area A is defined as follows:

$$F_D = C_D A \frac{1}{2} \rho V^2 \quad (4.123)$$

where C_D is the drag coefficient and $\frac{1}{2} \rho V^2$ is the dynamic pressure (q).

In the case of a round duct, the surface area A is

$$A = \pi D L$$

where D and L are respectively duct's diameter and length.

The drag force has to be balanced by a pressure force, corresponding to the pressure drop along the duct, which can be expressed as follows:

$$F_D = \Delta p^0 \left(\pi \frac{D^2}{4} \right) \quad (4.124)$$

Combining equations (4.123) and (4.124), the pressure drop can be derived:

$$\Delta p^0 = C_D \left(\frac{\pi D L}{\pi \frac{D^2}{4}} \right) q = 4 C_D \frac{L}{D} q$$

4.5. PRESSURE LOSSES IN THE CONNECTING PIPES

In a duct flow, the drag coefficient C_D is replaced by the Fanning friction factor f , so the final pressure drop equation is:

$$\Delta p^0 = 4 f \frac{L}{D} q \quad (4.125)$$

In the previous lines it has been explained how the velocity gradient, generated by viscosity, creates a drag force and a consequent pressure drop along the duct. It is therefore deduced that any change in duct's direction, cross sectional area or shape, with consequent change in the velocity profile, will cause a pressure loss. Losses of this type are expressed as follows:

$$\Delta p^0 = K_t q \quad (4.126)$$

where K_t is the pressure loss coefficient, which will be different depending on the type of loss.

4.5.2 Specific pressure losses data

4.5.2.1 Straight ducts

As discussed in the previous paragraph, the pressure loss due to friction in a straight duct is

$$\Delta p^0 = 4 f \frac{L}{D} q$$

For ducts of non-circular section, the diameter D is replaced by the hydraulic diameter (D_h), defined as

$$D_h = \frac{4 \cdot (\text{Cross-sectional area})}{\text{Wetted perimeter}}$$

The friction factor (f) depends on the Reynolds number and on the relative roughness (ϵ/D) of the duct, as shown in Figure 4.20.

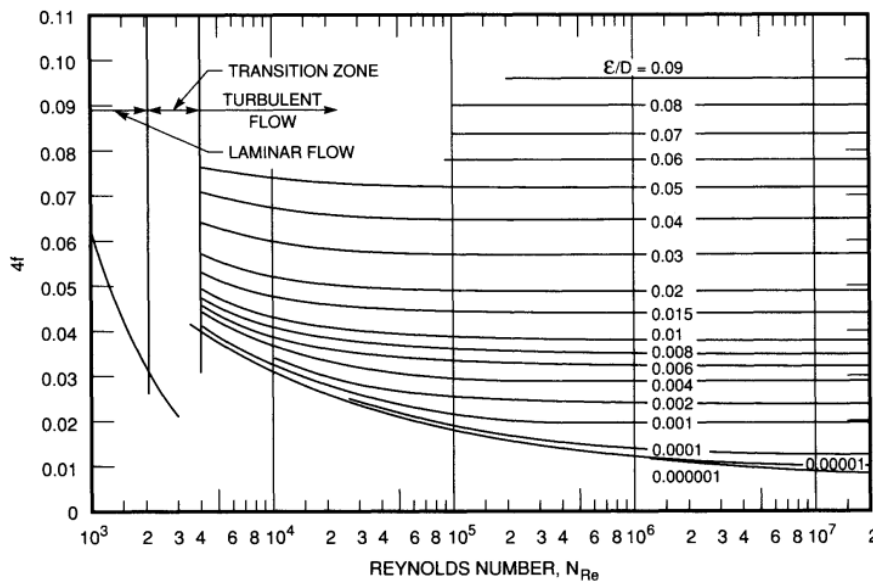


Figure 4.20: Friction factor vs. Reynolds number

For most aircraft ducting, the ducts can be treated as smooth tubes: this assumption will be applied in this thesis. The following formulas, approximating the data of Figure 4.20, are used to calculate the friction factor of a smooth tube as function of the Reynolds number:

$$f = \frac{16}{Re} \quad Re < 2100$$

$$f = \frac{0.0791}{Re^{0.25}} \quad 3000 < Re < 10000$$

$$f = \frac{0.046}{Re^{0.2}} \quad 10000 < Re < 5 \cdot 10^6$$

4.5.2.2 Elbows

The pressure loss in a general bend is

$$\Delta p^0 = \left(4f \frac{L}{D} + CK_{t90} \right) q$$

where

- L is the length along the centerline of the duct;
- K_{t90} is the pressure loss coefficient for an elbow (90° bend);
- C is the correction factor for bends other than 90° .

The first term is referred to the wall friction loss, the second term consists in the direction change loss.

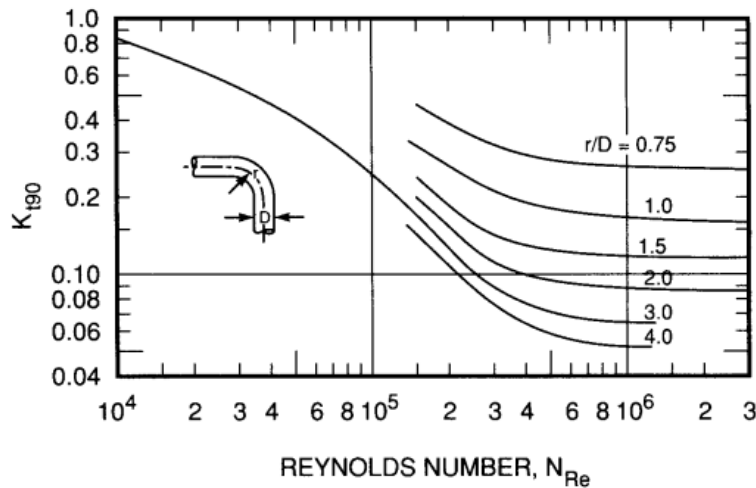


Figure 4.21: Loss coefficient vs. Reynolds number for 90° bends in circular ducts

Figure 4.21 shows the dependence of the loss coefficient K_{t90} on the Reynolds number. For values of Re above 10^5 there is a strong influence of the ratio r/D on the loss coefficient, where r is the curvature radius: in particular, the higher the ratio (which implies a smoother direction change), the lower the pressure loss.

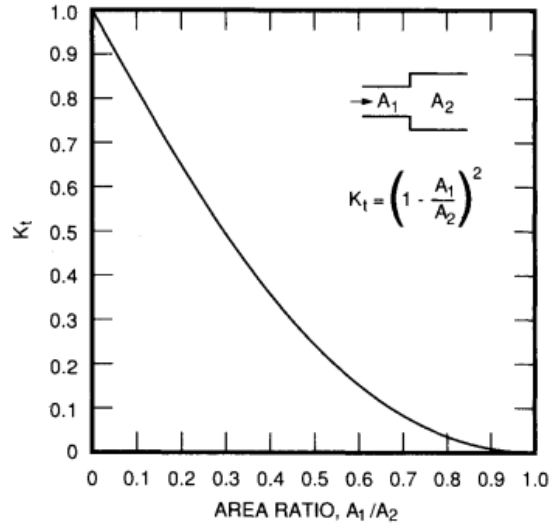
4.5. PRESSURE LOSSES IN THE CONNECTING PIPES

4.5.2.3 Duct area changes

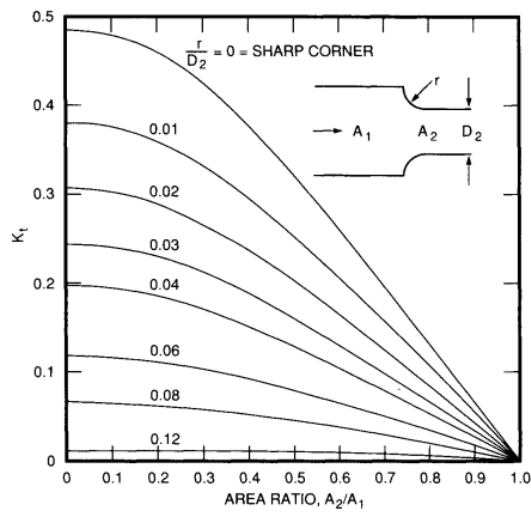
In order to be conservative, in this thesis the duct area changes will be treated as sudden contractions/expansions, instead of gradual ones. The pressure loss in this case is

$$\Delta p^0 = K_t q$$

where q is the dynamic pressure in the smaller area section.



(a) Sudden expansion



(b) Sudden contraction

Figure 4.22: Loss coefficient vs. area ratio in circular ducts for sudden area change

Figure 4.22 shows the dependence of the loss coefficient K_t on the area ratio in the cases of sudden expansion and sudden contraction. For sudden area changes, there is no influence of the Reynolds number on the loss coefficient.

Chapter 5

Component's size and system performance at Design Point

In this chapter the results of the sizing calculations and the system performance at Design Point conditions, obtained as described in the previous chapter, are discussed.

5.1 Direct Ram Air Design Point

The avionics box thermal control system shall operate through the complete flight envelope of aircraft, at any subsonic and supersonic conditions.

As already said, the system working mode is controlled by the pressure switch installed at the turbine inlet:

- the Reverse Bootstrap operates when the pressure difference between the turbine inlet and the ambient is higher than 14 kPa;
- the Direct Ram Air operates when the pressure difference between the turbine inlet and the ambient is lower or equal to 14 kPa.

As Direct Ram Air design point has been stated the flight at 16000 m altitude, 1.1 Mach number, ISA+20 temperature.

In order to avoid duct choking when the system is working in Direct mode, a diffuser has been placed at the beginning of the by-pass duct. It has been sized so that the Mach number at diffuser exit, at Design Point conditions, is 0.25: in this way, compressibility effects are avoided.

The main parameters relevant to the Direct Ram Air design point are shown in Table 5.1.

Direct System - Design Point		Q = 400 W Thermal Load	
Altitude	16000 m	Ambient temperature	236.7 K
Station	Flow rate	Total temperature	Total pressure
	<i>kg/s</i>	<i>K</i>	<i>kPa</i>
Before shock	0.0111	293.9	26.22
After shock	0.0111	293.9	26.19
Diffuser inlet	0.0111	293.9	23.63
Diffuser outlet	0.0111	293.9	22.77
Avionics inlet	0.0111	293.9	22.09
Avionics outlet	0.0111	329.7	18.24
		Ambient pressure	12.28 kPa
		Enthalpy	Humidity
		<i>kJ/kg</i>	<i>g/kg</i>
		295.2	0
		295.2	0
		295.2	0
		295.2	0
		295.2	0
		331.2	0
		Free Moisture	<i>g/kg</i>
		0	0
		0	0
		0	0
		0	0
		0	0

Table 5.1: Direct System Design point

5.2 Reverse Bootstrap operation Design Point

Several information are available in the literature about studies and research on the ideal performance of the new commercial supersonic aircraft; of course, these include also the mission profiles associated to such aircraft. The profile shown in Figure 5.1 has been selected for the study developed in this thesis.

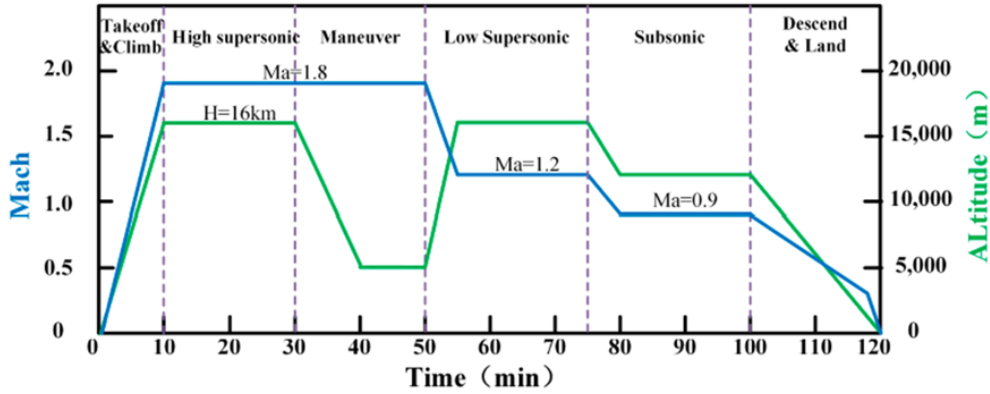


Figure 5.1: Typical mission profile of a modern supersonic aircraft

The following data have been set at Design Point:

Altitude	16000 <i>m</i>
Temperature	ISA+20
Flight Mach number	1.8
Humidity	0 <i>g/kg</i>
Avionics thermal load	500 <i>W</i>
Maximum avionics temperature	150°C

Table 5.2: Input parameters

5.2.1 Maximum avionics temperature

Excessive temperatures, above or below the limits the electronics is designed to work within, can cause problems from reduced reliability and service life to outright failure. In this thesis, the **IPC** standards for PCBs were consulted in order to define the maximum avionics temperature.

A **PCB** (Printed Circuit Board) is a medium used to connect electronic components to one another in a circuit: they consists of a flat sheet of insulating material and a layer of copper foil, laminated to the substrate.

IPC is a trade association aimed to standardize the assembly and production requirements of electronic equipment and assemblies, such as PCB's.

According to the IPC standards, class 3 PCBs can reach temperatures around 170°C. So, taking into account the thermal resistance of the avionics box faces, it has been chosen to set at design point the avionics box surface's maximum temperature to 150°C.

5.3 Shock wave and air intake

According to the conditions set at paragraph 5.2, we have the following data at the air intake station:

Total pressure before the shock	70.5	kPa
Total pressure after the shock	57.3	kPa
Total temperature before the shock	390	K
Total temperature after the shock	390	K
Flight Mach number	1.8	-
Mach number after the shock	0.616	-

Table 5.3: Shock wave and air intake parameters

The air mass flow rate needed to remove from the avionics the requested amount of heat, calculated as in paragraph 4.3.4.2, is:

$$\dot{m} = 0.0039 \text{ kg/s}$$

5.4 Air Cycle Machine (ACM)

5.4.1 Turbine

Size and thermodynamic parameters of the turbine, calculate as discussed in paragraphs 4.2.2 and 4.2.3, are reported in Table 5.4 and in Figures 5.3 and 5.4. The triangles of velocity at inlet and exhaust are shown in Figures 5.5 and 5.6.

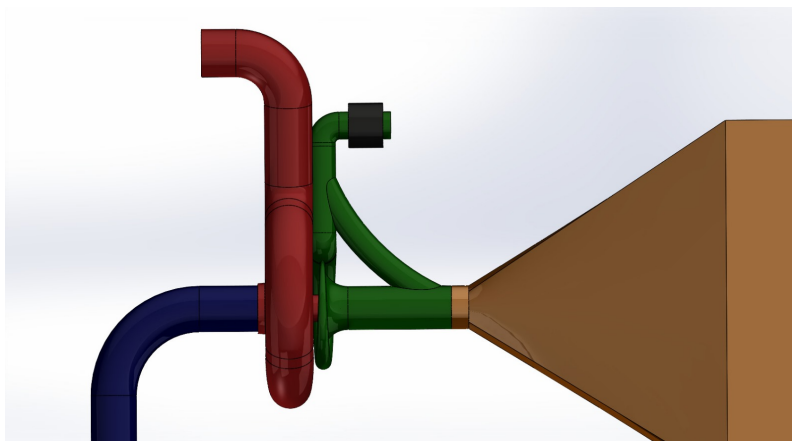


Figure 5.2: Air Cycle Machine CAD design

5.4. AIR CYCLE MACHINE (ACM)

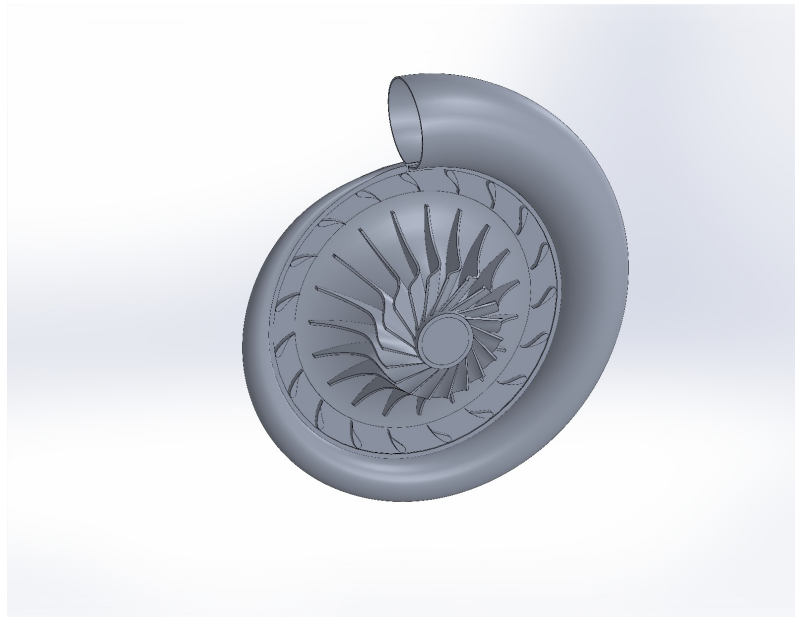


Figure 5.3: Turbine CAD design

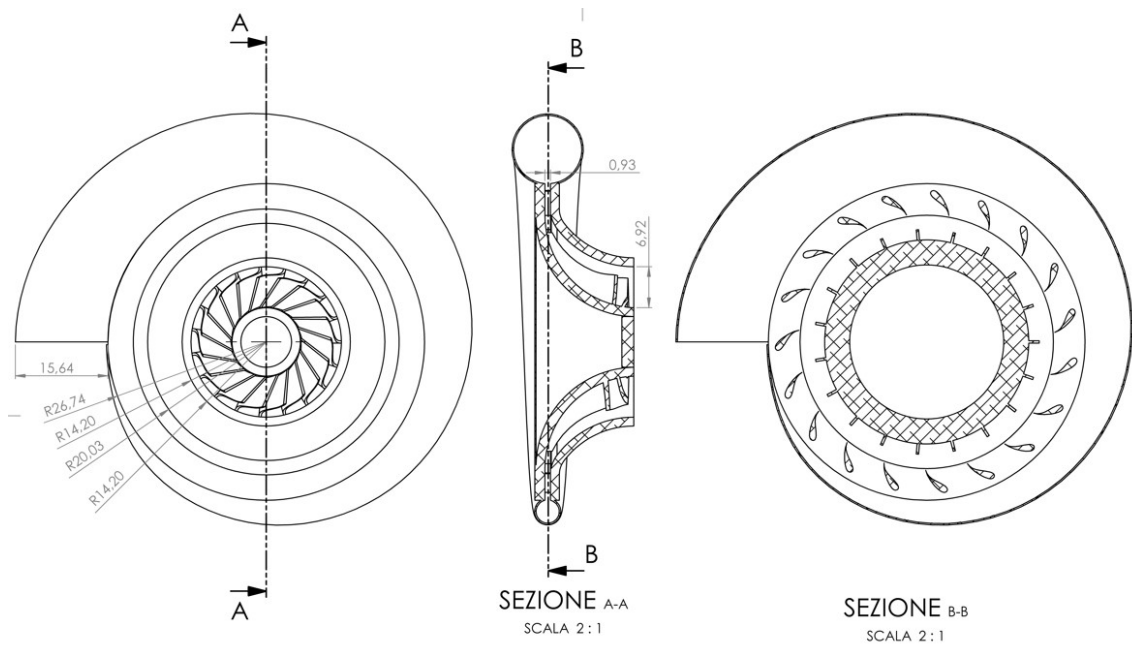


Figure 5.4: Turbine sections

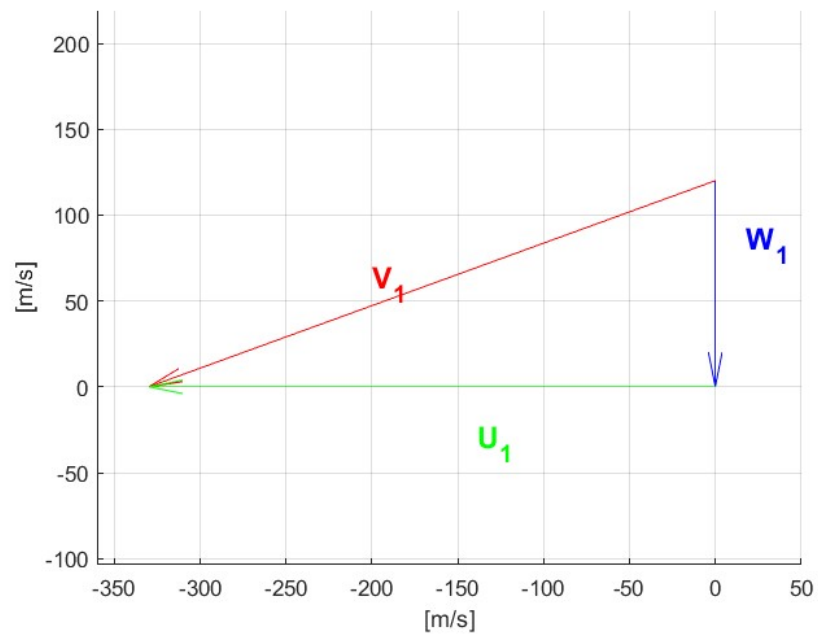


Figure 5.5: Triangles of velocity at turbine inlet

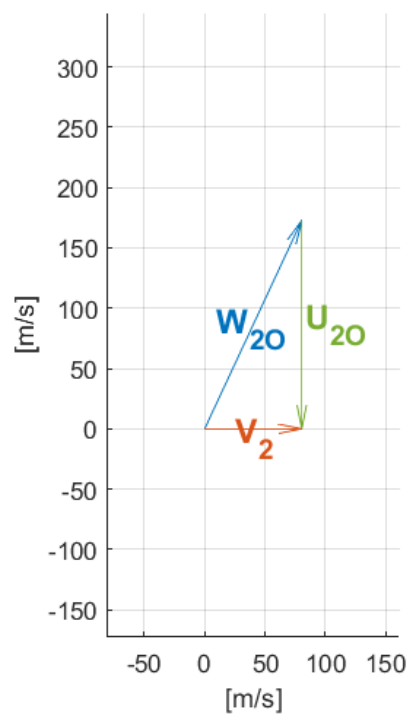


Figure 5.6: Triangles of velocity at turbine exhaust

5.4. AIR CYCLE MACHINE (ACM)

Turbine power	422.2	W
Rotational speed	147290	rpm
Expansion ratio	4.21	-
Total inlet pressure	51.7	kPa
Total exhaust pressure	15.3	kPa
Total inlet temperature	390	K
Total exhaust temperature	281.6	K
Inlet Mach number	0.616	-
Absolute speed angle at rotor inlet	70	°
Peripheral speed at rotor inlet	329.9	m/s
Rotor inlet absolute speed	351.1	m/s
Rotor inlet relative speed	120.1	m/s
Rotor inlet radial speed	120.1	m/s
Rotor inlet tangential speed	329.9	m/s
Peripheral speed at rotor exit (outer radius)	172.7	m/s
Rotor exit absolute speed (outer radius)	80.6	m/s
Rotor exit relative speed (outer radius)	190.6	m/s
Rotor exit radial speed	0	m/s
Rotor exit tangential speed	0	m/s
Relative speed angle at rotor exit	65	°
Exit Mach number	0.240	-
Total/static efficiency	0.825	-
Total/total efficiency	0.846	-
Number of rotor blades	17	-
Number of stator vanes	19	-

Table 5.4: Turbine parameters

5.4.2 Compressor

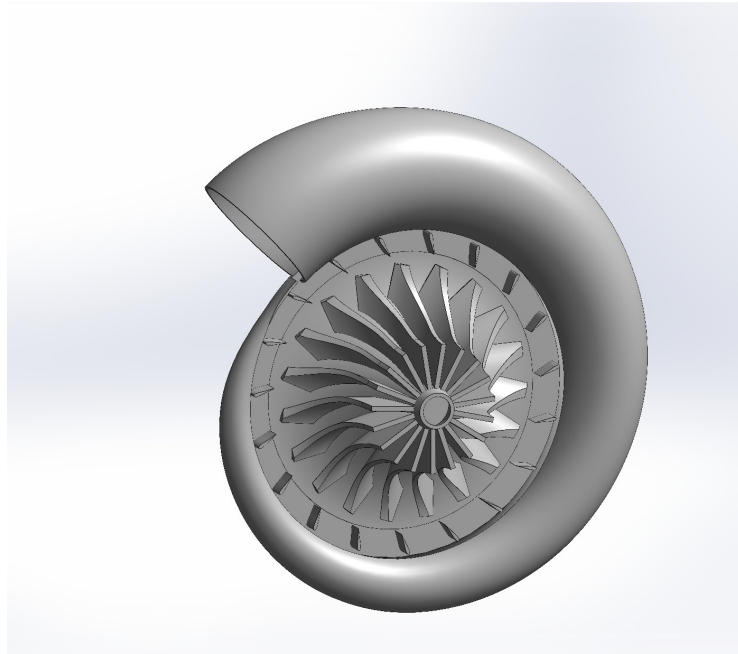


Figure 5.7: Compressor CAD design

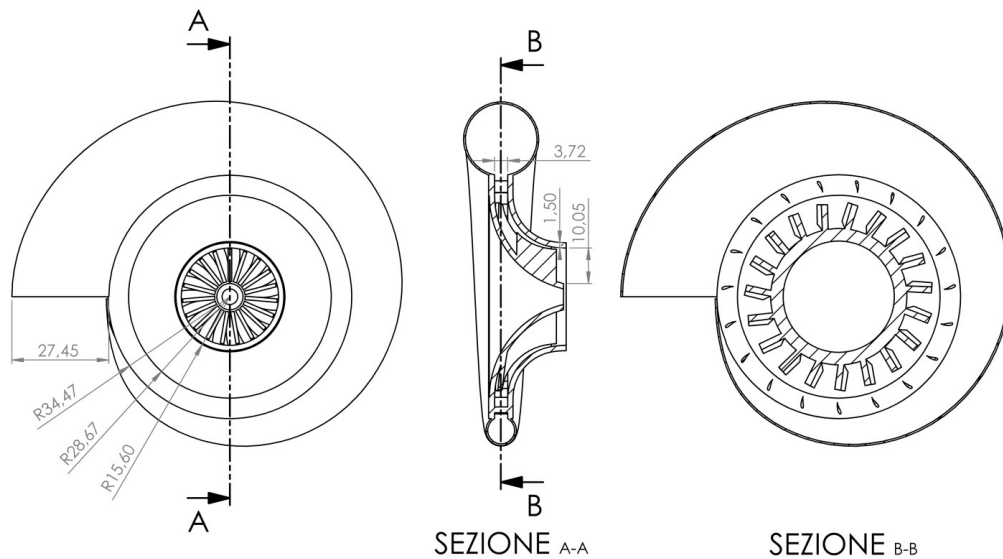


Figure 5.8: Compressor sections

Size and thermodynamic parameters of the compressor, calculate as discussed in paragraphs 4.4.2 and 4.4.3, are reported in Table 5.5 and in Figures 5.7 and 5.8. The triangles of velocity at inlet and exhaust are shown in Figures 5.9 and 5.10.

5.4. AIR CYCLE MACHINE (ACM)

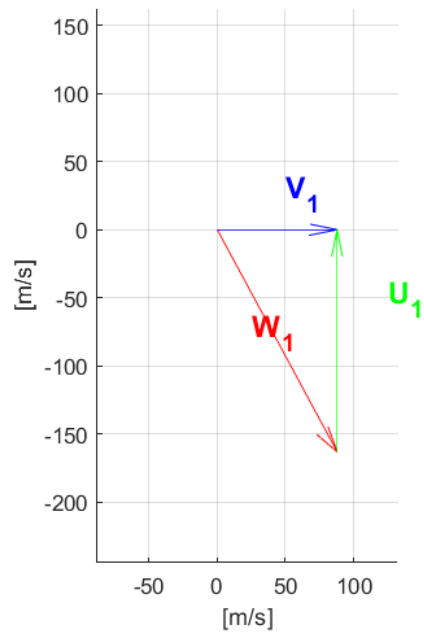


Figure 5.9: Triangles of velocity at compressor inlet

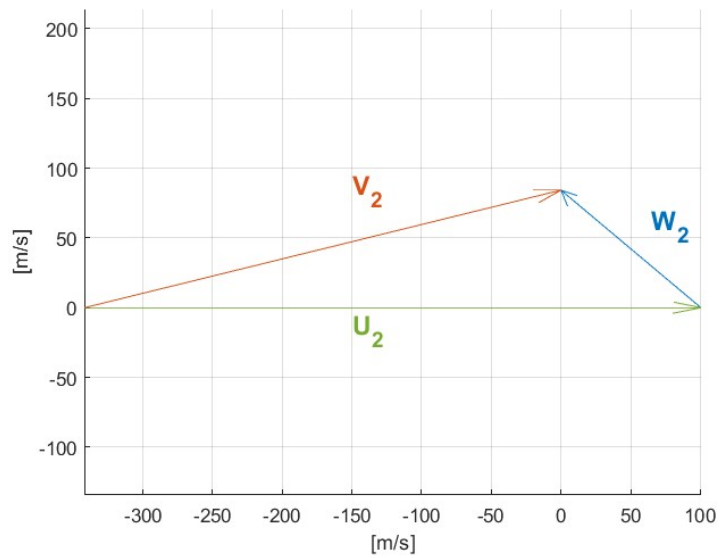


Figure 5.10: Triangles of velocity at compressor exhaust

Compressor power	422.2	W
Rotational speed	147290	rpm
Compression ratio	1.840	-
Total inlet pressure	9.1	kPa
Total exhaust pressure	16.7	kPa
Total inlet temperature	409.9	K
Total exhaust temperature	518.3	K
Inlet Mach number	0.218	-
Absolute speed angle at rotor inlet	0	°
Peripheral speed at rotor inlet (mean radius)	162.8	m/s
Rotor inlet absolute speed (mean radius)	87.9	m/s
Rotor inlet relative speed (mean radius)	185.1	m/s
Rotor inlet radial speed (mean radius)	0	m/s
Rotor inlet tangential speed (mean radius)	0	m/s
Peripheral speed at rotor exit	442.2	m/s
Rotor exit absolute speed	352.1	m/s
Rotor exit relative speed	131.0	m/s
Rotor exit radial speed	84.2	m/s
Rotor exit tangential speed	341.9	m/s
Relative speed angle at rotor exit	50	°
Slip factor	0.889	-
Exit Mach number	0.822	-
Total/static efficiency	0.568	-
Total/total efficiency	0.72	-
Number of rotor blades	19	-
Number of stator vanes	21	-

Table 5.5: Compressor parameters

5.5 Avionics box

5.5.1 Configuration

In the following figures, avionics box size and configuration are represented:

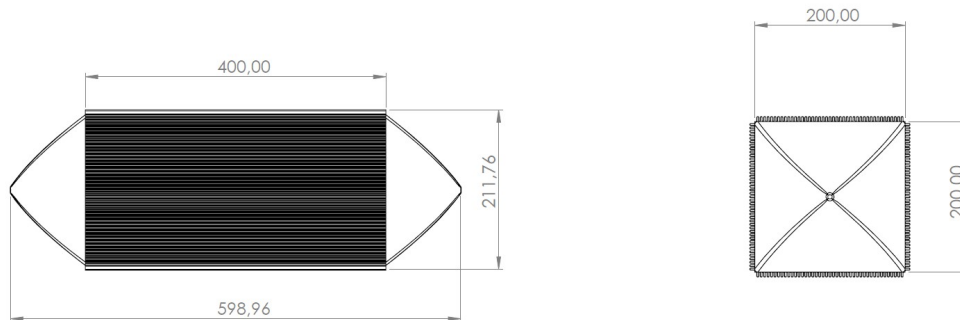


Figure 5.11: Avionics box sizes

5.5. AVIONICS BOX

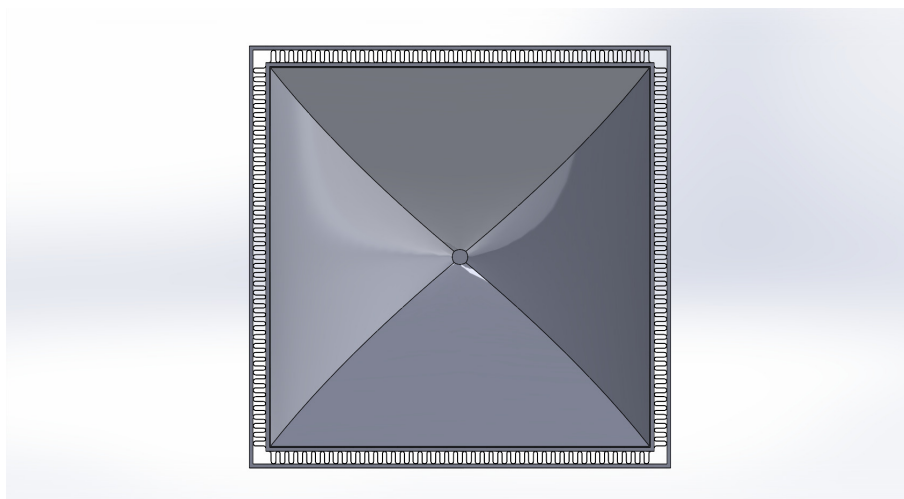


Figure 5.12: Avionics box CAD section

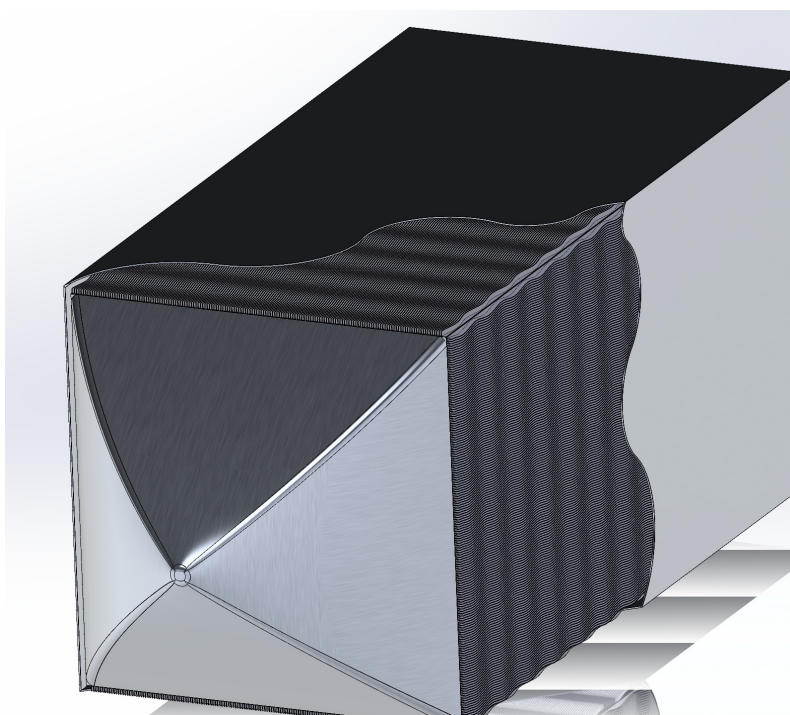


Figure 5.13: Avionics box cut view

5.5.2 Thermal parameters

The thermal parameters of the avionics box, calculated as discussed in paragraph 4.3, are reported in Table 5.6.

Heat load	500	W
Mass flow rate	0.0039	kg/s
Maximum avionics temperature	150	°C
Inlet total pressure	12.49	kPa
Exhaust total pressure	10.57	kPa
Inlet total temperature	281.6	K
Exhaust total temperature	409.9	K

Table 5.6: Avionics box parameters

5.5.3 Fin selection

The geometrical parameters of the fins designed for this application are reported in Table 5.7.

Hydraulic radius	0.378	mm
Fin height	2.70	mm
Fin thickness	0.150	mm
Fin spacing	1.20	mm
Fin wavelength	9.50	mm
Wave amplitude	0.985	mm
Transfer area/Volume between plates	2645.5	m^{-1}
Fin area/Total area	0.72	-

Table 5.7: Fin parameters

5.6 Connecting pipes

Size and pressure losses parameters of the connecting pipes, calculate as discussed in paragraph 4.5.1, are reported in Table 5.8.

From intake to turbine inlet	5%	
From turbine exhaust to avionics box inlet		
Inlet pressure	15.32	kPa
Exhaust pressure	12.49	kPa
$\Delta p/p$	18.5%	
From avionics box exhaust to compressor inlet		
Inlet pressure	10.57	kPa
Exhaust pressure	9.09	kPa
$\Delta p/p$	14%	

Table 5.8: Connecting pipes pressure losses

5.7 Complete system size and mass

The complete Avionics Box Thermal Control System is shown in Figure 5.14. The maximum envelope sizes are 0.983 m x 0.340 m x 0.207 m. As far as possible, the components are made of light alloy material.

However, due to the combination of temperatures and forces involved, acting on the compressor, imposes that this component shall be done in titanium alloy.

A detailed stress analysis and associated material selection is outside the purposes of this thesis.

The expected mass of the complete system (excluding the Avionics Box mass) is 1.995 kg. Each component mass is showed in table 5.9.

Therefore, if such a system were to be designed as part of the creation of a unit to be used in flight operations (development or exercise), an accurate stress analysis must be developed and an appropriate fabrication process shall be adopted in order to reach the minimum weight at the safest operating conditions.

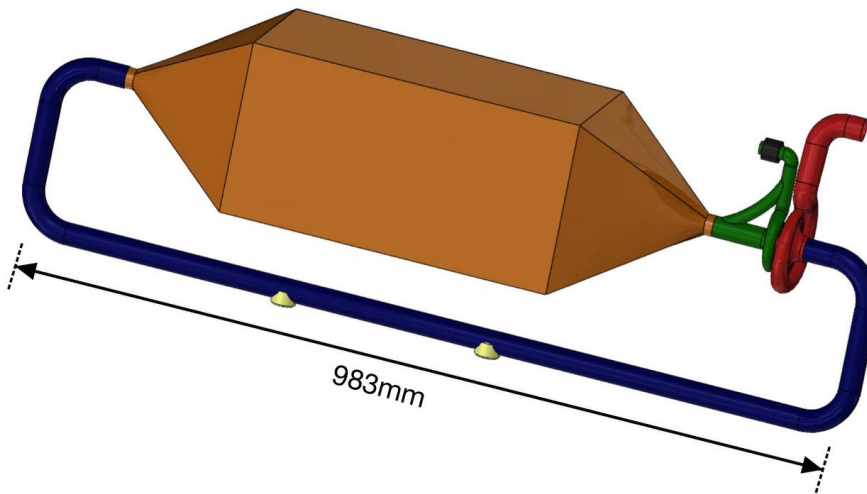


Figure 5.14: Avionics Box Thermal Control System CAD design

Component	Mass [kg]
Air Cycle Machine	0.268
Avionics box casing + fins	1.250
Water collector	0.075
Ducts	0.401

Table 5.9: Components mass

5.8 System performance at Design Point with Reverse Bootstrap operating

The thermodynamic cycle of the Reverse Bootstrap system object of the present thesis is reported in Figure 5.15 on the Temperature-Entropy plane. Stations from 0 to 6 are referred to the total conditions, while stations *amb* (ambient) and *e* (exhaust) are referred to the static conditions.

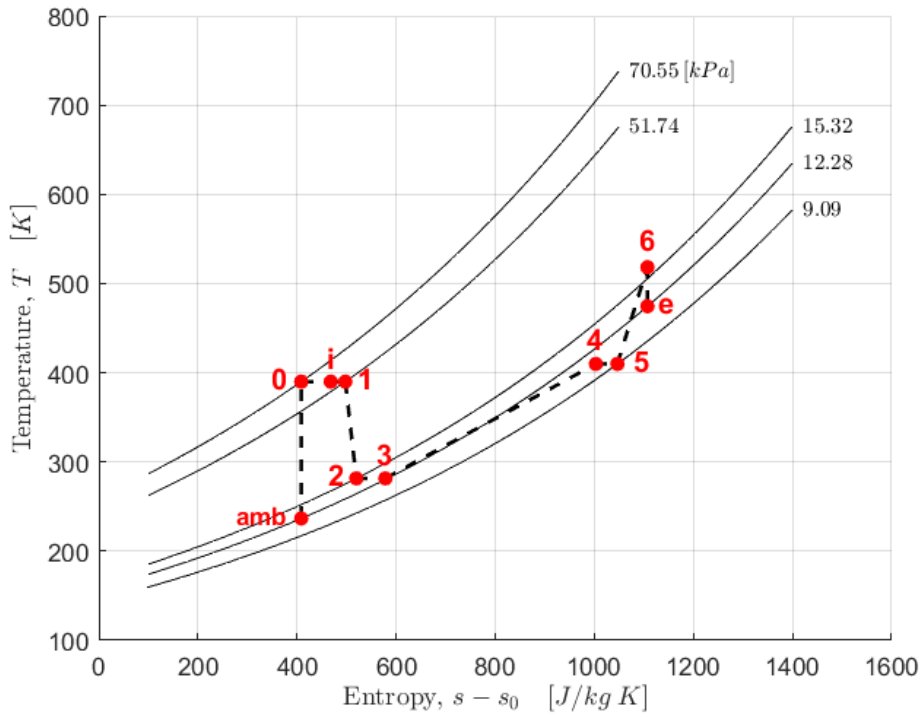


Figure 5.15: Thermodynamic cycle on the Temperature-Entropy plane

Station nomenclature

- *amb*: static ambient;
- *0*: environmental conditions;
- *i*: after shock;
- *1*: turbine inlet;
- *2*: turbine outlet;
- *3*: avionics box inlet;
- *4*: avionics box outlet;
- *5*: compressor inlet;
- *6*: compressor outlet;
- *e*: exhaust.

Reverse Bootstrap System - Design Point			Q = 500 W Thermal Load			
Altitude	16000 m	Ambient temperature	236.7 K	Ambient pressure	12.28 kPa	
Station	Flow rate <i>kg/s</i>	Total temperature <i>K</i>	Total pressure <i>kPa</i>	Enthalpy <i>kJ/kg</i>	Humidity <i>g/kg</i>	Free Moisture <i>g/kg</i>
Before shock	0.0039	390	70.55	391.75	0	0
After shock	0.0039	390	57.33	391.75	0	0
Turbine inlet	0.0039	390	51.74	391.75	0	0
Turbine outlet	0.0039	281.6	15.32	282.87	0	0
Avionics inlet	0.0039	281.6	12.49	282.87	0	0
Avionics outlet	0.0039	409.9	10.57	411.74	0	0
Compressor inlet	0.0039	409.9	9.09	411.74	0	0
Compressor outlet	0.0039	518.3	16.73	520.63	0	0
			TURBINE			
Pressure ratio	4.21	Power		422.2 W	Corrected speed	126572 rpm
Efficiency	0.825	Corrected flow		$0.0400 \frac{kg/s \sqrt{K}}{N}$	Mechanical speed	147290 rpm
			COMPRESSOR			
Pressure ratio	1.84	Power		422.2 W	Corrected speed	133442 rpm
Efficiency	0.72	Corrected flow		0.0516 <i>kg/s</i>	Mechanical speed	147290 rpm

Table 5.10: Reverse Bootstrap system Design point

Chapter 6

Off Design Point conditions

The present Avionics Box Thermal Control System has been sized according to the input shown in Table 5.2. Among these values, the avionics thermal load is 25% higher than the actual load in the same flight conditions. Following this approach, the sized system easily meets the actual requirements at any point of the flight envelope.

The Off-Design cases for which the system performances have been checked are shown in Table 6.1. A content of water vapor has been assumed in a few cases at different flight altitudes. This is specified in the following tables; in such cases, Wet Air Rated and Dry Air Rated Temperatures at turbine exhaust have been calculated, together with the associated liquid flow and moisture.

	Case 1	Case 2	Case 3
Altitude	16000 m	16000 m	5000 m
Temperature	ISA+20	ISA+20	ISA+20
Flight Mach number	1.8	1.2	1.8
Humidity	0 g/kg	0 g/kg	10.7 g/kg
Thermal load	400 W	400 W	1150 W
Maximum air temperature at avionics exhaust	170 °C	170 °C	170 °C

Table 6.1: Off Design conditions - Air cycle operation

	Case 4	Case 5
Altitude	12000 m	3000 m
Temperature	ISA+20	ISA+20
Flight Mach number	0.9	0.3
Humidity	0 g/kg	20 g/kg
Thermal load	400 W	1300 W
Maximum air temperature at avionics exhaust	170 °C	170 °C

Table 6.2: Off Design conditions - Direct cycle operation

6.1 Off Design point calculation procedure

In this section, the steps followed to calculate the system working point and performance at Off Design conditions are described. In the case of Direct cycle operation, the airflow will bypass the turbomachines, so the iteration process would not be needed.

1. Define the operating conditions:
 - Altitude
 - Temperature
 - Mach
 - Humidity
 - Thermal load
 - Max air temperature at avionics exhaust
2. Tentative assumptions:
 - Turbine corrected speed $N/\sqrt{\theta_T}$ (where $\theta_T = T_1^0/T_{st}$)
 - Turbine total-to-static expansion ratio $\beta_{T,ts}$
3. Enter turbine map shown in Figure 6.2 with $N/\sqrt{\theta_T}$ and $\beta_{T,ts}$, in order to find the corrected mass flow rate $\dot{m}\sqrt{T_1^0}/p_1^0 A_{th}$ (where A_{th} is the turbine throttling area);
4. Enter turbine map shown in Figure 6.1 with the corrected speed and $\beta_{T,ts}$ in order to find the turbine efficiency $\eta_{T,ts}$;
5. Calculate flow rate \dot{m} , speed N and turbine power;
6. Calculate compressor inlet conditions (ducts and avionics calculations are the same as the Design point);
7. Calculate the corresponding compression ratio that the compressor will have to provide;
8. Calculate compressor corrected speed N/θ_C and corrected mass flow rate $\dot{m}\sqrt{\theta_C}/\delta_C$ (where $\theta_C = T_5^0/T_{st}$ and $\delta_C = p_5^0/p_{st}$);
9. Enter compressor map in Figure 6.3 with N/θ_C and $\dot{m}\sqrt{\theta_C}/\delta_C$, so the compression ratio β_C can be found;
10. Enter compressor map in Figure 6.4 with N/θ_C and $\dot{m}\sqrt{\theta_C}/\delta_C$, obtaining the corrected adiabatic head $H_{ad}/\theta_C\eta_C$;
11. Calculate the adiabatic head H_{ad} from its definition (as in formula (4.117));
12. Since H_{ad} , θ_C and the corrected adiabatic head are known, the adiabatic efficiency of the compressor η_C can be calculated;
13. Calculate the power absorbed by the compressor;

6.1. OFF DESIGN POINT CALCULATION PROCEDURE

14. Compare the powers calculated in points 5 and 13 and the compression ratios obtained in points 7 and 9, noting the respective errors;
15. Iterate on the values of $N/\sqrt{\theta_T}$ and $\beta_{T,ts}$ assumed in point 2 until the errors highlighted in point 14 are within the tolerances. The iteration process is described in detail in Appendix C.

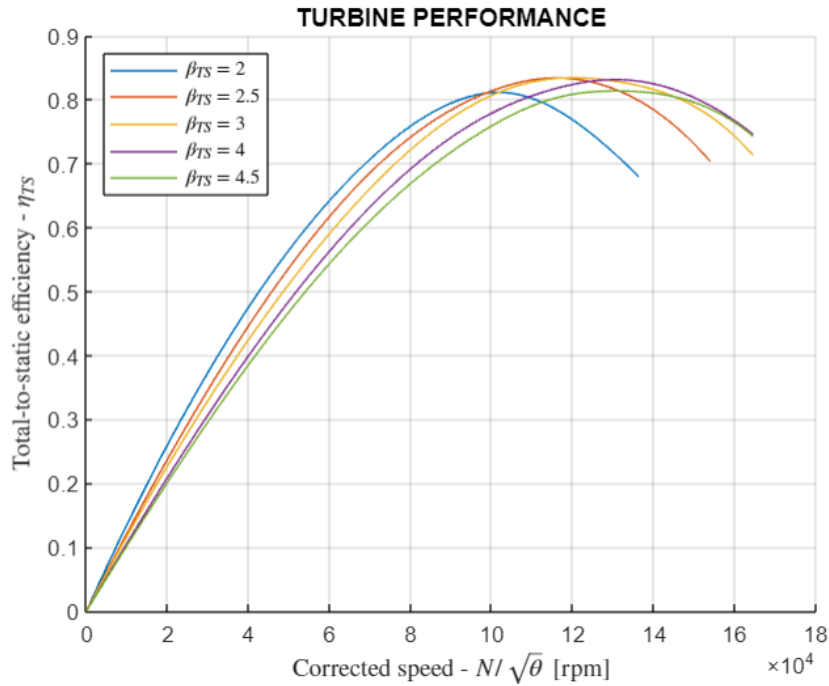


Figure 6.1: Turbine efficiency vs. Corrected speed

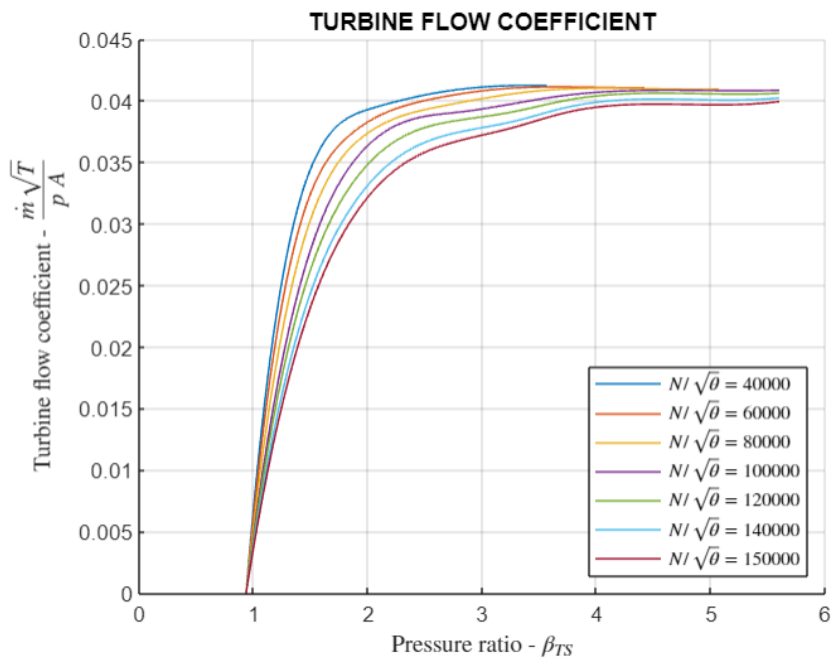


Figure 6.2: Turbine corrected mass flow vs. Expansion ratio

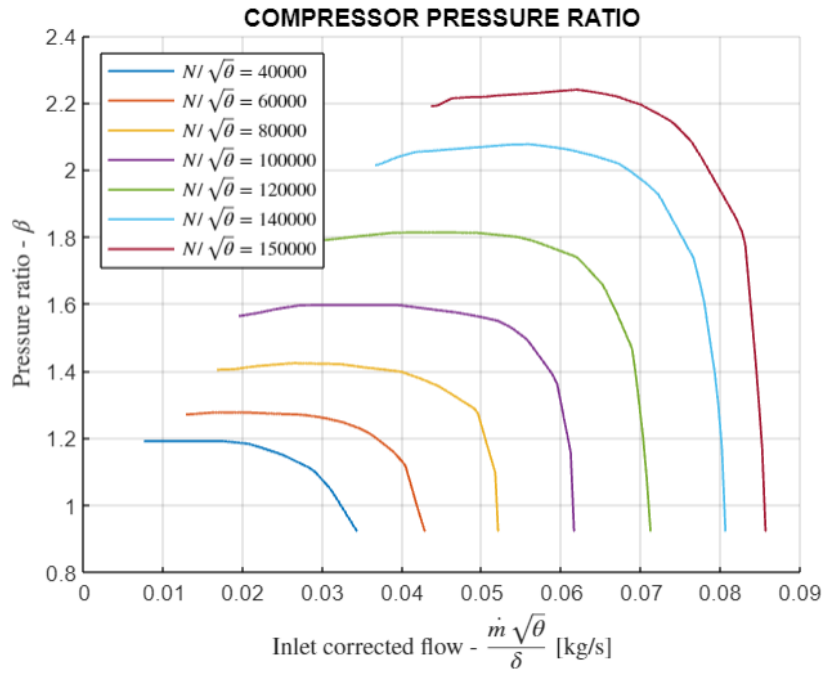


Figure 6.3: Compressor pressure ratio vs. Corrected mass flow

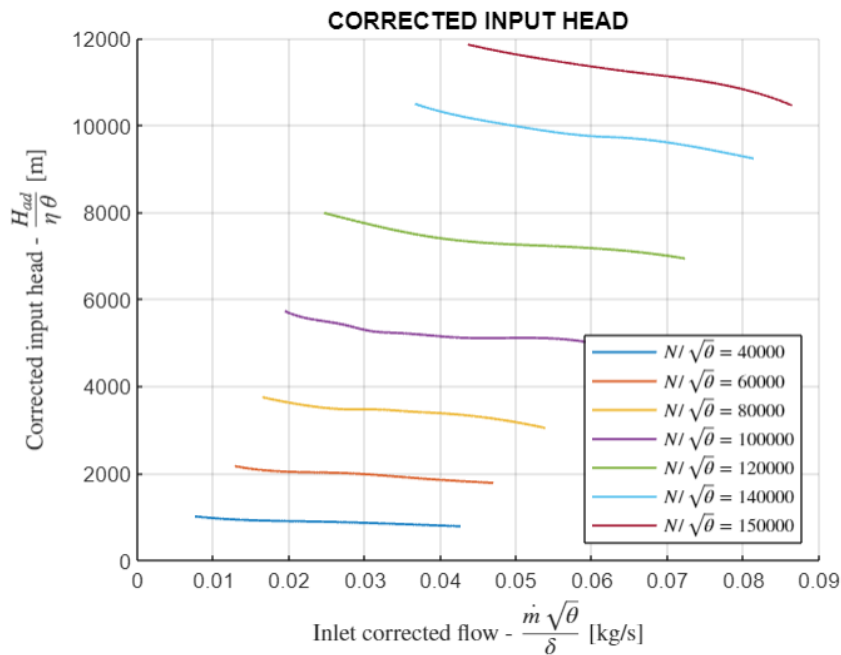


Figure 6.4: Compressor corrected head vs. Corrected mass flow

6.1.1 Impact of Humidity on the Turbine Exhaust Temperature

Among the Off-Design cases reported in Table 6.1, case n.3, being at an altitude of 5000 m, is a flight in humid air. The absolute humidity in these conditions, according to Figure 4.1 is 10.7 g/kg.

In these conditions, condensation of the water vapor could occur during expansion in the turbine, as already discussed in paragraph 4.1.1.1, with a consequent increase

6.1. OFF DESIGN POINT CALCULATION PROCEDURE

in the temperature at the turbine exhaust/avionics box inlet and the presence of liquid water. The procedure for calculating the air temperature and water flow rate at the turbine exhaust is reported in Appendix D.

In our case, following the procedure in Appendix D, we obtain that the saturation humidity in the given conditions of temperature and pressure at the turbine exhaust is $U_{sat} = 25.5$ g/kg which is clearly greater than the absolute humidity in ambient air. Since this absolute humidity remains constant in the evolution of the humid air in the Reverse Bootstrap system, we must conclude that in this case there is no condensation of the vapor, there is no increase in temperature, nor the presence of liquid water.

If, however, the combination of parameters characterizing the case under study had been such that the absolute humidity at the turbine exhaust was greater than the saturation humidity, we would have had a higher temperature and free water.

In order to demonstrate that the system can work also in presence of liquid water condensed in the turbine, another Off-Design case, not belonging to the flight envelope, has been analysed. In the selected flight conditions, the system works in Reverse Bootstrap mode, and the high ambient humidity leads to vapor condensation in the turbine.

Inputs of this Off-Design point are showed in Table 6.3.

Altitude	0 m
Temperature	ISA+20
Flight Mach number	0.6
Humidity	26 g/kg
Thermal load	1500 W
Maximum air temperature at avionics exhaust	170°C

Table 6.3: Off-Design case with vapor condensation

Following the procedure reported in Appendix D, it has been calculated that, in this conditions, the saturation humidity at the turbine exhaust is $U_{sat} = 11.2$ g/kg, significantly lower than the ambient humidity. This leads to the condensation of water vapor in the turbine, with a consequent presence of liquid water ($L = 14.8$ g/kg) at the turbine exhaust.

The temperature of the air exiting the turbine ($T_{WET} = -2.3^\circ\text{C}$) is significantly higher than the T_{DAR} (the temperature achieved by the air if the carried water could totally re-evaporate), which reaches $T_{DAR} = -37.5^\circ\text{C}$.

Because of the temperature control at the turbine exhaust, the humid air enters the Avionics box at 2°C .

However, it has been demonstrated that the air, in this conditions, can still refrigerate the Avionics box, without exceeding the maximum allowed temperature: according to the calculations, the humid air, at the Avionics box exhaust has a temperature of 150.5°C , which is within the safe range.

It is important to reiterate that this calculations do not take into account the re-evaporation (partial or entire) of the liquid water in the gap around the Avionics box. As discussed in paragraph 4.2.2.1, this is a conservative assumption, since it does not consider the latent evaporation heat removed from the air and the consequent reduction of its temperature.

6.2 Performances at Off Design points

The operative points concerning the three Off-Design cases object of study are shown in Figures from 6.5 to 6.8. Then, the system performance in all these cases are described in Tables from 6.4 to 6.8.

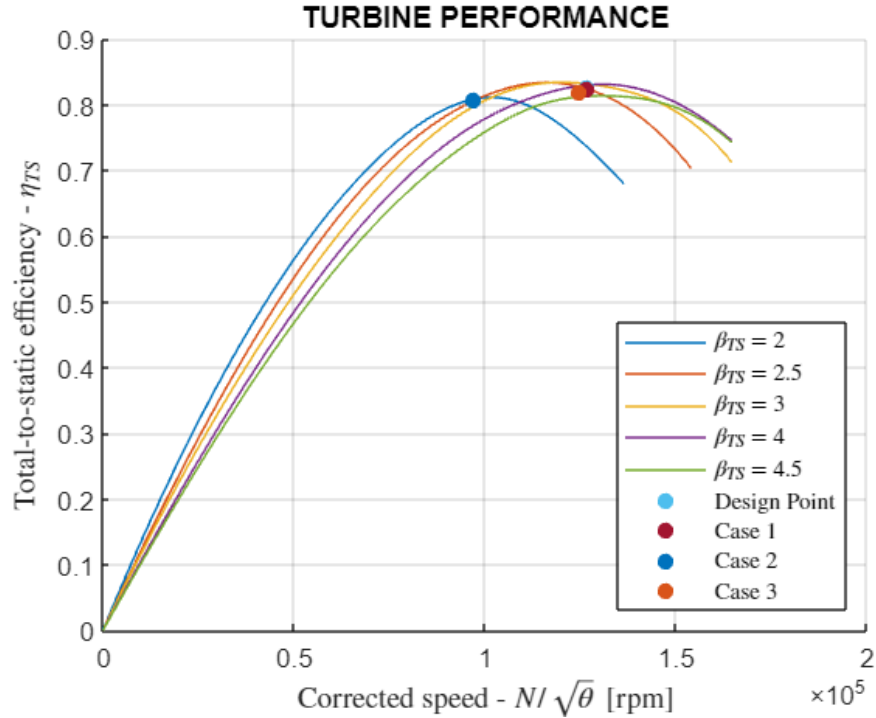


Figure 6.5: Turbine Performance at Off-Design conditions

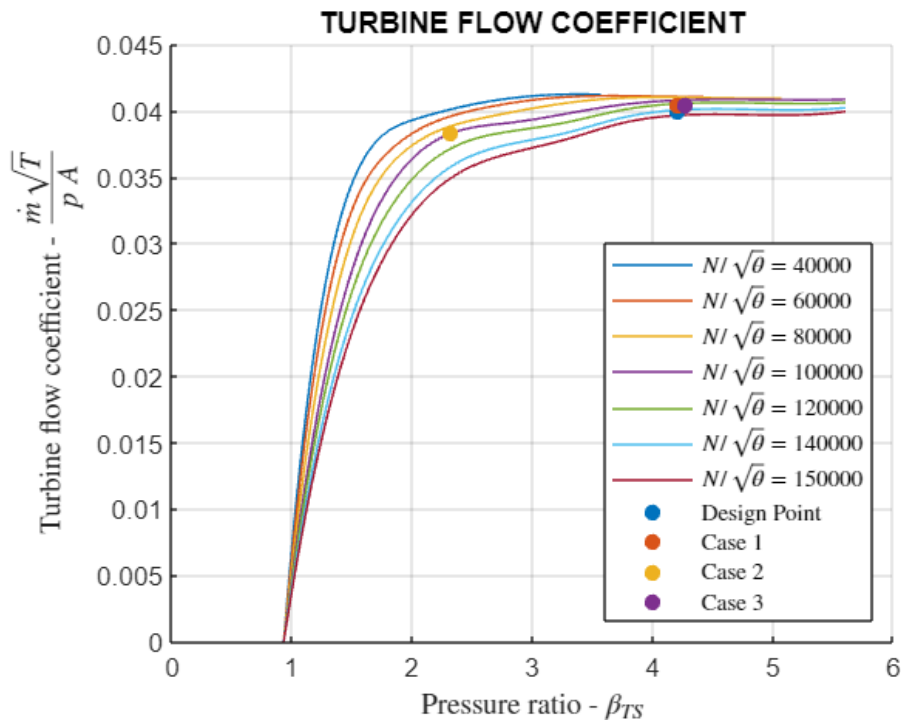


Figure 6.6: Turbine Flow Coefficient at Off-Design conditions

6.2. PERFORMANCES AT OFF DESIGN POINTS

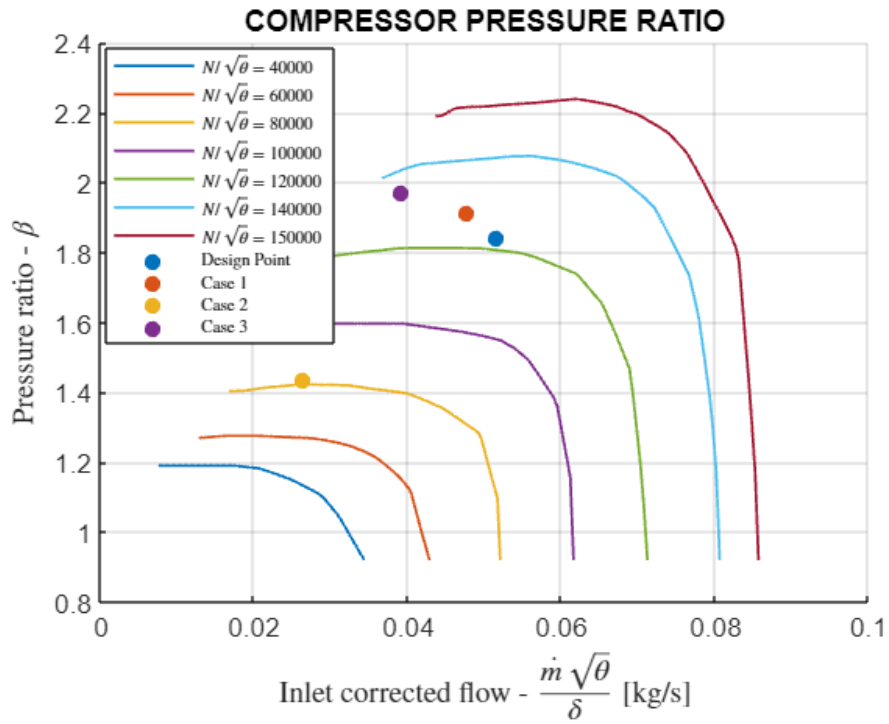


Figure 6.7: Compressor Pressure Ratio at Off-Design conditions

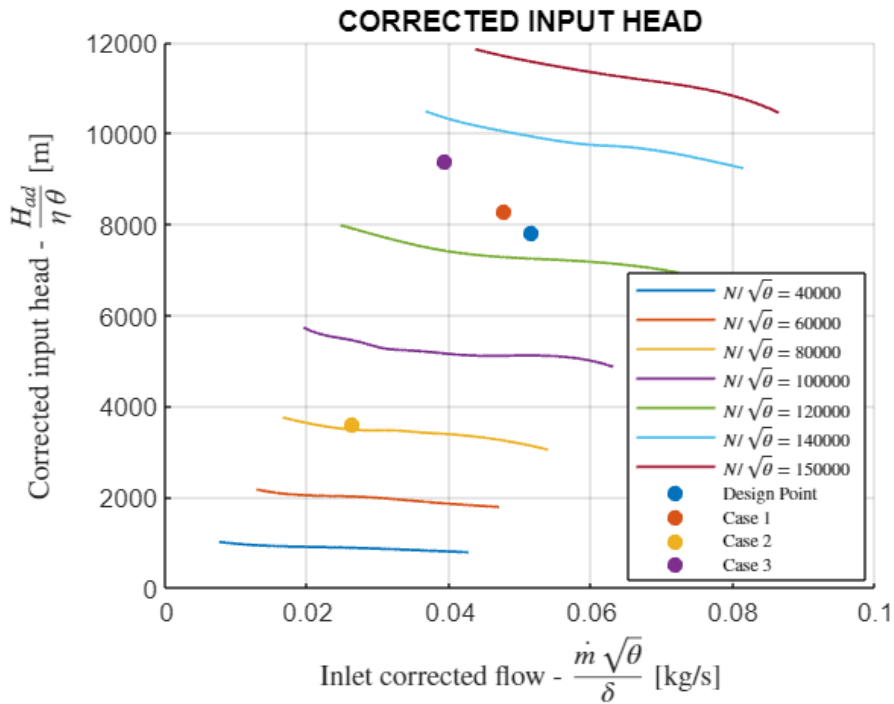


Figure 6.8: Corrected Adiabatic Head at Off-Design conditions

Reverse Bootstrap System - Case 1**Q = 400 W Thermal Load**

Station	Flow rate	Total temperature	Total pressure	Enthalpy	Humidity	Free Moisture
	<i>kg/s</i>	<i>K</i>	<i>kPa</i>	<i>kJ/kg</i>	<i>g/kg</i>	<i>g/kg</i>
Altitude	16000 m	Ambient temperature	236.7 K	Ambient pressure	12.28 kPa	
Before shock	0.0039	390	70.55	391.7	0	0
After shock	0.0039	390	57.33	391.7	0	0
Turbine inlet	0.0039	390	51.74	391.7	0	0
Turbine outlet	0.0039	281.9	12.79	283.2	0	0
Avionics inlet	0.0039	281.9	12.72	283.2	0	0
Avionics outlet	0.0039	383.7	10.91	385.4	0	0
Compressor inlet	0.0039	383.7	9.59	385.4	0	0
Compressor outlet	0.0039	491.4	18.34	493.6	0	0
TURBINE						
Pressure ratio	4.21	Power	424.8 W	Corrected speed	126572 rpm	
Efficiency	0.823	Corrected flow	0.0404 $\frac{kg/s\sqrt{K}}{N}$	Mechanical speed	147290 rpm	
COMPRESSOR						
Pressure ratio	1.91	Power	424.8 W	Corrected speed	127610 rpm	
Efficiency	0.725	Corrected flow	0.0477 $\frac{kg/s}{N}$	Mechanical speed	147290 rpm	

Table 6.4: Reverse Bootstrap - Off design Case 1

Reverse Bootstrap System - Case 2

Altitude 16000 m

Q = 400 W Thermal Load

Ambient temperature 236.7 K Ambient pressure 12.28 kPa

Station	Flow rate <i>kg/s</i>	Total temperature <i>K</i>	Total pressure <i>kPa</i>	Enthalpy <i>kJ/kg</i>	Humidity <i>g/kg</i>	Free Moisture <i>g/kg</i>
Before shock	0.0022	304.8	29.77	306.2	0	0
After shock	0.0022	304.8	29.56	306.2	0	0
Turbine inlet	0.0022	304.8	26.68	306.2	0	0
Turbine outlet	0.0022	252.2	11.74	253.3	0	0
Avionics inlet	0.0022	252.2	11.69	253.3	0	0
Avionics outlet	0.0022	435.8	10.78	437.8	0	0
Compressor inlet	0.0022	435.8	10.26	437.8	0	0
Compressor outlet	0.0022	488.8	14.70	491.0	0	0

TURBINE

Pressure ratio	2.32	Power	114.7 W	Corrected speed	97138 rpm
Efficiency	0.807	Corrected flow	$0.0384 \frac{kg/s\sqrt{K}}{N}$	Mechanical speed	99932 rpm

COMPRESSOR

Pressure ratio	1.43	Power	114.7 W	Corrected speed	81240 rpm
Efficiency	0.890	Corrected flow	0.0263 kg/s	Mechanical speed	99932 rpm

Table 6.5: Reverse Bootstrap - Off design Case 2

Reverse Bootstrap System - Case 3**Q = 1150 W Thermal Load**

Station	Altitude	Flow rate	Ambient temperature	Total temperature	Total pressure	Ambient pressure	Enthalpy	Humidity	Free Moisture
	5000 m	kg/s	K	K	kPa	kPa	kJ/kg	g/kg	g/kg
Before shock		0.0168	460.7	328.7	328.7	471.8	10.7	0	
After shock		0.0168	460.7	267.7	267.7	471.8	10.7	0	
Turbine inlet		0.0168	460.7	241.6	241.6	471.8	10.7	0	
Turbine outlet		0.0168	329.7	58.64	58.64	337.6	10.7	0	
Avionics inlet		0.0168	329.7	58.36	58.36	337.6	10.7	0	
Avionics outlet		0.0168	396.3	55.64	55.64	405.8	10.7	0	
Compressor inlet		0.0168	396.3	51.15	51.15	405.8	10.7	0	
Compressor outlet		0.0168	527.1	101.1	101.1	539.7	10.7	0	
TURBINE									
Pressure ratio	4.29		Power	2260 W		Corrected speed	124376 rpm		
Efficiency	0.819		Corrected flow	0.0405 $\frac{kg/s\sqrt{K}}{N}$		Mechanical speed	157303 rpm		
COMPRESSOR									
Pressure ratio	1.98		Power	2260 W		Corrected speed	134091 rpm		
Efficiency	0.670		Corrected flow	0.0391 kg/s		Mechanical speed	157303 rpm		

Table 6.6: Reverse Bootstrap - Off design Case 3

Direct System - Case 4		Q = 400 W Thermal Load				
Altitude	12000 m	Ambient temperature	236.7 K	Ambient pressure	21.88 kPa	
Station	Flow rate	Total temperature	Total pressure	Enthalpy	Humidity	Free Moisture
	<i>kg/s</i>	<i>K</i>	<i>kPa</i>	<i>kJ/kg</i>	<i>g/kg</i>	<i>g/kg</i>
Before shock	0.0163	275.0	37.00	295.2	0	0
After shock	-	-	-	-	-	-
Diffuser inlet	0.0163	275.0	33.40	295.2	0	0
Diffuser outlet	0.0163	275.0	32.39	295.2	0	0
Avionics inlet	0.0163	275.0	31.45	295.2	0	0
Avionics outlet	0.0163	299.5	27.52	331.2	0	0

Table 6.7: Direct system - Off design Case 4

Direct System - Case 5		Ambient temperature		Ambient pressure		Q = 1300 W Thermal Load	
Station	Flow rate	Total temperature	Total pressure	Enthalpy	Humidity	Free Moisture	
	<i>kg/s</i>	<i>K</i>	<i>kPa</i>	<i>kJ/kg</i>	<i>g/kg</i>	<i>g/kg</i>	
Altitude	3000 m		288.7 K		72.62 kPa		
Before shock	0.0162	294.2	77.40	306.3	20	0	
After shock	-	-	-	-	-	-	
Diffuser inlet	0.0162	294.2	69.85	306.3	20	0	
Diffuser outlet	0.0162	294.2	69.47	306.3	20	0	
Avionics inlet	0.0162	294.2	69.00	306.3	20	0	
Avionics outlet	0.0162	371.4	66.98	386.6	20	0	

Table 6.8: Direct system - Off design Case 5

Chapter 7

Reliability

The Reliability [33] of any device is the probability that it will work correctly for a given time and under certain specified conditions. The definition of mission is fundamental in determining of reliability: a long operating time or severe conditions lower the level of reliability.

Any product or process is characterized by its reliability, whatever its complexity. A simple object or a system made up of several components, or a complicate organization can be analyzed at level of each single component/activity or can be viewed as a unitary entity if detailed study is not of interest.

Reliability, like performance, weight, volume, etc., plays a key role and must therefore be developed from the earliest stages of a design study, growing and developing with the project. Finally, it becomes increasingly important to ensure safety with maintenance activities during operation.

7.1 Types of reliability

Several definitions of reliability exist:

Logistical reliability probability of failures not occurring (for a certain time under certain conditions);

Dispatch reliability probability of failures not occurring (for a certain amount of time under certain conditions) that prevent the departure on time;

Mission reliability probability that for a given (started) mission no failure will occur that prevents its achievement;

Security probability of dangerous failures not occurring (for a certain time under certain conditions)

In this chapter, a logistical methodology will be adopted, studying the time the system can remain in service without failures.

7.2 Mean Time Between Failures (MTBF) and Failure Rate (λ)

The MTBF, is a critical reliability indicator which has wide application in maintenance management. This value represents the expected period between the start of one failure and the start of the next one.

MTBF provides an important statistical indication for plant management or maintenance managers, enabling them to gain a better understanding of machine behavior and to plan maintenance activities more efficiently. Therefore, the MTBF is a key parameter in any reliability analysis; it shall be calculate in the early stage of a new project, starting with statistical data applied to similar components or activities, growing and improving in terms of data quality together with the product itself being analyzed.

MTBF is expressed in hours (h) passed between two consecutive failures.

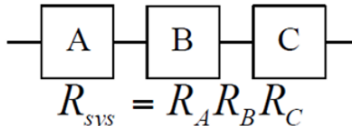
The inverse of the MTBF is the Failure Rate (λ) which is therefore the number of failures that occur on average over the course of an hour.

7.3 Reliability relations between system components

From a reliability point of view, the functioning of a system can be depicted graphically with one or more appropriately interconnected block diagrams where each block represents a subsystem or component.

In studying the reliability of an entire system, the individual components are grouped in series or in parallel, depending on their behavior from a reliability point of view.

If the system we are analyzing can only work if all its components work simultaneously, this system is graphically represented by many elements connected together in series. In this definition the electrical similarity from which (Figure 7.1) derives is evident.

$$R_{sys} = \prod_{i=1}^N R_i$$


$R_{sys} = R_A R_B R_C$

Figure 7.1: Electrical similarity

In this case, if $R_{A,B,C}$ is the probability of failure of each component (value between 0 and 1), the reliability of the set of these R_{sys} components will be given by the product of the individual reliability.

However, if we want to be more certain of operation in particular conditions (greater guarantee of good functioning or, even more importantly, increased safety) we must install other components equal to the one we consider critical in parallel with each other (redundancy). This reassures us about the achievement of our objective,

7.4. PRELIMINARY RELIABILITY CALCULATION FOR THE REVERSE BOOTSTRAP THERMAL SYSTEM DISCUSSED IN THIS THESIS

but has a negative impact in terms of logistical reliability because by necessarily increasing the number of components, the probability of failure also increases, but without negative impacts on performance and/or safety.

Still referring to the electrical similarity, we have the diagram in Figure 7.2.

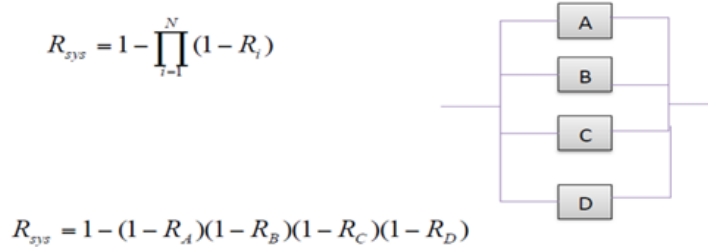


Figure 7.2: Electrical similarity with redundant components

Considering the scheme in Figure 7.2 it is clear that, for the system to work, at least one of the four components connected in parallel needs to work. The mathematical expressions that allow the calculation of the reliability of the system are shown in the same figure.

From what has been said about reliability connections in series and parallel and remembering the definitions of the various types of reliability, it is clear that Logistics Reliability is characterized by series connections because we want to know what the average operating time of a system is without failures of any kind occur. In these conditions, the probability of failure increases with the number of components installed.

From these considerations the importance of seriously dealing with Reliability from the early stages of our project is even clearer.

7.4 Preliminary Reliability calculation for the Reverse Bootstrap Thermal Control System discussed in this thesis

Let us now apply the considerations reported in the previous paragraphs to the thermal control system of the Avionics Box which is the subject of this thesis.

The block diagram of the system for analysing Logistics Reliability is represented in Fig(7.3)

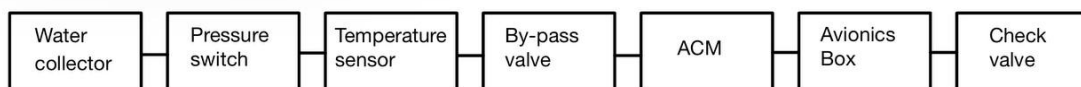


Figure 7.3: System block diagram

Following the considerations already made, dealing with Logistic Reliability, all the components are connected to each other in series, including the two exhaust check

valves (in by/pass operation) of the air coming from the Avionics Box, even if they work in parallel.

On Table (7.1) the list of components with their respective failure rates is shown.

Component	N	λ	$N \cdot \lambda$
Water collector	1	10	10
Pressure switch	1	11,7	11,7
Temperature sensor	1	11,7	11,7
By-pass valve	1	28,5	28,5
ACM	1	10	10
Avionics box	1	7,7	7,7
Check valve	2	2,6	5,2

Table 7.1: Failure rates table

The following mathematical expression provides the MTBF value as a function of the failure rates of the individual components, in the case of a series connection of the blocks which represent the behaviour of the components from a reliability point of view¹.

$$MTBF = \frac{1}{\sum \lambda_i} \quad (7.1)$$

The relationship confirms that, in a series system, as the number of components increases, the more reliability decreases, and that the reliability of the system will still be less than that of the least reliable single component.

From failure values shown in the Table 7.1, we obtain that the Thermal Control System MTBF, related to Logistic Reliability, is equal to:

$$MTBF = 12200 \text{ hours}$$

If we believe that this value calculated with the procedure discussed here can satisfy our reliability objectives, we must keep it constantly under control during all development phases, not only of the design, but also and even more effectively during the operation of our product.

It is therefore necessary to develop an adequate strategy and equip ourselves with the appropriate tools to implement it.

7.5 Failure Mode and Effect Analysis (FMEA)

The tool used to monitor the development of reliability and to decide whether to carry out improvement interventions and which of the possible ones is the Failure Mode and Effect Analysis (FMEA): a systematic analysis of how each detail or component can fail to perform correctly operation, considering the different possible failure modes as separate items.

¹This is the result of calculation processes and probabilistic/statistical reasoning which are omitted

7.6. FAILURE MODES EFFECTS AND CRITICALITY ANALYSIS (FMECA)

FMEA is carried out starting in the early design phase, of all the defects that may occur on the system; this allows us to prevent defects, at least the most serious ones and those that are easiest to correct, gradually providing the most convincing indication of the level of reliability achieved and drawing conclusions, related to that phase, on the validity of the path being followed.

For these reasons, FMEA must start as soon as possible, even if in the initial phases of the project it will undoubtedly be not very detailed, to gradually acquire new voices and provide increasingly focused and detailed analyses as the project progresses. In particular, the failure rate values will be estimated empirically; subsequently they will be increasingly reliable values, until they are confirmed by experimentation.

FMEA is based on three elements:

1. *Failure Modes*: this refers to the different ways in which a system can fail in its operation. These may include malfunctions, mechanical failures, electrical failures, or other problems that may occur during system operation.
2. *Effects*: represents the consequences or impacts of such failures on the overall operation of the system. Effects may range from physical damage to financial losses, or even security risks.
3. *Corrections*: repair (if possible and convenient) or replacement of the unit in order to restart the operation of the system in the fastest, cheapest, safest way according to the present needs (testing, development, service...)

The first FMEA of the Thermal Control System of the Avionics Box is shown in Table 7.2.

7.6 Failure Modes Effects and Criticality Analysis (FMECA)

A further step in the development of the reliability is FMECA (Failure Modes, Effects, and Criticality Analysis) is a reliability assessment methodology widely employed in fields like process analysis and industrial maintenance. Developed in 1949, FMECA gained significant traction during the Apollo space program, where it proved instrumental in predicting system failures and implementing necessary corrective measures. Subsequently, the United States Department of Defense established MIL-STD-1629A, a military standard originating from FMECA's naval applications within the US Navy.

This standard, updated until 1984, outlines the purposes, procedures, and evolution of the FMECA methodology.

In addition to the principles of FMEA, FMECA adds a semi-quantitative path to estimate the level of criticality of the problems identified through the attribution of a "criticality index".

The activities that characterize the FMECA and distinguish it from the FMEA are:

- establish the severity of each defect;
- in order of severity, hypothesize the causes;

Component	Failure Modes	Effects	Corrections
Water collector	- Leakage through the joints or welding seams	- Airflow to turbine reduction	- Correct connections tightening - Check/repair welding seams
Temperature sensor	- Incorrect temperature measurement	- The bypass valve does not operate correctly	- Recalibration or replacement
Bypass valve	- Valve does not operate according to signals from sensor/switch	- Incorrect operation of Direct/Air Cycle modes - Anti-ice protection lost	- Valve replacement
Air Cycle Machine	- Air bearings malfunction - Shaft seized	- Vibration; power loss; system performance not achieved - Turbine overspeed	- Replace ACM - Replace ACM
Avionics box ^a	- Operative temperature exceeding the tolerated limits	- Damage to avionics box electronics	- Clean the ducts between the plate fins
Check valve	- Valve does not operate correctly with the cooling mode (direct or ACM)	-Change the air flow and pressure upstream of the compressor / cannot dissipate the air flow in direct mode	- Valve replacement
Pressure Switch	- Incorrect pressure difference measurement	-Change mode too early/too late	- Recalibration or replacement

Table 7.2: FMEA of the Thermal Control System of the Avionics Box

^aMonitoring and protection of the Avionics Box are responsibility of the Customer. Reciprocal impacts and correction shall be agreed.

7.6. FAILURE MODES EFFECTS AND CRITICALITY ANALYSIS (FMECA)

- plan the identified actions and monitor their implementation.

An example of a scheme for the construction of the FMECA is shown in Table 7.3. In the FMECA table, after the columns in which the name of the process step or component/subsystem we are analysing must be entered, a column called EVALUATION appears. The sub-columns of EVALUATION contain the values of four indices:

- **S Severity (Severity - S)**: Severity of the effects of the defect on the process.
- **O Probability (Occurrence - O)**: Probability of the defect occurring due to a certain cause.
- **D Detection (D)**: Probability that the defect will be detected during the validation phases of the project.
- **RPN (Risk Priority Number)**: The priority with which actions should be carried out to eliminate or limit the risk of failure

Scales from 1 to 10 are used to estimate the value of the S, O, D indices, which allow situations to be interpreted and their values to be associated with them.

Occurrence

Occurrence indicates the probability of a given type of failure occurring. For a correct assessment, it is based on similarity with previous experiences, also carefully analysing the applicable procedures and methods already used in the company.

Detection

Detection indicates the probability that the failure mode will be intercepted, once it has occurred. The higher the value of the index, the greater the probability that the fault, if any, will not be intercepted.

N°	Component name	Failure mode	Failure effects	Corrective actions	Evaluation			Interventions to be performed	Manager and date of intervention	Solution			Priority
					S, O, D value					New S, O, D value			
					S	O	D			RPN	S	O	

Table 7.3: An example of FMECA layout table

7.6. FAILURE MODES EFFECTS AND CRITICALITY ANALYSIS (FMECA)

Ranking	Occurrence	Comments
1	1 in 1.500.000	Remote probability of occurrence; unreasonable to expect failure to occur
2	1 in 150.000	Very low failure rate. Similar to past design that has, had low failure rates for given volume/loads
3	1 in 15.000	Low failure rate based on similar design for given volume/loads
4	1 in 2000	Occasional failure rate. Similar to past design that had, in the past, similar failure rates for given volume/loads
5	1 in 400	Moderate failure rate. Similar to past design having moderate failure rates for given volume/loads
6	1 in 80	Moderate to high failure rate. Similar to past design having moderate failure rates for given volume/loads
7	1 in 20	High failure rate. Similar to past design having frequent failures that caused problems
8	1 in 8	High failure rate. Similar to past design having frequent failures that caused problems
9	1 in 3	Very high failure rate. Almost certain to cause problems
10	1 in 2+	Very high failure rate. Almost certain to cause problems

Table 7.4: Occurrence classification

Detectability	Evaluation Criterion	Index
Impossible	Existing design controls are unable to detect potential causes or subsequent failure modes	10
Very remote	Very remote ability of existing design controls to detect potential causes or consequent failure modes	9
Remote	Remote capability of existing design controls to detect potential causes or consequent failure modes	8
Very low	Very low ability of existing design controls to detect potential causes or consequent failure modes	7
Low	Low ability of existing design controls to detect potential causes or consequent failure modes	6
Medium	Medium capacity of existing design controls to detect potential causes or consequent failure modes	5
Quite high	Quite capability of existing design controls to detect potential causes or consequent failure modes	4
High	High capacity of existing design controls to detect potential causes or consequent failure modes	3
Very High	Very high capability of existing design controls to detect potential causes or consequent failure modes	2
Certain	Existing design controls certainly detect potential causes or consequent failure modes	1

Table 7.5: Detection classification

Severity

It indicates the severity of the failure mode. A first indication is given by the type of characteristic.

- A safety characteristic always has a Severity 9 or 10;
- A critical characteristic may have a Severity 7 or 8.

Ranking	Effect	Comments
1	None	No reason to expect failure to have any effect on safety, health, environment or mission
2	Very low	Minor disruption to facility function. Repair to failure can be accomplished during trouble call
3	Low	Minor disruption to facility function. Repair to failure may be longer than trouble call but does not delay mission
4	Low to moderate	Moderate disruption to facility function. Some portion of mission may need to be reworked or process delayed
5	Moderate	Moderate disruption to facility function. 100 % of mission may need to be reworked or process delayed
6	Moderate to high	Moderate disruption to facility function. Some portion of mission is lost. Moderate delay in restoring function
7	High	High disruption to facility function. Some portion of mission is lost. Significant delay in restoring function
8	Very high	High disruption to facility function. All of mission is lost. Significant delay in restoring function
9	Hazard	Potential safety, Health or environmental issue. Failure will occur with warning
10	Hazard	Potential safety, Health or environmental issue. Failure will occur without warning

Table 7.6: Severity classification

RPN

RPN (Risk Priority Number) is an index of the order that must be followed, when determining what action to take, to eliminate or limit the risk of failure. RPN is calculated as the product of S(everity) x O(ccurrence) x D(etection). Higher values of RPN indicate effects on which action should be taken sooner.

The RPN must be continuously updated after making the changes suggested by FMECA to ensure that it is lower than the previous one. Each of the magnitudes Occurrence, Severity, Detection, is expressed on a scale from 1 (lowest value) to 10 (highest value). The criticality must be as low as possible to be successful.

Once the RPN parameter has been identified, it must be decided whether to carry out corrective actions and their type. Corrective actions can never change the Severity as this index is unrelated to the process and is an intrinsic characteristic of the failure mode under consideration. The corrective action can therefore lower the Occurrence and/or Detection index.

Chapter 8

Comments and conclusions

8.1 Comments

The work presented here demonstrated the feasibility of an avionics thermal control system based on a Reverse Bootstrap air cycle. The suitability of such solution has been demonstrated by design and result analysis in both humid and dry air; moreover, for humid air, a simplified, but very conservative calculation approach has been adopted with very good results.

We now ask ourselves whether this solution is convenient from different points of view: performance, weight, size, reliability, maintenance, energy cost, sustainability. To compare the various alternatives, it would be necessary to know the characteristics of the other solutions that we currently ignore. However, we can make some considerations in this regard and identify at least qualitative answers.

- The usual solution to thermally control the on-board electronics is to integrate the avionics thermal control into the complete Environmental Control System (ECS) of the aircraft, installing the avionics equipment at the exhaust of the conditioned environments (cockpit, passenger cabin), using for the avionics cooling, which tolerate temperatures much higher than those of the inhabited compartments, the exhaust air at a temperature of approximately $30^{\circ}C$, while selected avionics can tolerate up to $80^{\circ}C$ ¹.

We must also take into account the architecture of the system, i.e. whether the loop is open or closed. In fact, if it is open, the impact of the avionics on the entire ECS consists only of a slight increase in pressure, without influence on the temperature of the inhabited compartments; if, however, the cycle is closed, the heat removed from the avionics remains in circulation and is a component of the thermal load of the entire system.

- Another important factor impacting the selection of the thermal control system type is the availability of the bleed air from the engine; more in general that depends also from the type of the engines: will they be "air breathing"(eso-reactors) engines or endo-reactors or both?

If the engines will be eso-reactors, bleeds are theoretically available, but on the modern engines it is preferred to avoid the bleed in order to not penalize

¹ $80^{\circ}C$ is the usual limit for electronics used for space or military applications, while for commercial use it is around $50^{\circ}C$. Modern special electronics have a much wider tolerance and are guaranteed at least up to $170^{\circ}C$.

8.2. CONCLUSIONS

- 95 Exhaust air;
- 102 Heat load;
- 104 Heat exchanger;
- 135 Turbine;
- 155 Compressor;
- 160 Shaft;
- 170 Motor;
- 180 Turbine by-pass valve;
- 190 Compressor by-pass valve.

- The application of the system shown in Figure 8.1 could be advantageous to avoid partially or totally the engine compressor bleed through the complete flight envelope. In this way, a zero energy or near-zero energy ECS could be realized.

8.2 Conclusions

1. The feasibility of a light and compact air cycle Reversed Bootstrap system for the thermal control of the avionics onboard of a supersonic civil aircraft has been theoretically demonstrated.
2. The designed Thermal Control System has a thermal load of 1500 W at sea level and extreme absolute humidity of 26g/kg, till to 400 W at 16000 m and Mach 1.8 with 0 g/kg humidity.
3. Overall dimensions of the system are 0.983 m x 0.340 m x 0.207 m; its mass (excluding the avionics) is 1.995 kg. The calculated MTBF is more than 12000 hours.
4. All components of the system were sized at the mean-line in order to evaluate their performance, dimensions and weight at the design point. The calculations were performed using software prepared by the candidates.
5. The performance of the entire system was calculated at the design point and verified at several other points representative of the aircraft's mission.
6. For what concerns the energy cost of the system here discussed, we are not in a position to compare it with any other solution because we don't know the details of such alternative solution. We can only state with certainty that the solution discussed here does not involve any energy cost (thanks to the absence of air bleed from the engine) despite the presence of the air intake (whose aerodynamic design is outside our objectives) which operates with a minimum airflow lower than 0.004 kg/s through the flight envelope.
7. Possible developments of the Reverse Bootstrap technology have been proposed, including the extension of its application to the ECS of inhabited compartments.

Appendix A

MatLab-Simulink model

The main objective of this appendix is to provide a clear understanding of the operation of the MatLab-Simulink model and each function block in the context of the overall system, highlighting the dynamic interactions between them. Through the detailed analysis of the simulations performed, it is intended to provide an in-depth overview of the expected performance and responses of the system.

Each block has a similar structure:

- **Input ports** - take output values from the previous block, needed to set the calculation;
- **Calculation subsystems** - where calculations are made;
- **Output ports** - make data available to the following block .

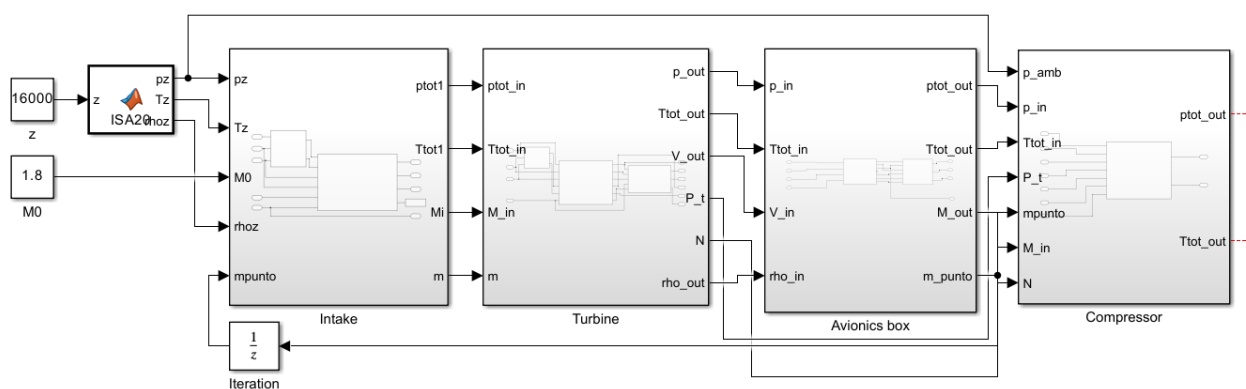


Figure A.1: Simulink model

In addition to the system blocks, there are:

- Two input blocks, altitude and flight Mach, to initialise the calculation;
- A block for calculating temperature, pressure and density values from flight altitude (block name : ISA20);
- A block for iterating the flow rate value.

A.1 Input blocks & ISA20 block

The Mach and flight altitude as input to the Simulink model define a given flight condition, providing information about the state of airflow needed to size the machines.

In the Steady-State case:

- **Mach**=1.8;
- **Flight altitude**=16000 [m];

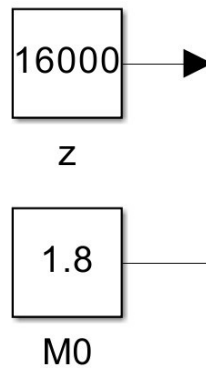


Figure A.2: Input blocks

Block ISA20 contains within it all the equations for calculating temperature (T), pressure (p), and density (ρ) dependent on altitude by including both troposphere and tropopause relationships.

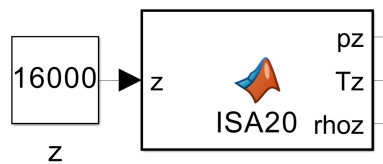


Figure A.3: ISA20 block

A.2 Intake block

The intake block is connected to *ISA20* and M_0 : the equations within it are used to calculate the conditions downstream to a normal and stationary shock wave, under the assumption of an ideal gas. Special attention should be paid to the iteration block: it gives a starting value to the mass flow rate, in order to start the iteration, then it takes the value of \dot{m} calculated in the Avionics Box block and brings it back to the Intake block.

A.3. TURBINE BLOCK

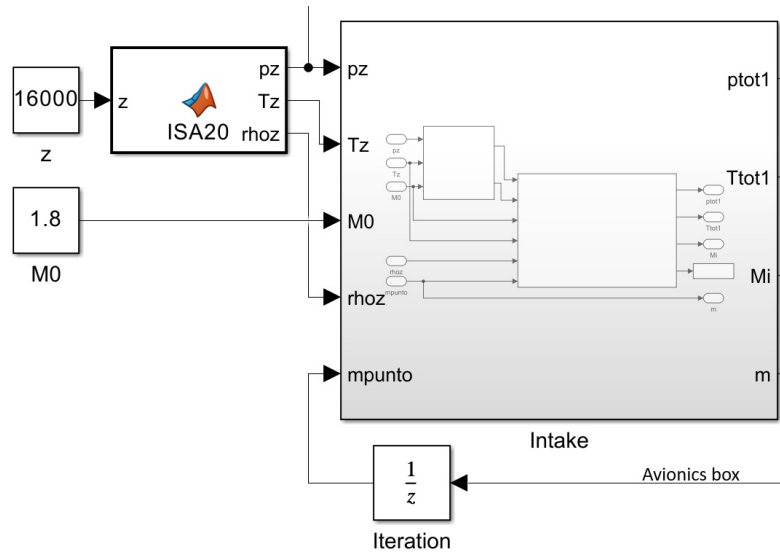


Figure A.4: Connections to intake

Within the Intake block there are:

1. A block for calculating T_0 , p_0 and ρ_0 ;
2. The block for sizing the intake;
3. A display to show the intake size in the current configuration.

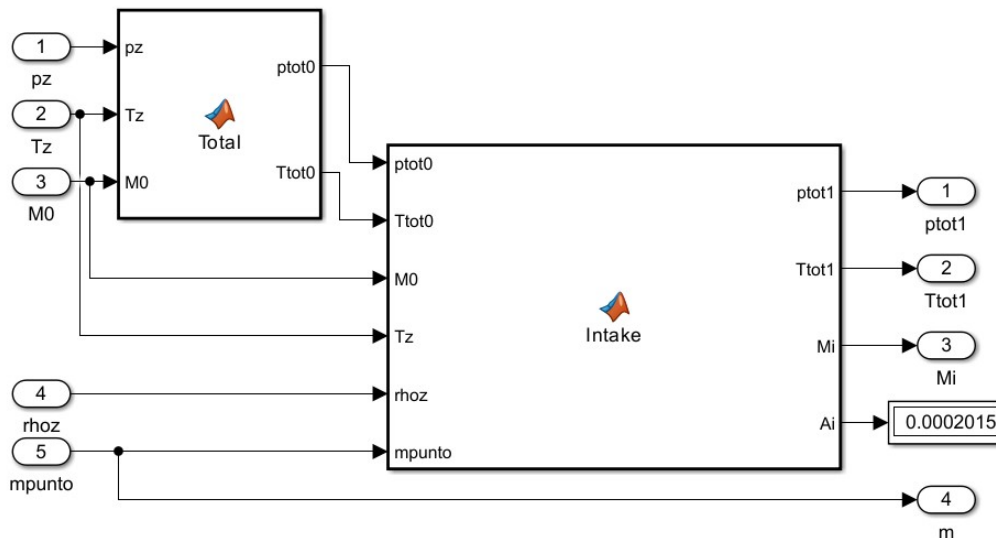


Figure A.5: Subsystem intake block

A.3 Turbine block

This block has the following functions:

- Obtain pressure, temperature, Mach and output velocity;
- Size rotor, volute, stator and meridian duct;

- Calculate the minimum number of blades;
- Obtain the power output of the turbine;
- Draw meridian duct and velocity triangles at turbine inlet and outlet.

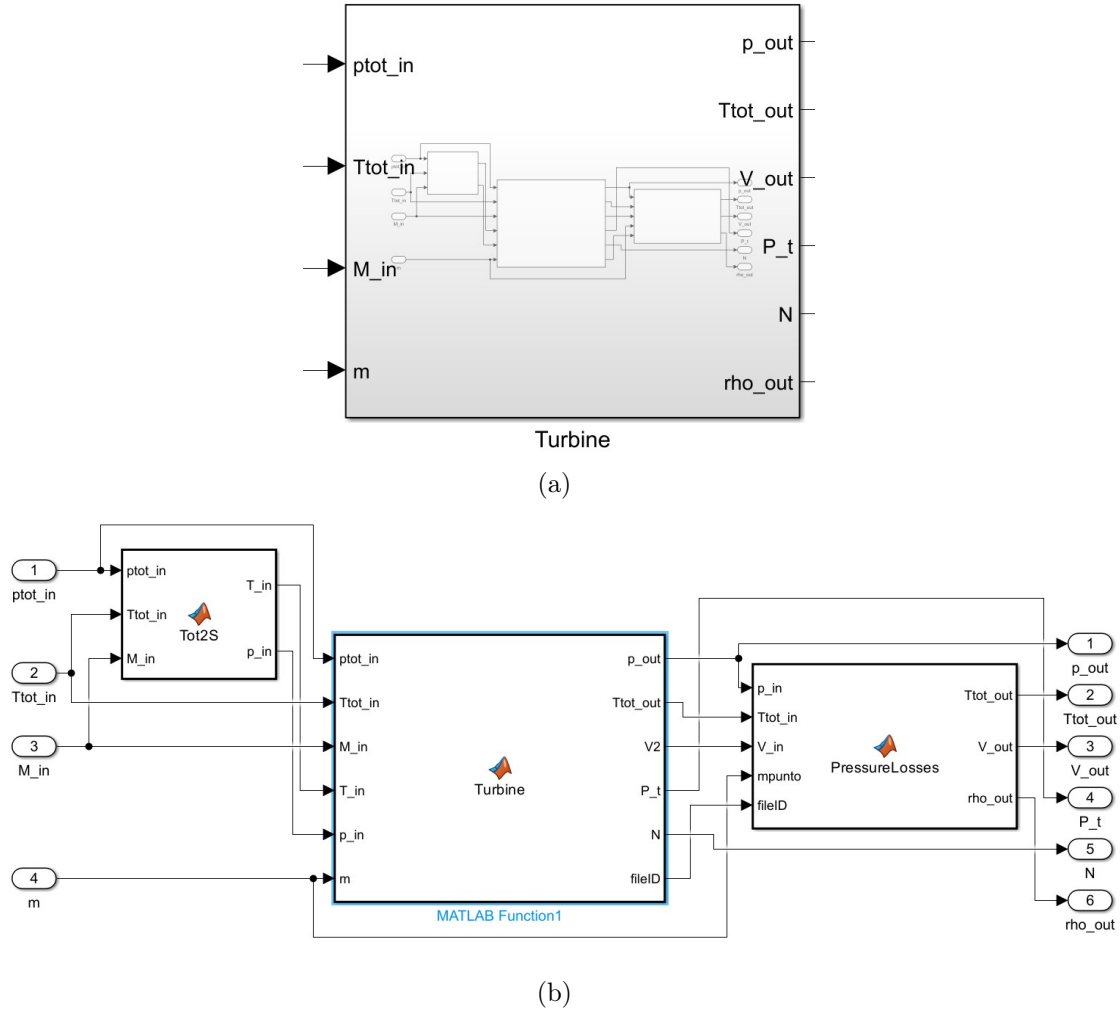


Figure A.6: Turbine block (a) and subsystem turbine block (b)

In addition, there are two blocks:

- **Tot2S** which calculates static quantities;
- **PressureLosses** which calculates the percentage losses in the tubes in the transition from turbine to avionics.

A.4 Avionics box block

The avionics box block is for the purpose of calculating the flow rate required to dispose of the heat generated by the electronic components.

The box has fins for optimal heat dissipation, the heat transfer of which is obtained by testing the graphs in the book Compact Heat Exchangers [17], processed by the Matlab code.

A.5. COMPRESSOR BLOCK

The function of *PressureLosses2* is the same as *PressureLosses*, with the difference that the connection considered is between the avionics box and the compressor.

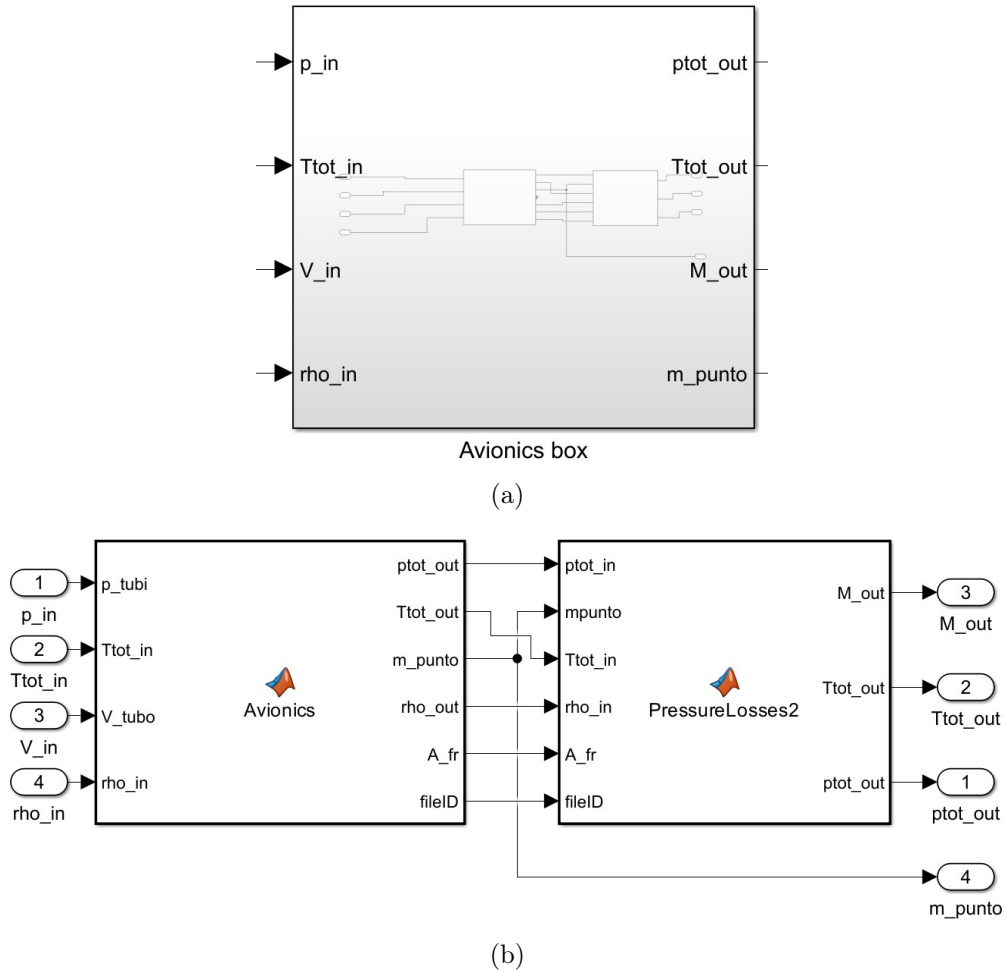


Figure A.7: Avionics box block (a) and subsystem avionics box block (b)

In the figure A.8 you can see the flow rate branch in the iteration block.

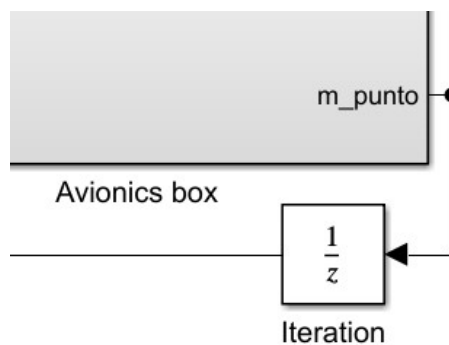
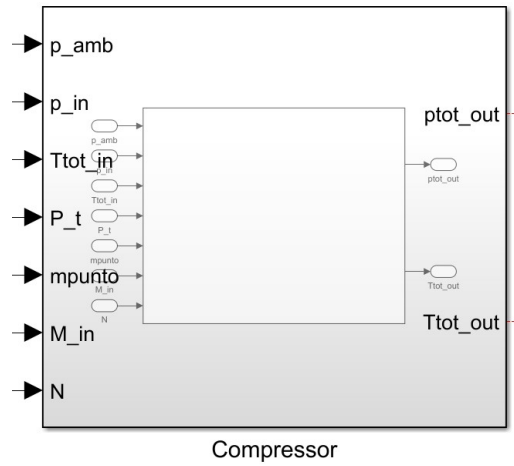


Figure A.8: Connections between avionics box and iteration box

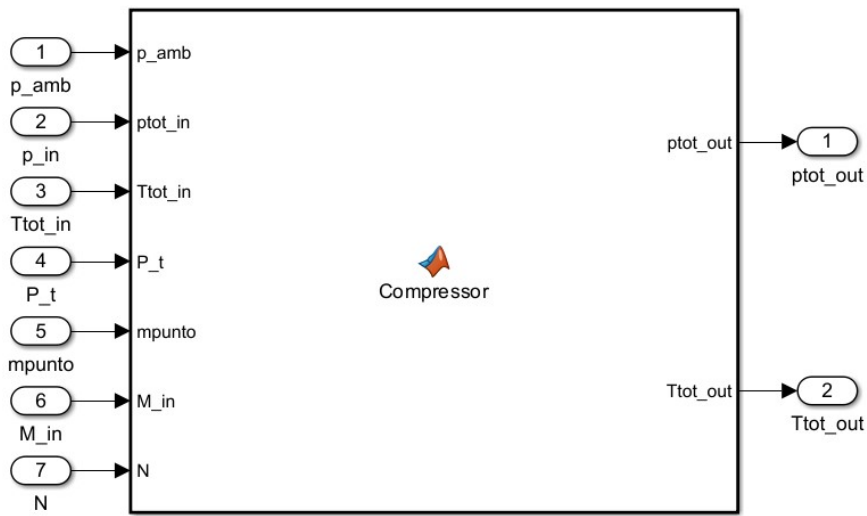
A.5 Compressor block

Finally, the compressor block has similar functions to the turbine block :

- Calculate temperature and output pressure;
- Size rotor, diffuser, meridian duct;
- Validate the efficiency;
- Draw the meridian duct and speed triangles;
- Calculate the minimum number of blades and the slip factor;



(a)



(b)

Figure A.9: Compressor block (a) and subsystem compressor block (b)

Appendix B

Component maps construction

In order to calculate and analyse the performance at the Off Design points of a system whose performance at the design point is known, it is necessary to know the so-called maps of each component: diagrams that show the behaviour of the components when one or more inputs vary.

Such maps are derived experimentally, running the prototype components on dedicated test benches, duly instrumented.

However, in the case of this thesis, with brand new components specifically designed, the experimental maps of course are not available. It is necessary to select one of two different procedures:

1. define the new maps by applying similarity theorems and dimensional analysis;
2. use experimental maps of similar components, appropriately scaled to fit the new components.

The second procedure has been applied, since experimental maps of Environmental Control System components are available.

The component maps, already scaled to the present application, are reported in Figures from 6.1 to 6.4.

Appendix C

Off Design iteration process

In paragraph 6.1 it is described how, using turbine and compressor maps, it is possible to derive the system performance at Off Design conditions. However, the process starts with the assumption of the value of two parameters:

1. the turbine corrected speed $N/\sqrt{\theta_T}$;
2. the turbine expansion ratio $\beta_{T,ts}$.

Since it is almost impossible that both this assumptions are true, at the end of the calculations two errors are found:

- a mismatch between the power generated by the turbine and the power absorbed by the compressor ($P_T \neq P_C$): it is an error since, in this application, all the power generated by the turbine is used to move the compressor;
- the calculated compressor discharge area is different from the one obtained from sizing: it is an error because this geometrical area is fixed.

The iteration process aims to update the attempt parameters in order to reduce the errors below the tolerance.

To do that, it is necessary to understand how the variation of the attempt parameters affects the errors: therefore, the partial derivatives of the errors with respect to both of the parameters have to be found. Since the relation between the errors and the attempt parameters is not linear, the partial derivatives need to be calculated at each step of the iteration.

The partial derivatives of the errors (e_1 and e_2) with respect to the attempt parameters (x_1 and x_2) are calculated by giving, in turn, an infinitesimal variation δx to x_1 and x_2 ; then, repeating all the steps described in paragraph 6.1, the consequent variation of the errors δe can be found.

$$\delta e_1 = \frac{\delta e_1}{\delta x_1} \delta x_1 + \frac{\delta e_1}{\delta x_2} \delta x_2$$

$$\delta e_2 = \frac{\delta e_2}{\delta x_1} \delta x_1 + \frac{\delta e_2}{\delta x_2} \delta x_2$$

Now, it is possible to calculate the variations of the attempt parameters (Δx_1 and Δx_2) which brings the errors e_1 and e_2 to zero. It is done by solving the following

linear system:

$$\begin{cases} \frac{\delta e_1}{\delta x_1} \Delta x_1 + \frac{\delta e_1}{\delta x_2} \Delta x_2 = -e_1 \\ \frac{\delta e_2}{\delta x_1} \Delta x_1 + \frac{\delta e_2}{\delta x_2} \Delta x_2 = -e_2 \end{cases}$$

Obviously the errors will probably not go to zero at the first iteration step since, as already discussed, their relation to δx_1 and δx_2 is not linear. So, it is necessary to repeat this process until convergence.

Appendix D

T_{DAR} and T_{WAR} at the turbine exhaust

If water vapor is present at the turbine inlet, during the expansion phase, due to the temperature drop and decreasing pressure till to the turbine exhaust, vapor condensation will occur accompanied by an exothermic reaction which will introduce unwanted heat into the air flow that we intend to cool.

We need to calculate if, during the expansion, the condensation of the water vapor happens together with sensible temperature increase at the turbine exhaust and production of liquid water.

In such case, the exhaust temperature measured by a dry bulb thermometer is called Wet Air Rated Temperature T_{WAR} , while T_{DAR} is the temperature reached after the re-evaporation of the liquid water.

In our case we know the absolute air humidity which is constant through the system. This is the Ambient Humidity U_{amb} [kg/kg].

The following relations concerning the humidity apply:

$$p_{sat} == \exp(16.6536 \sim 4030.183/(t + 235)) \quad (D.1)$$

$$U_{sat} = 0.622 p_{sat}/(p - p_{sat}) \quad (D.2)$$

$$H = c_{p,a}T + U_{sat}(C_{w,lat} + c_{p,w}T) \quad (D.3)$$

$$c_{p,u} = c_{p,a} + U_{amb} \cdot c_{p,w} \quad (D.4)$$

where:

air specific heat at constant pressure	$c_{p,a} = 1.0045$	$kJ/kg K$
water specific heat at constant pressure	$c_{p,w} = 1.820$	$kJ/kg K$
humid air specific heat at constant pressure	$c_{p,u}$	$kJ/kg K$
water latent heat at 0°C	$C_{w,lat} = 2500$	$kJ/kg K$
dry air/water vapor mixture total pressure	p	[kPa]
saturation pressure	p_{sat}	[kPa]
dry air/water vapor mixture total temperature	t	[°C]
ambient air absolute humidity	U_{amb}	[kg/kg]
saturation humidity at turbine exhaust	U_{sat}	[kg/kg]

Calculation process

- Calculate the humid air enthalpy at turbine inlet $H_{t,in}$, by means of formula (D.3) above, knowing U_{amb} , temperature and pressure at turbine inlet;

- b. Assume a tentative value for temperature t_{tent} that we want to calculate at turbine exhaust;
- c. Calculate saturation pressure at turbine exhaust p_{sat} by mean of (D.1), using t of step b.;
- d. Calculate U_{sat} by mean of (D.2), being p the air-vapor mix pressure at turbine exhaust;
- e. Calculate tentative humid air enthalpy $H_{t,ex,tent}$ by mean of (D.3), having supposed t_{tent} of step b. and U_{sat} calculated in d.;
- f. Calculate $L_{t,tent} = H_{t,in} - H_{t,ex,tent}$;
- g. $L_{t,tent}$ must be equal to L_t (obtained from system calculation with T_{DAR});
- h. If the statement g. is not true, change t_{tent} assumed in b. and reiterate till to the final convergence according to g.;
- i. The saturation humidity at turbine exhaust $U_{sat,ex,t}$ is given by (D.2) where p_{sat} is calculated by (D.1) with the last value of t of step b. which is the exhaust temperature of the humid air (T_{WAR}) measured by a dry bulb thermometer;
- j. The liquid water at the turbine exhaust is given by:

$$U_{liq,ex,t} = U_{amb} - U_{sat,ex,t}$$

- k. Equation in step j. makes sense if $U_{amb} > U_{sat,ex,t}$, otherwise there is no condensation in turbine ;
- l. If step k. is not true, liquid water (moisture) is not produced and the temperature at turbine exhaust is directly calculated by the system program.

Bibliography

- [1] ACTON, O., Turbomacchine, UTET, 1986.
- [2] AGRVAAL G. L., Foil Air/Gas Bearing Technology - An Overview, ASME Publication 97-GT-347, 1997.
- [3] ASTARITA, T., Onde d'urto normali e oblique, Università degli Studi di Napoli Federico II.
- [4] BALJE, O.E. Turbomachines, A Guide to Design, Selection, and Theory, 1981.
- [5] BAR-SHALOM, D., Altitude effects on heat transfer processes in aircraft electronic equipment cooling, Massachusetts Institute of Technology, 1989.
- [6] CHESHIRE, L.J. The design and development of centrifugal compressors for aircraft gas turbines, Proceedings of the Institution of Mechanical Engineers, 153, 1945.
- [7] CHIESA S., Affidabilità, Sicurezza e Manutenzione nel progetto dei sistemi, CLUT, 1988
- [8] COHEN, H., ROGERS G.F.C. and SARAVANAMUTTOO, H.I.H., Gas Turbine Theory, 4th edition, 1996.
- [9] CSANADY, G.T., Theory of Turbomachines, McGraw Hill, 1964.
- [10] DEFRANCESCO G.L., Applications of the Reverse-Bootstrap Air Cycle Environmental Control System, United Technologies Hamilton Standard.
- [11] DEFRANCESCO G.L., HO T. European Patent Application Ep 3 733518 A1, 2019.
- [12] FACCHETTI, S., Concorde: l'aereo supersonico da oltre 2.000 km/h tornerà, ma sarà più silenzioso, HDMOTORI.it, 2018.
- [13] GRABOW R. M. et al., A Ram Air Driven Air Cycle Cooling System for Avionics Pods, Ford Aerospace and Communications Corp., Newport Beach, CA, 1986.
- [14] HAYNES, T., Why NASA used the Tupolev TU-144, Key.Aero, 2021.
- [15] HERBERT, M.V., A method of performance prediction for centrifugal compressors, Aeronautical Research Council, R&M No. 3843 (HMSO, 1980).

- [16] ISMAIL, L.S., RANGANAYAKULU, CH., Heat Transfer and Flow Friction correlations for Compact Wavy Plate Fin Heat Exchangers.
- [17] KAYS, W.M., LONDON, A.L. Compact Heat Exchangers, 1964.
- [18] KOFSKEY, M.G., NUSBAUM, W.J., Effects of specific speed on experimental performance of a radial-inflow turbine, 1972.
- [19] LARENAS, N, American compra 20 Aereo supersonico Boom Overture, 2022.
- [20] MAO Yu-Feng et al., Cooling Ability/Capacity and Exergy Penalty Analysis of Each Heat Sink of Modern Supersonic Aircraft. Beihang University, Beijing 10091MDPI, 20191, China, 2019.
- [21] MIAO L. et al., Heat Transfer and Pressure Drop Characteristic Research of Sine Wavy Flying-Wing Fins, School of Mechanical and Electrical Engineering, Xuzhou University of Technology, Jiangsu 221000, China, 2023.
- [22] NOVAIS W.R.I. et al., Thermodynamic and Heat Transfer Analysis Of Cooling Technologies: a Comparative Study.
- [23] OSNAGHI C., Teoria delle Turbomacchine, Società Editrice Esculapio, 2013 .
- [24] OVERLI, J.M. Stramnings Maskiner, Bind 3, Termiske Maskiner, 2. utgave, 1992.
- [25] RODGERS, C., Development of a high specific speed centrifugal compressor, The American Society of Mechanical Engineers, paper 96-GT-353, 1996.
- [26] RODGERS, C., The Efficiencies of Single-Stage Centrifugal Compressors for Aircraft Applications, The American Society of Mechanical Engineers, paper 91-GT-77, 1991.
- [27] ROHLIK, H.E., Analytical Determination of Radial Inflow Turbine Design, 1968.
- [28] SHEIK ISMAIL L. et al., Heat Transfer And Flow Friction Correlation For Compact Wavy Plate Fin Heat Exchangers.
- [29] Thermodynamics of Incompressible and Compressible Fluid Flow AIR1168/1, SAE Aerospace Information Report, 2008.
- [30] TURGUT, E.T., USANMAZ, O., An analysis of vertical profiles of wind and humidity based on long term radiosonde data in Turkey, 2016.
- [31] VAVRA, M.H., Radial Inflow Turbines, Monterey, California, Naval Postgraduate School, 1964.
- [32] VAVRA, M.H., Radial Turbines, von Karman Insitute for Fluid Dynamics, 1968.
- [33] VERMA, A. K. et al., Reliability and Safety Engineering, Springer, 2016.

Ringraziamenti

A conclusione di questo lavoro, vorrei in primis ringraziare coloro che vi hanno partecipato. Ringrazio il Professor Paolo Maggiore, per avermi dato la possibilità di svolgere questo progetto. Ringrazio l'Ing. Achille Mannini, per avermi seguito meticolosamente durante questo percorso, con passione e dedizione, permettendomi di imparare e migliorare. Ringrazio Umberto, per essersi confermato un compagno ed amico di valore, per aver sempre trovato il tempo di aiutare, e per aver tolto quelle frecce dalle slide.

Desidero poi ringraziare le persone che mi hanno accompagnato in un altro tipo di percorso, altrettanto difficile e tortuoso, come quello della vita.

Ringrazio tutti i miei amici, per aver sopportato quel ragazzino scontroso, antipatico e decisamente strano, contribuendo a renderlo la persona calma, simpatica e decisamente strana che sono oggi. Grazie per aver reso speciali i momenti belli, ma soprattutto per aver reso meno amari quelli difficili.

In particolare ringrazio Steve e Andrea, per essermi stati vicino più di tutti in questi anni, per essersi beccati il meglio e il peggio di me, ed essere qui oggi, nonostante tutto.

Ringrazio Mamma e Papà, per avermi voluto bene quando era difficile volermi bene, per aver sempre cercato di spianarmi la strada per far sì che arrivassi dove sono ora. Non sono bravo ad esprimere riconoscenza, in particolare con voi, ma spero di riuscire a farlo con queste poche righe. Vi voglio bene.

Ringrazio Dario, perchè so che, sotto sotto, un po' mi vuoi bene e sei contento per me.

Ringrazio Nonna Lia. Con la tua dolcezza, la tua generosità ed il tuo altruismo (per non parlare della tua genovese!) sei stata e continui ad essere la persona migliore che abbia mai conosciuto. Spero di valere, come nipote, la metà della nonna che sei per me.

Ringrazio Nonno Pino, per essere stato il nonno per definizione: ore di traffico per accompagnarmi ovunque, partite di basket in casa (con rottura di crocifisso annessa) e frasi emblematiche ripetute mille volte, ascoltate sempre col sorriso.

Ringrazio Nonno Teo, per avermi accompagnato, mano nella mano, durante la prima parte della mia vita, indirizzandola verso il traguardo che raggiungo adesso. Spero tu sia fiero, ma so che si può sempre fare di più.

Luca